AN ABSTRACT OF THE THESIS OF

Larry Wise for the degree of Master of Science in Civil Engineering presented on July 20, 1999. Title: Numerical and Physical Modeling of Wave Forces on A-Jacks Units.

Abstract approved: Redacted for Privacy

William G. McDougal

A numerical model is developed to estimate wave forces on A-Jacks armor units. The forces include drag, inertia, buoyancy, and slamming as the unit penetrates the free surface. The wave force model is used to determine the rigid body motions of the units. Bulk forces on a matrix of units are also estimated. Wave flume tests are used to provide preliminary verification of the wave force model.

The wave force model discretizes the A-Jacks into a number of small elements. The Morison equation is used for submerged elements with stretch linear wave theory employed for wave kinematics. For elements that penetrate the free surface, slamming force calculations are based on the von Karman method. The calculated wave forces are used to determine the rigid body rotation of a single, unrestrained A-Jacks. The axes of rotation are defined by the three contacts between the unit and the under layer. The model allows for an individual A-Jacks unit to rotate with one degree of freedom about the axis of rotation with the minimum stability. Adjacent units do not restrain the rotation and interactions with other units in the matrix are not included. The equation of motion

is integrated in time to determine the rotation. This technique is used to determine the incipient motion conditions for a single, unrestrained A-Jacks. This is verified with experimental observations. The wave force model is found to be in agreement with the incipient rotational motion experiment results. The angular velocity at the instant when a leg of the unit rocks back and impacts the under layer can also be used to determine the impact force on the leg.

A single, unrestrained A-Jacks is a simplistic idealization. In reality, there is a high degree of interaction among the units. The interaction results in partial sheltering from wave forces and additional motion restraint. The bulk forces on a matrix of A-Jacks units are estimated by applying an empirical factor to the calculated forces to account for the sheltering effects among units. A calibration and preliminary verification of the bulk force models is obtained by measuring forces exerted on a matrix of units mounted on a load-frame. The A-Jacks were subjected to a variety of wave conditions in a 10 m wave flume. The measured bulk force on a matrix of units was fit with the numerical model output using a consistent set of sheltering coefficients.

Numerical and Physical Modeling of Wave Forces on A-Jacks Units

by

Larry Wise

A THESIS

submitted to

Oregon State University

in partial fulfillment of
the requirements for the
degree of

Masters of Science

Presented July 20, 1999
Commencement June 2000

Master of Science thesis of Larry Wise presented July 20, 1999

APPROVED:

Redacted for Privacy

Major Professor, representing Civil Engineering

Redacted for Privacy

Chair of Department of Civil, Construction, and Environmental Engineering

Redacted for Privacy

Dean of Graduate School

I understand that my thesis will become part of the permanent collection of Oregon State University libraries. My signature below authorizes release of my thesis to any reader upon request.

Redacted for Privacy

Larry Wise, Author

ACKNOWLEDGEMENT

I would like to thank several people who have helped me throughout this project. Support for this project was provided by Lee Brick and Block of Bowling Green, Kentucky. The O.H. Hinsdale Wave Research Laboratory provided some of the equipment used for the physical model experiments and Terry Dibble helped set up the wave gage and the data acquisition system for the bulk forces experiments. Ben Thornton assisted by running and analyzing the majority of the bulk forces experimental runs. William McDougal provided his time and computers for the modeling effort and helped guide me through this research project. Lastly, my wife Marie provided editing and proofreading which was greatly appreciated.

TABLE OF CONTENTS

TABLE OF CONTENTS (Continued)

LIST OF FIGURES

LIST OF FIGURES (Continued)

LIST OF FIGURES (CONTINUED)

LIST OF FIGURES (CONTINUED)

LIST OF FIGURES (CONTINUED)

LIST OF FIGURES (Continued)

LIST OF TABLES

NUMERICAL AND PHYSICAL MODELING OF WAVE FORCES ON A-JACKS UNITS

1. INTRODUCTION

The purpose of this project is to develop and verify a numerical wave force model for A-Jacks armor units. A three dimensional wave force model is developed for a single unit which includes drag, inertia, slamming, and buoyancy forces. The model can integrate the equation of motion to determine the rotational response of the unit to the wave forces. The model developed for a single unit is empirically extended to predict the forces which are experienced by an armor unit nested in a group of other units. The numerical model is verified by a series of laboratory tests.

Chapter 1 contains a brief description of A-Jacks armor units and a statement of the problem which is to be investigated. Chapter 2 gives background information on how similar problems have been approached by past researchers, including classic methods upon which design standards have been based and methods similar to the research conducted for this problem. Chapter 3 presents detailed theoretical information on how the numerical model was developed and briefly discusses the operation of the model. Chapter 4 discusses the convergence of the numerical model, presents typical graphical output from the model, and presents a parametric analysis of nearly five thousand model simulations. Chapter 5 discusses three physical experiments which were conducted: (1) incipient rotational motion experiments, (2) steady flow drag force experiments, and (3) bulk forces on uniformly placed units experiments. The physical model results are

compared to the predictions of the numerical model. Finally, Chapter 6 summarizes the results and draws conclusions from the research work.

A-Jacks units are six legged concrete armor units with a filleted central hub that gives structural strength and determines the in-place armor unit spacing. The size of the unit is specified by its length which is defined as the distance between the endpoints of two co-linear legs. Typical prototype scale units have sizes ranging from 2 ft. to 12 ft. A-Jacks are typically placed in a single unit thick layer and may be installed in either uniform or random placement patterns. The interlocking matrix of A-Jacks yields high hydraulic stability in comparison with other armor units.

The primary goal for the development of the numerical wave force model for A-Jacks armor units is to provide an estimate of the forces on a single unit for structural analysis. The structural analysis of individual units, using finite element modeling techniques, is being conducted at Auburn University in conjunction with the development of this wave force model. The force directly induced by waves, and impact forces caused by the wave induced motions of the A-Jacks, can be an input to the structural analysis. The return of a rotating unit to its resting position will result in an impact which can lead to large stresses. For this reason, the rotational motion of A-Jacks units about the ends of the three legs upon which they rest was modeled.

A single, unrestrained A-Jacks is a simplistic idealization. In reality, there is a high degree of interaction among the units. The interaction results in partial sheltering from wave forces and additional motion restraint. The bulk forces on a matrix of A-Jacks units are estimated by applying an empirical factor to the calculated forces to account for the sheltering effects among units. A preliminary verification of the bulk force model is

obtained by measuring forces exerted on a matrix of units mounted on a load-frame. The A-Jacks were subjected to a variety of wave conditions in a 10 m wave flume. The measured bulk forces on a matrix of units were fit with the numerical model output using a consistent set of sheltering coefficients.

The design of concrete armor unit cover layers for breakwaters and other coastal structures has historically been based on empirical design equations. The equations have been developed from large amounts of laboratory and field data on structure successes and failures. This method provides an adequate design procedure, particularly for randomly placed quarry stone. However, this method does not accurately represent the response of highly interlocking armor units.

The numerical wave force model for a single A-Jacks armor unit, and its extension to matrices of interlocked units, provides one step towards the development of a deterministic stability model for A-Jacks armor units. This wave force model may be integrated into future work on the structural response of the entire interlocked matrix of units on a structure slope and the flow fields surrounding such structures. At this stage, it may be realistic to begin to look at design methods based on deterministic approaches in addition to the traditional empirical approaches.

2. BACKGROUND

Coastal structures, such as jetties and breakwaters, have been constructed for harbor protection for over four thousand years. Early structures were sometimes constructed using cut stone blocks; however, by the time of the Roman civilization the ease of construction of rubble mound structures was realized (Whalin, 1994). As with many ancient construction practices, and those that survived through the European middle ages, experience of the constructors dictated the design. Only at the beginning of this century did systematic and scientific study of such structures begin, and only after the middle of this century were concrete armor units used as a replacement for quarry stone.

The stability of a rubble mound structure is affected by a number of parameters ranging from characteristics of the breakwater, such as geometry, construction materials, porosity, density, size, and interlocking, to characteristics of the environment, such as wave height, water depth, wave period, and wave breaking characteristics. With such a large number of variables in a very complex and energetic environment, study of these structures has occupied engineers for decades. Bruun (1990) presents issues concerning the stability and design of rubble mound structures and discusses three categories: overall stability, unit-in-place stability, and unit structural stability. The overall stability is the stability of an entire structure against all types of failure, the unit-in-place stability refers to the stability of individual armor units against significant movement, and the unit structural stability is the ability of individual units to resist the stresses within the units.

The overall stability and unit-in-place stability have been studied, generally as a single category, since the 1930s. The first empirical design formula to gain popular

usage in the harbor engineering field was that presented by the Spanish engineer R. Iribarren (1938). His equation determined the necessary weight of armor stone for a breakwater cover layer. A similar formulation was derived by Epstein and Tyrrell (1949).

In the 1950s the U.S. Army Corp of Engineers (USACE) begin scientific investigation into the stability of armor stones at their Waterways Experiment Station (WES) in Vicksburg, Mississippi. The USACE is charged with the maintenance of navigable waterways of the United States and under this mission has constructed and maintains most of the large breakwaters in the United States. In 1958 R. Y. Hudson of the WES introduced a new, simplified formulation for determining the required weight of armor stones:

$$W_r = \frac{\gamma_r H^3}{K_d m (S_r - 1)^3} \tag{1}$$

where W_r is the minimum required weight for an armor stone of the primary cover layer, H is the design wave height at the structure, K_d is the Hudson's equation stability coefficient, m is the structure slope expressed as run over rise (1:m), γ_r is the unit weight (weight per volume) of the armor stone, γ_w is the unit weight (weight per volume) of the surrounding water, and

$$S_r = \frac{\gamma_r}{\gamma_w} \tag{2}$$

This equation, known as Hudson's equation, is based on numerous large and small scale laboratory tests. In the laboratory experiments, the structure was tested to failure,

typically defined as the unacceptable movement of a percentage of armor units. The stability coefficient is fitted as the bottom envelope of the data (most conservative).

The stability number, N_s, is an alternative way to write the Hudson stability relationship and is given as:

$$N_s = \frac{\gamma_r^{1/3} H}{W_r^{1/3}(S_r - 1)} \tag{3}$$

The stability number and the Hudson stability coefficient are related as:

$$N_s = (K_d m)^{1/3} \tag{4}$$

Over the past forty years the stability formulations have been used to design breakwaters around the world. Due to its simplicity and wide ranging applicability, Hudson's equation has become the primary design equation for cover layers.

Hudson's equation does have several important omissions. Among the more frequent criticisms are that the wave period, characteristics of the wave breaking on the structure, core permeability, intensity and duration of the wave event, and the shape and interlocking patterns of the armor layer units are not explicitly included. Despite these criticisms, and perhaps because the formulation implicitly combines all of these variables into the stability coefficient, the equation has continued to be the most widely used of its type. Several attempts have been made to improve upon Hudson's equation. The reformulation perhaps gaining the most support being Van der Meer's equation (1988) which explicitly included several of the parameters not included in Hudson's equation.

Due to uncertainties in the design formulas and site specific conditions, laboratory testing is often recommended before the construction of large breakwaters or jetties. These laboratory tests are costly, and costs are increased if several design alternatives are

to be investigated. Laboratory tests also have their own set of uncertainties including extrapolating the results from laboratory scale to prototype scale. However, the laboratory costs often represent an insignificant fraction of the construction cost.

Many studies have been conducted in the last fifteen years in an attempt to predict the unit-in-place stability of armor layer units using numerical models or force predictions based on measured flow fields. Such models are the first step in modeling the overall stability of a structure. The development of an accurate model for unit-in-place stability would allow engineers to test design alternatives at a relatively low cost before conducting laboratory tests. In addition, a predictive model may lead to further optimization of breakwater design and minimize the need for or lower the cost of laboratory testing.

Several researchers have attempted to measure and predict the wave forces on idealized armor layer units, typically spheres. Juhl and Jensen (1990) measured the forces, including slamming and buoyancy, in an armor layer consisting of parallel cylinders and used their measurements to estimate the required weight of such units. Sulisz and McDougal (1990) and Sulisz (1994) proposed numerical estimates for the required weight for the rubble base of a composite breakwater (a breakwater comprised of a caisson on a rubble base). Their model solved for the flow field in and around the rubble base and estimated forces using modifications of Morison's equation (a semi-empirical wave force model for small bodies). The quarry stones of the armor layer were treated as spheres and critical conditions for the displacement of these spheres were found with the model. Silva and Losada (1997) used a similar model to investigate submerged breakwaters. Rufin et al. (1996) used laboratory measurements of forces on

and flow fields around spherical armor units on a submerged breakwater to estimate the required weight of such units. They also used a modified Morison's equation to predict forces based on the measured flow field and applied these forces to several stability criteria to predict the unit-in-place stability. Using the measured forces and flow field they were able to show the validity of Morison's equation for the top layer of armor units under a variety of wave conditions. Kobayashi and Otta (1987) developed a wave forces model for spherical armor units using a finite amplitude wave. The hydrodynamics of the model were improved upon by Kobayashi and Wurjanto (1990) and extended to irregular waves by Kobayashi et al. (1990).

Concrete armor units began to be used in the 1950s. Since that time numerous designs have be developed and deployed. Concrete armor units are generally used where quarry stone of the size required for the cover layer is either not available or is economically unjustifiable. The primary advantage of these concrete armor units is that their design allows them to be interlocking, thus increasing their stability and allowing lighter units to be used. However, three major disadvantages can also be cited: (1) the concrete units may break and thus significantly decrease their stability, (2) the units may possess very little reserve hydraulic stability meaning that once design conditions are exceeded complete structure failure could rapidly occur, and (3) until recently there has been little information available on structural design procedures (Bruun, 1990).

With concrete armor units, the third stability category described by Bruun (1990), unit structural stability, becomes most critical. A number of researchers have measured the stresses in concrete armor units in both laboratory and prototype studies. Burcharth (1981) dynamically tested dolos armor units to failure using drop tests, where a rotational

impact was used, and pendulum tests, where the unit was struck with a weight. Howell (1988) presented measurements of stresses, static and dynamic, in prototype scale dolos armor units at the Crescent City, California breakwater.

Less work has been done on predicting the forces that induce these stresses. McDougal et al. (1987) developed a numerical model to predict the wave forces, including slamming, on dolos concrete armor units. Dolos are a randomly placed armor unit; however, the numerical model was developed for a single, idealized orientation. The wave force model was used to predict rotational motions for the specific orientation. These forces and rotational motions were used as input to a finite element structural model (Tedesco et al., 1987). Their structural analysis yielded insight into possible failure mechanisms for dolos units.

This brief coverage of previous research on armor layer units shows that there is progression towards more deterministic design models. In 1983 Burcharth wrote that "a deterministic calculation of the stresses in the units is practically impossible, mainly because of the randomness of the ways in which the [armor] units are supported and because of the difficulties in determining the actual wave forces." For A-Jacks armor units, uniform placement makes the first cause of impossibility solvable, and the numerical model presented here is one step towards solving the second cause of impossibility.

3. THEORETICAL DEVELOPMENT

This chapter presents the theoretical development of the wave force model. The first section describes the coordinate systems used and the transformation between the systems. The next section discusses the wave theory used to determine the hydrodynamics of the model. This is followed by an introduction of the modified form of Morison's equation used to calculate the inertia and drag forces on the unit. Then the basis of the slamming force model is developed. Following this is a discussion of how the force calculations are implemented in the numerical model. Finally, the last section discusses the basis of the prediction of the rotational motion of the units and how this is incorporated in the numerical model.

3.1 Coordinate Systems and Transforms

Two coordinate systems are used in the formulation of the A-Jacks wave force model. These are the global coordinate system (X,Y,Z), which is aligned with the incident waves, and the body coordinate system (x,y,z), which is aligned with the A-Jacks unit legs. Figure 1 shows an A-Jacks unit with the global and body coordinate systems identified.

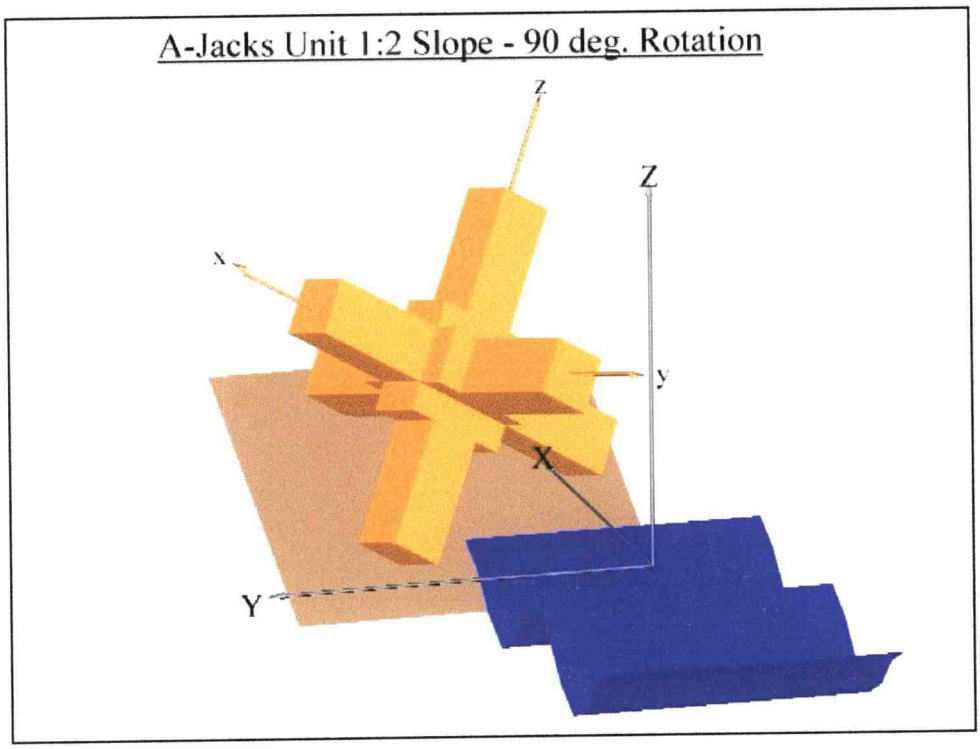

Figure 1: A-Jacks unit on a 1:2 slope with the body x axis rotated +90° with respect to the global X axis.

The global coordinate system is aligned such that incident waves propagate in the $+X$ direction. The global coordinate system vertical datum is at the still water level and the direction of the $+Z$ axis is defined such that the gravitational acceleration vector, g, has a negative sign. The position of the horizontal coordinate system origin (X=0, Y=0) relative to the unit of interest is input by the program user. The user inputs the values of the X and Y coordinates of the unit centroid, $X0$ and $Y0$, and the depth of the centroid below the still water level, d. The direction of the $+Y$ axis, along the wave crest, is chosen to yield a right-handed coordinate system.

A-Jacks units have fillets at their central hub. However, due to the fabrication technique, there are no fillets along the axis of one leg. The body coordinate system is defined such that the leg which has no fillets perpendicular to its axis corresponds to the x axis. Furthermore, the $+x$ direction points away from the plane on which the unit rests. The body coordinate system vector defining the direction of this leg is $\vec{a}$. The origin of the body coordinate system is at the centroid of the unit. The vector has a unit length and extends from the origin (x=0, y=0, z=0) in the $+x$ direction. The global coordinate system vector along this leg is $\vec{A}$. The y and z axes are chosen to obey the right hand rule and are defined such that the positive directions for the two axes point away from the plane on which the unit rests. The vectors $\vec{b}$, in body coordinates, and $\vec{B}$, in global coordinates, correspond to the leg in the y direction. The vectors $\vec{c}$, in body coordinates, and $\vec{C}$, in global coordinates, correspond to the leg in the z direction. The vectors $\vec{b}$ and $\vec{c}$ have unit lengths and extend from the origin (x=0, y=0, z=0) in the $+y$ direction and $+z$ direction, respectively.

The legs of the unit are referred to as leg A, leg B, and leg C corresponding to the legs parallel to the vectors $\vec{a}$, $\vec{b}$, and $\vec{c}$ (or, likewise, $\vec{A}$, $\vec{B}$, and $\vec{C}$). The endpoints of each leg corresponding to the $+\vec{a}$, $+\vec{b}$, and $+\vec{c}$ directions are denoted as $a1$, $b1$, and $c1$, respectively (or $A1$, $B1$, and $C1$ in global coordinates). The opposite endpoints of each leg, which rest on the structure slope, are denoted as $a0$, $b0$, and $c0$, respectively (or $A0$, $B0$, and $C0$ in global coordinates). The distance from one end of a leg to the opposite end of the leg defines the length of a unit, D. The width of the leg, w, is:

$$w = rD \tag{1}$$

where D is the length of the A-Jacks unit and r is the waist ratio. A typical value for the waist ratio is $r = 1/6.5$. Along legs B and C, fillets extend away from the union of the three legs. The fillet length, s, is:

$$s = frD \tag{2}$$

where f is the fillet ratio. A typical value is $f = 1/2$.

A-Jacks units are most often used to provide wave protection for jetties, breakwaters, or other coastal structures. As such, the units are generally placed on a slope, typically in the range of 1.5H:1V to 3H:1V. In addition, waves may approach the structure at an angle. Both of these angles, the orientation of the unit on the slope, and the angles the legs of a unit make with the plane on which it rests are necessary to define the relationship between the body and global coordinate systems. For the present purposes, it is assumed that a unit rests on a plane that is inclined relative to the horizontal plane (the global XY plane) according to the nominal slope of the structure. This is, of course, an idealization that does not account for variability in the underlying rubble layer or armor unit layer upon which a unit would normally rest.

The slope of the structure is defined as m, where m is a number greater than zero. A value of m=2 would correspond to a 1:2 slope (1 vertical:2 horizontal). A value of m=∞ would correspond to no slope, or a horizontal plane (the global XY plane). The angle between the horizontal plane and the plane of the slope, μ, is:

$$\mu = \tan^{-1}\left(\frac{1}{m}\right) = \cot^{-1}(m) \tag{3}$$

The angle that the incident waves make with the up-slope direction is denoted by ψ. The angle ψ=0 corresponds to a wave which propagates in the same direction as the

up-slope direction, or alternatively a wave which is normally incident to the toe of the structure. ψ increases as the wave angle increases in a counter-clockwise manner. Figure 2 shows the definition of the wave angle.

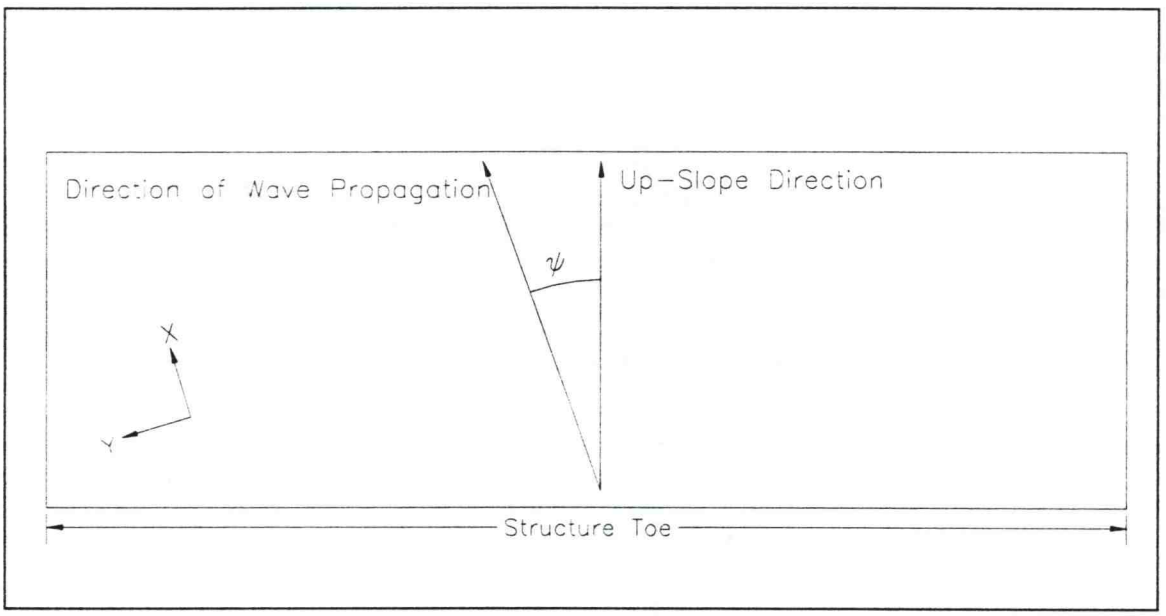

Figure 2: Definition sketch for the angle of wave approach.

The angles that an A-Jacks unit makes with the plane on which it rests are also important to the geometry of the force model. The A-Jacks unit has three legs in contact with the subgrade. The endpoints of these legs form an equilateral triangle on the plane of the subgrade. It can be shown through the use of the Pythagereom theorem and the laws of sines and cosines that the angle of intersection between a leg and the plane, ϕ, is:

$$\phi = \tan^{-1}(\sqrt{1/2}) \cong 35.26° \tag{4}$$

Furthermore, the angles in the plane of the structure slope of the direction of each leg are separated by 120° (or $2\pi/3$). The angle which leg A makes with the up-slope direction of the structure, measured counter-clockwise from the up-slope direction, is defined as θ. Figure 3 shows a unit on a slope with the angles θ, ϕ, and μ denoted.

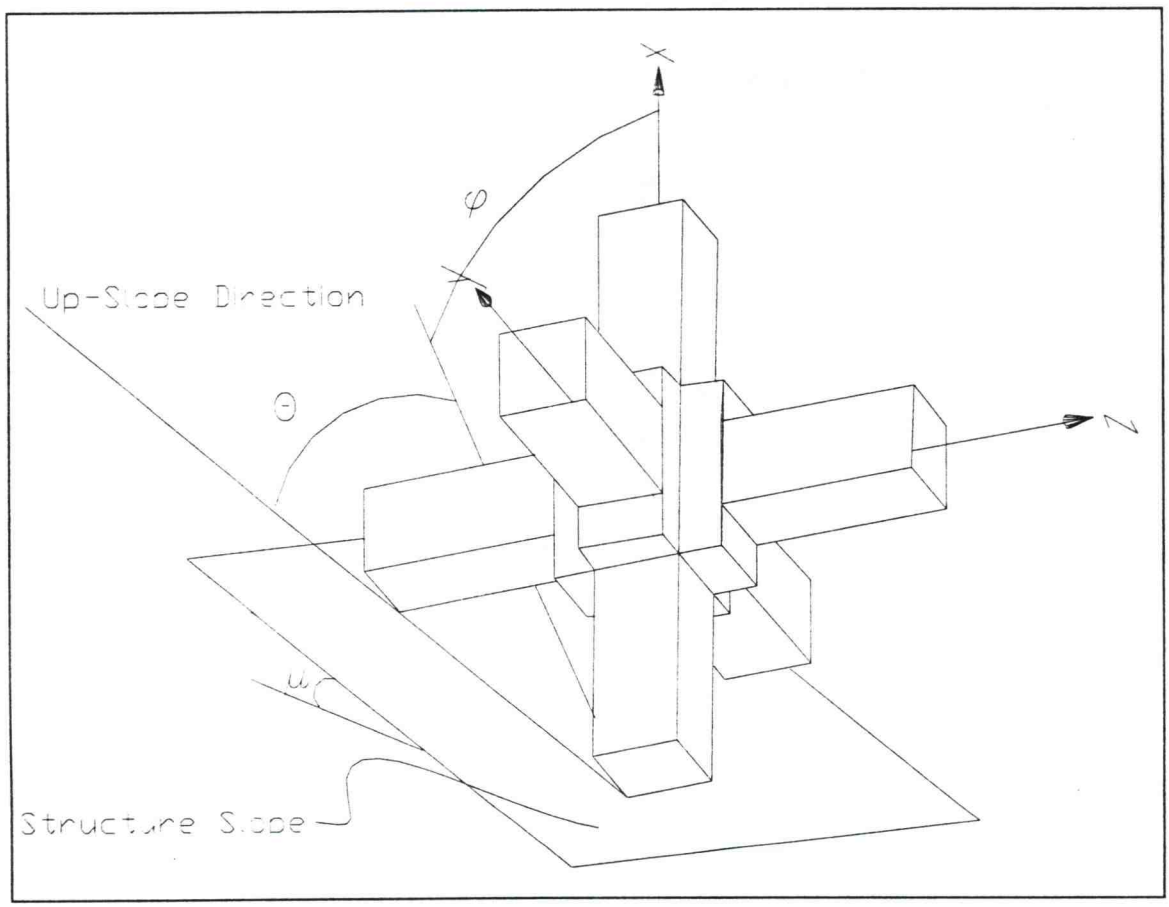

Figure 3: A-Jacks unit on slope showing slope angle, rotation of unit on slope, and the angle each leg makes with the slope surface.

With knowledge of the alignment of the two coordinate systems, a transformation can be derived to allow vectors to be transformed from one coordinate system to the other. This simplifies the force model by allowing the calculation of wave kinematics in

the global coordinate system, where they are more easily defined, and the calculation of forces and moments in the body coordinate system, where they are more easily defined. The transformation is performed in steps, with the first transformation being from body coordinates to an intermediate coordinate system corresponding to a unit on a horizontal slope (global XY plane). After this transformation is made, a further transformation is made to account for the slope of the structure, μ, and the angle of wave approach, ψ. Finally, a translation is applied to place the origin of the global coordinate system at the correct location as defined by the user input.

The directions of the vectors $\vec{a}$, $\vec{b}$, and $\vec{c}$ are first defined for the unit resting on a horizontal plane. This first transformation forms an intermediate coordinate system (X',Y',Z') which corresponds to the unit sitting on an m=∞ slope with incident waves. Thus, the $+X'$ direction is perpendicular to the toe of the structure (essentially the up-slope direction after the rotational transformation for the slope is applied) and the acceleration of gravity is in the $-Z'$ direction. The origin of the intermediate coordinate system is at the centroid of the unit (eliminating the need for a translation at this stage). The unit is rotated by an angle θ in the horizontal plane (measured between the $+x$ direction and the $+X'$ direction) and each leg makes an angle ϕ with the horizontal plane. The body coordinate system unit vectors $\vec{x}$, $\vec{y}$, and $\vec{z}$ are then given in the intermediate coordinate system as:

$$\begin{aligned}
\vec{x} &= (\cos\phi\cos\theta)\hat{i} + (\cos\phi\sin\theta)\hat{j} + (\sin\phi)\hat{k} = l_{11}\hat{i} + l_{21}\hat{j} + l_{31}\hat{k} \\
\vec{y} &= (\cos\phi\cos(\theta + \frac{2\pi}{3}))\hat{i} + (\cos\phi\sin(\theta + \frac{2\pi}{3}))\hat{j} + (\sin\phi)\hat{k} = l_{12}\hat{i} + l_{22}\hat{j} + l_{32}\hat{k} \\
\vec{z} &= (\cos\phi\cos(\theta + \frac{4\pi}{3}))\hat{i} + (\cos\phi\sin(\theta + \frac{4\pi}{3}))\hat{j} + (\sin\phi)\hat{k} = l_{13}\hat{i} + l_{23}\hat{j} + l_{33}\hat{k}
\end{aligned} \tag{5}$$

where l_{ij} are the direction cosines.

The three vectors in Equation (5) are mutually orthogonal and the rotational transformation matrix **R** can be written as (Chisholm, 1978):

$$\mathbf{R}_1 = \begin{bmatrix} l_{11} & l_{12} & l_{13} \\ l_{21} & l_{22} & l_{23} \\ l_{31} & l_{32} & l_{33} \end{bmatrix} \tag{6}$$

The matrix $\mathbf{R}_1$ allows any intermediate coordinate system vector, $\vec{Q}$, to be transformed to a body coordinate system vector, $\vec{q}$, and vice versa by the formulas:

$$\begin{aligned} \vec{q} &= \mathbf{R}_1 \vec{Q} \\ \vec{Q} &= \mathbf{R}_1^{-1} \vec{q} \end{aligned} \tag{7}$$

Since it is an orthogonal matrix, $\mathbf{R}_1$, has the special properties that (Chisholm, 1978):

$$\begin{aligned} \mathrm{Det}(\mathbf{R}_1) &= 1 \\ \mathbf{R}_1^{\mathrm{T}} &= \mathbf{R}_1^{-1} \end{aligned} \tag{8}$$

where Det( ) is the determinant of the matrix.

For example, given the angle $\phi \cong 35.26°$ and using the angle $\theta = 0$ gives the body coordinate system unit vectors as:

$$\begin{aligned}
\vec{x} &= (\cos(35.26^\circ)\cos(0))\hat{i} + (\cos(35.26^\circ)\sin(0))\hat{j} + (\sin(35.26^\circ))\hat{k} \\
&= 0.8165\hat{i} + 0\hat{j} + 0.5773\hat{k} \\
\vec{y} &= (\cos(35.26^\circ)\cos(\frac{2\pi}{3}))\hat{i} + (\cos(35.26^\circ)\sin(\frac{2\pi}{3}))\hat{j} + (\sin(35.26^\circ))\hat{k} \\
&= -0.4083\hat{i} + 0.7071\hat{j} + 0.5773\hat{k} \\
\vec{z} &= (\cos(35.26^\circ)\cos(\frac{4\pi}{3}))\hat{i} + (\cos(35.26^\circ)\sin(\frac{4\pi}{3}))\hat{j} + (\sin(35.26^\circ))\hat{k} \\
&= -0.4083\hat{i} - 0.7071\hat{j} + 0.5773\hat{k}
\end{aligned} \tag{9}$$

Thus, the leg A has components in the $+X'$ and $+Z'$ directions, leg B has components in the $-X'$, $+Y'$, and $+Z'$ directions, and leg C has components in the $-X'$, $-Y'$, and $+Z'$ directions. Then the rotational transformation $\mathbf{R_1}$ is given as:

$$\mathbf{R}_1 = \begin{bmatrix} 0.8165 & -0.4083 & -0.4083 \\ 0 & 0.7071 & -0.7071 \\ 0.5773 & 0.5773 & 0.5773 \end{bmatrix} \tag{10}$$

The determinant of this matrix is found to be 1.

Now rotational transformation matrices, $\mathbf{R}_1$ and $\mathbf{R}_1^{-1}$, have been defined to transform body coordinate system vectors to intermediate coordinate system vectors and vice versa. A second set of rotational transformation matrices, $\mathbf{R}_2$ and $\mathbf{R}_2^{-1}$, and a translation vector, $\mathbf{C}_t$, are need to convert from the intermediate coordinate system to the global coordinate system. This second set of rotational transformation matrices will account for the slope of the structure and the angle of wave approach. Since the rotational transformations are linear operators, super-position is valid and the total rotational transformation matrices for body coordinates to global coordinates and vice versa are the product of the two transformation matrices, $\mathbf{R}_1\mathbf{R}_2^T$ and $\mathbf{R}_1^T\mathbf{R}_2$. In addition, the matrix $\mathbf{R}_2$ is the product of two rotation matrices; a matrix for the rotation about the

global Y axis by the angle of μ, $\mathbf{R}_\mu$, and a matrix for a rotation about the new Z axis by the angle of ψ, $\mathbf{R}_\psi$.

$$\mathbf{R}_\mu = \begin{bmatrix} \cos\mu & 0 & -\sin\mu \\ 0 & 1 & 0 \\ \sin\mu & 0 & \cos\mu \end{bmatrix}$$

$$\mathbf{R}_\psi = \begin{bmatrix} \cos\psi & \sin\psi & 0 \\ -\sin\psi & \cos\psi & 0 \\ 0 & 0 & 1 \end{bmatrix} \tag{11}$$

$$\mathbf{R}_2 = \mathbf{R}_\mu \mathbf{R}_\psi = \begin{bmatrix} \cos\mu\cos\psi & \cos\mu\sin\psi & -\sin\mu \\ -\sin\psi & \cos\psi & 0 \\ \sin\mu\cos\psi & \sin\mu\sin\psi & \cos\mu \end{bmatrix}$$

For example, given a slope of 1:2 (μ=-26.57°) and a normally incident wave (ψ=0), $\mathbf{R}_2$ is found to be:

$$\mathbf{R}_2 = \begin{bmatrix} 0.8944 & 0 & 0.4472 \\ 0 & 1 & 0 \\ -0.4472 & 0 & 0.8944 \end{bmatrix} \tag{12}$$

Finally, a translation must be applied to place the origin of the unit at the desired location, ($X0$, $Y0$, $-d$). This translation vector is defined as:

$$\mathbf{C}_t = \begin{bmatrix} X0 \\ Y0 \\ -d \end{bmatrix} \tag{13}$$

The total transformations for any vector from a body coordinate vector, $\vec{q}$, to a global coordinate vector, $\vec{Q}$, and the inverse are:

$$\vec{q} = (\vec{Q} - \mathbf{C}_t)\mathbf{R}_1\mathbf{R}_2^T$$
$$\vec{Q} = \mathbf{R}_1^T\mathbf{R}_2\vec{q} + \mathbf{C}_t \tag{14}$$

For a unit at a depth of 20 ft. below the still water level and $X0=Y0=0$ with a rotation on the slope of $\theta=0$, on a 1:2 slope (μ=-26.57°), with a normally incident wave ($\psi=0$) the total coordinate system transform is (units of ft.):

$$\vec{q} = \left(\vec{Q} - \begin{bmatrix} 0 \\ 0 \\ -20 \end{bmatrix} \right) \begin{bmatrix} 0.4721 & -0.6233 & -0.6233 \\ 0 & 0.7071 & -0.7071 \\ 0.8815 & 0.3338 & 0.3338 \end{bmatrix}$$
$$\vec{Q} = \begin{bmatrix} 0.4721 & 0 & 0.8815 \\ -0.6233 & 0.7071 & 0.3338 \\ -0.6233 & -0.7071 & 0.3338 \end{bmatrix} \vec{q} + \begin{bmatrix} 0 \\ 0 \\ -20 \end{bmatrix} \tag{15}$$

For a 4 ft. A-Jacks unit with the placement used in Equation (15) the global coordinates of the endpoints of the unit are found to be (units of ft.):

$$A0 = \begin{bmatrix} -0.9442 \\ 0 \\ -21.7631 \end{bmatrix} \quad B0 = \begin{bmatrix} 1.2464 \\ -1.4142 \\ -20.6676 \end{bmatrix} \quad C0 = \begin{bmatrix} 1.2467 \\ 1.4142 \\ -20.6676 \end{bmatrix}$$
$$A1 = \begin{bmatrix} 0.9442 \\ 0 \\ -18.2369 \end{bmatrix} \quad B1 = \begin{bmatrix} -1.2467 \\ 1.4142 \\ -19.3324 \end{bmatrix} \quad C1 = \begin{bmatrix} -1.2467 \\ -1.4142 \\ -19.3324 \end{bmatrix} \tag{16}$$

It is observed that leg A (defined by the vector from $A0$ to $A1$), has no component in the global Y direction. This is due to the fact that the angles θ and ψ both being zero. It is also noted that the beginning coordinate for leg A ($A0$) has a lower Z value than the

beginning coordinate of legs B or C ($B0$ or $C0$, respectively) because the structure slope is such that $A0$ is sitting at a lower elevation.

3.2 Linear and Stretch Linear Wave Theories

To determine the hydrodynamic forces on an A-Jacks unit, the wave kinematics must be estimated. A number of wave theories that estimate the hydrodynamics under various wave conditions have been developed. Of the wave theories developed, linear wave theory (or Airy wave theory) is the most basic and has a large range of conditions under which it is acceptably accurate. Linear wave theory has been used for the development of this wave force model due to its ease of implementation and relatively broad region of validity. However, it should be noted that although it has broad applicability, linear wave theory does not take into account the complexities of flows in and around breakwater structures which may be dominating factors in the real world.

Using linear wave theory, the instantaneous water level, η, water particle velocity, $\vec{U}$, and water particle acceleration, $\dot{\vec{U}}$, are:

$$\begin{aligned}
\eta(X,t) &= \frac{H}{2}\cos(kX-\omega t) \\
\vec{U}(X,Z,t) &= u\hat{i}+v\hat{k} \\
&= \frac{H}{2}\frac{gk}{\omega}\left[\frac{\cosh k(h+Z)}{\cosh kh}\cos(kX-\omega t)\hat{i}+\frac{\sinh k(h+Z)}{\cosh kh}\sin(kX-\omega t)\hat{k}\right] \\
\dot{\vec{U}}(X,Z,t) &= \frac{\partial u}{\partial t}\hat{i}+\frac{\partial v}{\partial t}\hat{k} \\
&= \frac{H}{2}gk\left[\frac{\cosh k(h+Z)}{\cosh kh}\sin(kX-\omega t)\hat{i}-\frac{\sinh k(h+Z)}{\cosh kh}\cos(kX-\omega t)\hat{k}\right]
\end{aligned} \tag{17}$$

where u is the horizontal water particle velocity, v is the vertical water particle velocity, H is the wave height, k is the wave number, ω is the angular wave frequency, h is the water depth, and t is the time.

Linear wave theory is based on the assumption of infinitesimally small wave amplitudes, and the water particle velocities and accelerations are not defined above the still water level. However, in the case where part or all of the body of interest lay above the still water level, it is necessary to either change the domain of the linear wave theory solution to cover the entire water column, extrapolate the linear wave theory above the still water level, or use a higher order wave theory. Chakrabarti (1987) discusses a number of methods of extrapolating the kinematics of linear wave theory above the still water level including hyperbolic extrapolation, constant value extrapolation using the values at the still water level, and linear extrapolation; all of these methods result in overly conservative forces. The approach of changing the domain of the linear wave theory solution to cover the entire water column has been taken for the A-Jacks wave forces model. Chakrabarti (1987) discusses two methods of changing, or stretching, the domain of the linear wave theory to cover the entire water column ($-h<Z<\eta$). The form used for this model is the form developed by Chakrabarti, where:

$$\begin{aligned}
\vec{U}(X,Z,t) &= u\hat{i} + v\hat{k} \\
&= \frac{H}{2}\frac{gk}{\omega}\left[\frac{\cosh k(h+Z)}{\cosh k(h+\eta)}\cos(kX-\omega t)\hat{i} + \frac{\sinh k(h+Z)}{\cosh(h+\eta)}\sin(kX-\omega t)\hat{k}\right] \\
\dot{\vec{U}}(X,Z,t) &= \frac{\partial u}{\partial t}\hat{i} + \frac{\partial v}{\partial t}\hat{k} \\
&= \frac{H}{2}gk\left[\frac{\cosh k(h+Z)}{\cosh(h+\eta)}\sin(kX-\omega t)\hat{i} - \frac{\sinh k(h+Z)}{\cosh(h+\eta)}\cos(kX-\omega t)\hat{k}\right]
\end{aligned} \tag{18}$$

In effect, stretch linear wave theory conserves the velocity and acceleration at the free surface, but changes the velocity and accelerations in the rest of the water column. Where $h >> \frac{H}{2}$ the effect of the stretching is small. Unfortunately, stretch linear wave theory does not satisfy Laplace's equation (the continuity equation) unless the term $(h+\eta)$ is treated as a constant in the differentiation of the velocity potential with respect to X and Z (Chakrabarti, 1987).

3.3 Morison's Equation for Inclined Cylinders

Morison's equation is widely used for vertical and inclined small diameter cross-section members (Sarpkaya and Isaacson, 1981). The basic requirement for the application of the equation is that the diameter of the body must be small in relationship to the wave length so that diffraction does not occur. Morison's equation is also applicable to other small body cross-sections if the force coefficients are properly defined. This section outlines how Morison's equation is applied to the A-Jacks wave force model.

The general form of Morison's equation applied to a discrete section of an inclined body (over the length of which the velocity and acceleration are assumed constant) is (Sarpkaya and Isaacson, 1981):

$$d\vec{F} = dL\left[\frac{1}{2}\rho C_d D_f \left|\vec{U}_n\right|\vec{U}_n + \rho C_m A_c \dot{\vec{U}}_n\right] \tag{19}$$

where $d\vec{F}$ is the force on the section being considered, dL is the longitudinal (axial) length of the section being considered , ρ is the fluid density, C_d is the drag coefficient

for the section being considered, D_f is the projected area per unit length of the section being considered, $\vec{U}_n$ is the normal fluid velocity vector (normal to the longitudinal axis of the section), C_m is the inertia coefficient for the section being considered with $C_m = (1+C_a)$, C_a is the added mass coefficient for the section being considered, A_c is the longitudinal area of the section being considered (e.g., $\frac{1}{4}\pi D^2$ for a circular cylinder of diameter D), and $\dot{\vec{U}}_n$ is the normal fluid acceleration vector (normal to the longitudinal axis of the section).

In addition to the Morison's equation forces, which are orthogonal to the centerline axis of each leg, an additional drag force term is used for the component of drag caused by flow parallel to the axis of the leg. This drag force for axial flow past the end elements of the leg is estimated as:

$$d\vec{F}_d = \frac{1}{2}\rho C_d^f A_f^f \left|\vec{U}_l\right|\vec{U}_l \tag{20}$$

where $d\vec{F}_d$ is the drag force along the axis of the section being considered, C_d^f is the drag coefficient for flow along the axis of a terminal section (end element) being considered, $\dot{\vec{U}}_l$ is the longitudinal fluid acceleration vector, and A_f^f is the projected frontal area (normal to the axial flow) of the terminal section (e.g., $\frac{1}{4}\pi D^2$ for a circular cylinder of diameter D).

The Morison's equation force for each discrete section is applied at the axial center of that section at a point on the centerline axis of the leg. The axial length of the discrete section must be chosen such that the assumption that the fluid velocity and

acceleration are constant along that section is true within reasonable limits. These limits are achieved by choosing sufficiently small elements to obtain the desired accuracy of the model.

The normal components of velocity and acceleration are determined by the orientation of the leg under consideration. For example, the normal components of velocity and acceleration for a section of leg A, parallel to the vector $\vec{A}$ (in global coordinates), are given by (Sarpkaya and Isaacson, 1981):

$$\begin{aligned} \vec{U}_n &= \vec{A}\times(\vec{U}\times\vec{A}) \\ \dot{\vec{U}}_n &= \vec{A}\times(\dot{\vec{U}}\times\vec{A}) \\ \vec{U}_l &= \vec{U}-\vec{U}_n \end{aligned} \tag{21}$$

where $\vec{U}$ is the total fluid velocity vector (in global coordinates) and $\dot{\vec{U}}$ is the total fluid acceleration vector (in global coordinates). The absolute value of $\vec{U}_n$, $\left|\vec{U}_n\right|$, is the vector length of $\vec{U}_n$ and is given as:

$$\left|\vec{U}_n\right| = \left[\vec{U}_n \bullet \vec{U}_n\right]^{1/2} = \left[u_n^2 + v_n^2\right]^{1/2} \tag{22}$$

where u_n is the component of the normal velocity vector in the X direction and v_n is the component of the normal velocity in the Z direction. Equations (21) and (22) can readily be adapted for use in the body coordinate system after transforming the velocity and leg direction vectors to body coordinates (the second part of Equation (22) must be modified because three components of velocity will be present in the body coordinate system).

The projected area per unit length, D_f, the cross-sectional area, A_c, and the projected frontal area of a terminal section, A_f^f, must be defined before Equations (19) and (20) can be used. The cross-sectional area and frontal area of a terminal section are easily defined as:

$$A_c = A_f^f = w^2 \tag{23}$$

where w is the width of a leg. Defining the projected area per unit length is more problematic. To simplify calculations, a circle is transcribed around the square cross-section being considered, and the diameter of this circle is used for the projected transverse length, thus:

$$D_f = \sqrt{2}w \tag{24}$$

This prevents D_f from being a function of the angle the normal velocity vector makes with the cross-section and instead considers the "worst case" angle of 45° (which maximizes the projected transverse length and results in a higher drag force).

Finally, before Equation (19) can be applied to the present problem the appropriate drag and inertia coefficients must be chosen. The drag and inertia coefficients are functions of the cross-sectional shape and of the Reynolds number, $\mathbf{R_e}$, or the Keulegan-Carpenter number, **KC**, which can be calculated by:

$$\mathbf{KC} = \left|\vec{U}_n\right| \frac{T}{D} \tag{25}$$

$$\mathbf{R_e} = \left|\vec{U}_n\right| \frac{D}{\upsilon} \tag{26}$$

where v is the kinematic viscosity of the fluid. Equation (19) uses the same drag and inertia coefficients as are appropriate for a vertical member with the same cross-section and $\mathbf{R_e}$.

The drag coefficient is determined by interpolation between experimentally determined drag coefficients for square cylinders (Mott, 1990). The interpolation is based on the angle of attack, Ω, of the normal velocity vector and $\mathbf{R_e}$. The angle of attack, Ω, is defined as:

$$\Omega = \left(\tan^{-1}\left(\frac{|U_{n1}|}{|U_{n2}|} \right) \right) \tag{27}$$

where $0<\Omega<\pi/2$, U_{n1} is the component of the normal velocity parallel to the primary face, and U_{n2} is the component of the normal velocity perpendicular to the primary face. Figure 4 gives a definition sketch for the angle of attack. The primary face can be any of the four faces of the square section; for this model it is the face with a $-z$ direction outward normal for leg A, the face with an $-x$ direction outward normal for leg B, and the face with a $-y$ direction outward normal for leg C. The appropriate drag coefficient is linearly interpolated from the data in Table 1 (Mott, 1990). In cases where $\mathbf{R_e}$ lies outside of the range in Table 1 the C_d value at the same Ω and the nearest value of $\mathbf{R_e}$ is used. Equation (20) uses a single value for C_d^f of 1.60 (Mott, 1990).

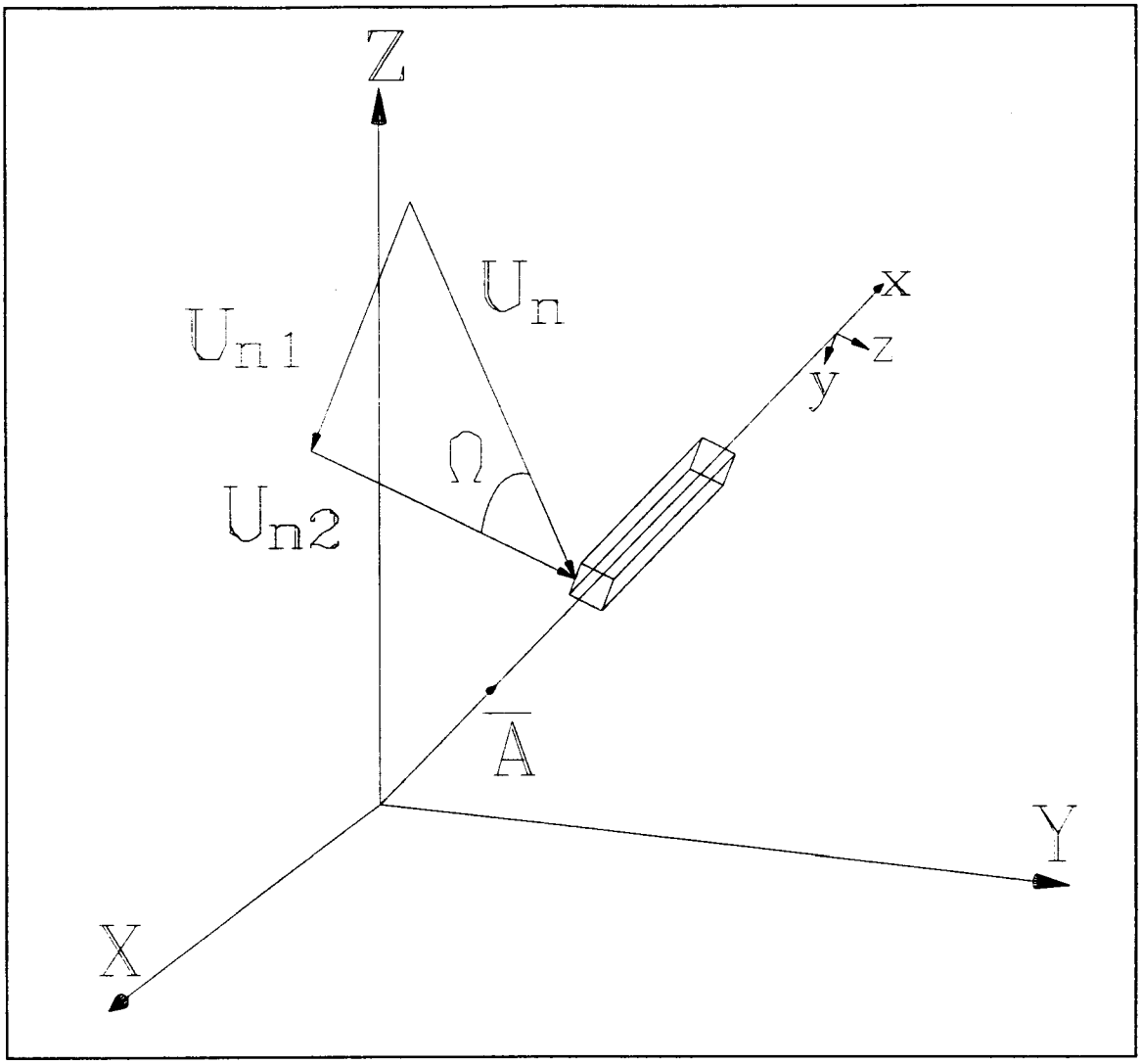

Figure 4: Definition sketch for angle of attack

Table 1: Angle of attack and Reynold's number dependent drag coefficients

Ω	$\mathbf{R_e}$	C_d
0°/90°	3.5×10^3	1.60
0°/90°	1×10^4	1.90
0°/90°	3×10^4	2.05
0°/90°	8×10^4	2.05
45°	2×10^4	1.60
45°	8×10^4	1.60

The coefficient of inertia, C_m, is obtained from the theoretically determined added mass coefficients reported by Blevins (1979). For a square cylinder the added mass coefficient for flow perpendicular to one face of the cylinder is:

$$C_a = 1.51 \quad C_m = C_a + 1 = 2.51 \tag{28}$$

Blevins (1979) also shows that since the section is symmetrical about both axes in the plane of the fluid normal acceleration (normal to the axis of the leg) that there are no cross-coupled added mass terms. In addition, the added mass for fluid normal acceleration at an arbitrary angle of attack (in the plane normal to the axis of the leg) is identical to the added mass for a zero angle of attack. The added masses for rotary acceleration about the axes of the leg and high-frequency ($f >> 1/T_{wave}$) forced vibrations are assumed to be negligible.

3.4 Slamming Forces

Slamming forces occur when a body penetrates a free surface. The forces arise due to the change in the added mass of the fluid which must be accelerated around the body thus causing a change in momentum. Prior to entering the fluid, the mass of the system is simply the mass of the body. As the body enters the fluid, the added mass changes from zero to a finite value. The added mass increases as the body penetrates the free surface. Even if the velocity is constant as the body enters the fluid, this creates a time-rate of change in the momentum of the system which results in a force. However, the velocity of the body is rarely a constant and is generally dependent on the slamming force. Therefore, this becomes a non-linear problem.

The result of a body entering a still fluid in a Lagrangian coordinate system is identical to the result for a fluid impinging upon a still body if examined in an Eulerian coordinate system based upon the position of the body. The problem of a wave impinging on a stationary body at or near the still water level is similar to the latter. However, a problem arises of creating a convenient coordinate system in which to express the slamming force problem. The slamming force is in the direction of the velocity of water particles on the free surface which is not necessarily conveniently expressed in either the body or global coordinate system.

To solve this problem, an intermediate coordinate system is created which is defined by the water particle velocities on the wave surface. Then the geometry of the sections cut through the legs of the unit is determined so that the slamming force problem can be solved in two dimensions. Thus it is necessary to determine the surface velocity

field which is done using the kinematic free surface boundary condition (KFSBC) of linear wave theory. The KFSBC is that the velocity of a particle on the free surface is equal to the velocity of the free surface. For linear wave theory (LWT) the KFSBC gives:

$$\dot{\eta} = \frac{\partial \eta}{\partial t} = w = -\frac{\partial \Phi}{\partial Z}|_{z=0} \tag{29}$$

Where Φ is the velocity potential in global coordinates. So the velocity at the surface is the time rate of change of the free surface level.

To determine the slamming force at each point along a leg, the leg is discretized into parallelogram sections whose plane is normal to the water surface plane (idealized as a plane since the length of the A-Jacks is small relative to the wave length). The axial centers of these parallelogram sections correspond to the points where the Morison's equation forces are calculated. The geometry of the sections to which the slamming force is applied is a function of the angle between leg and the outward water surface normal.

The geometry of the slamming sections is derived in Subsection 3.4.1. Then the slamming force is derived and distributed over the areas that it affects in Subsection 3.4.2. Finally, a limit to the slamming force, which can give unreasonably large forces, is defined.

3.4.1 Slamming Section Geometry

The geometry of the section of the body which is subject to slamming forces is dependent on the angles at which the water surface plane intersects the body. The

derivation of the geometry of the section follows Gasson (1983) and is developed for leg C. The axis of leg C is parallel to the z axis as shown in Figure 5a. Figure 5 shows leg C being intersected by the plane of the water surface. The water surface plane intersects the body coordinate x axis at the angle α and the y axis at the angle β. The quantities ε, $d3$, and $d4$ are the basis for the solution of the slamming force problem and, therefore, the objective of this geometric analysis.

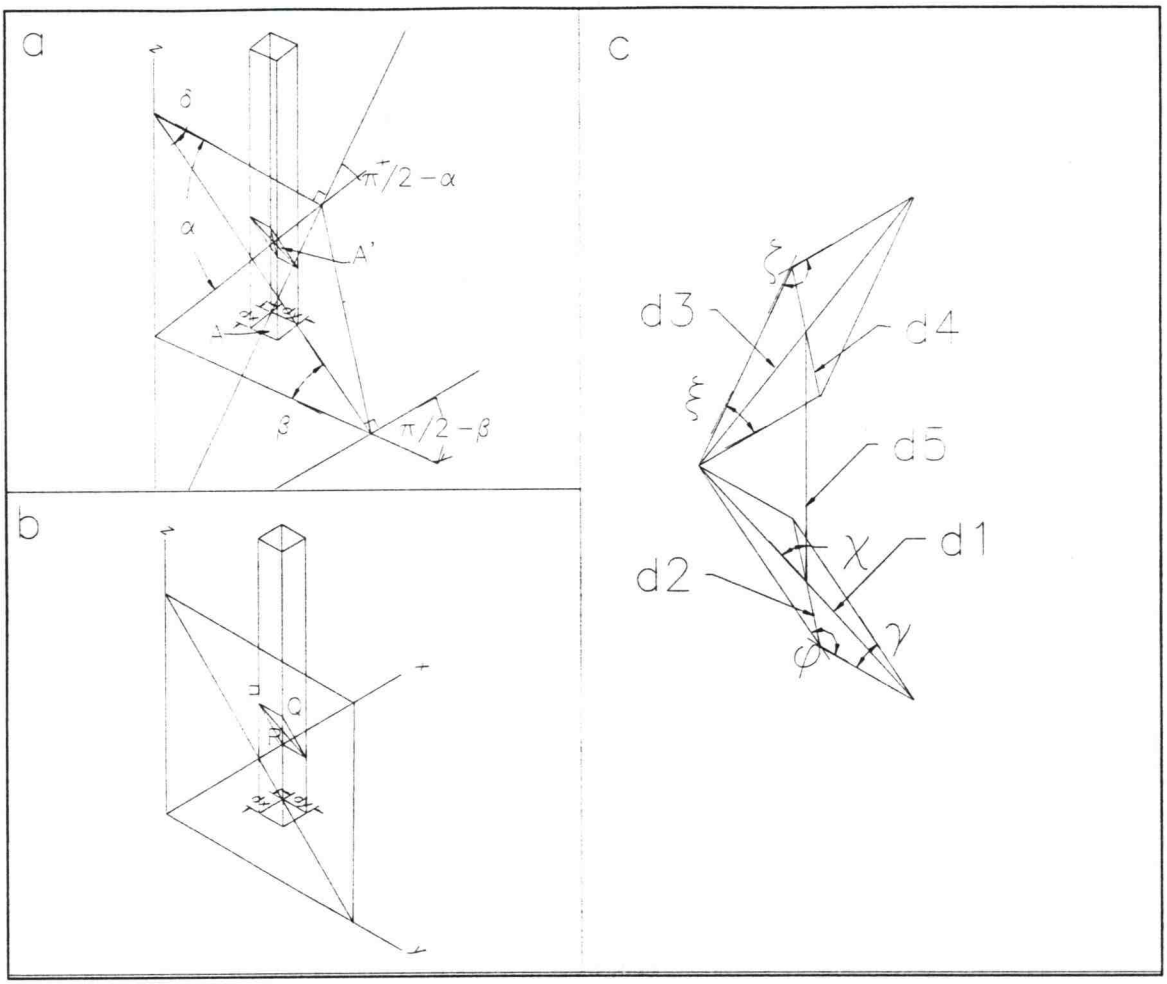

Figure 5: Definition sketches for the slamming section geometry. (a) Water surface plane intersection with body coordinate axes (b) Parallelogram defined by water plane intersection with body (c) Parallelogram created by water surface plane and plane normal to the water surface.

The cross-sectional area (in the *xy* plane), *A*, of the leg is:

$$A = dx \cdot dy = w^2 \tag{30}$$

where dx is the width of the leg in the x direction, dy is the width of the leg in the y direction, and w is the width of the leg. The lengths of segments $\overline{AB}$, $\overline{AC}$, and $\overline{BC}$, and the angles α and β are found by Pythagoreom's theorem and the law of sines to be:

$$\overline{AB} = \sqrt{\bar{a}^2 + \bar{b}^2} \quad \overline{AC} = \sqrt{\bar{a}^2 + \bar{c}^2} \quad \overline{BC} = \sqrt{\bar{b}^2 + \bar{c}^2} \tag{31}$$

$$\sin\alpha = \frac{\bar{c}}{\overline{AC}} = \frac{\bar{c}}{\sqrt{\bar{a}^2 + \bar{c}^2}} \quad \sin\beta = \frac{\bar{c}}{\overline{BC}} = \frac{\bar{c}}{\sqrt{\bar{b}^2 + \bar{c}^2}} \tag{32}$$

The third angle, δ, can then be determined by using the law of cosines, Pythagoreom's theorem, and Equations (31) and (32):

$$\begin{aligned} \overline{BA}^2 &= \overline{AC}^2 + \overline{BC}^2 - 2(\overline{AC})(\overline{BC})\cos\delta \\ (\bar{a}^2 + \bar{b}^2) &= (\bar{a}^2 + \bar{c}^2) + (\bar{b}^2 + \bar{c}^2) - 2\sqrt{\bar{a}^2 + \bar{c}^2}\sqrt{\bar{b}^2 + \bar{c}^2}\cos\delta \\ -2\bar{c}^2 &= -2\sqrt{\bar{a}^2 + \bar{c}^2}\sqrt{\bar{b}^2 + \bar{c}^2}\cos\delta \\ \cos\delta &= \frac{\bar{c}}{\sqrt{\bar{a}^2 + \bar{c}^2}}\frac{\bar{c}}{\sqrt{\bar{b}^2 + \bar{c}^2}} = \sin\alpha\sin\beta \end{aligned} \tag{33}$$

$$\begin{aligned} &\cos^2\delta + \sin^2\delta = 1 \\ &\delta = \sin^{-1}\left(\sqrt{1-\cos^2\delta}\right) = \sin^{-1}\left(\sqrt{1-\sin^2\alpha\sin^2\beta}\right) \end{aligned} \tag{34}$$

By the law of cosines, the length of the segments $|PQ|$ and $|PR|$ on the leg of interest are:

$$\begin{aligned} |PQ| &= \frac{dx}{\cos\alpha} = \frac{w}{\cos\alpha} \\ |PR| &= \frac{dx}{\cos\beta} = \frac{w}{\cos\beta} \end{aligned} \tag{35}$$

The angle γ is, by similar triangles, equal to the angle δ:

$$\gamma = \delta = \sin^{-1}\left(\sqrt{1-\sin^2\alpha\sin^2\beta}\right) \tag{36}$$

The area of the section cut through the leg by the water surface plane, A', is found using the equation for the area of a parallelogram (Gieck and Gieck, 1990) and Equations (35) and (36) to be:

$$A' = |PQ| \cdot |PR| \cdot \sin\gamma = \frac{w^2}{\cos\alpha\cos\beta}\sin\gamma = \frac{w^2}{\cos\alpha\cos\beta}\sqrt{1-\sin^2\alpha\sin^2\beta} \tag{37}$$

The other interior angle of the parallelogram can now be found, using the fact that the sum of interior angles in a parallelogram is equal to 2π, to be:

$$\phi = \pi - \gamma \tag{38}$$

The lengths $d1$ and $d2$ are found, using the formula for the major axis lengths of a parallelogram (Gieck and Gieck, 1990), to be:

$$d1 = \sqrt{\left(\overline{PQ} + h\cot\gamma\right)^2 + h^2} = \sqrt{\left(\frac{w}{\cos\alpha} + \frac{w}{\cos\beta}\sin\gamma\cot\gamma\right)^2 + \left(\frac{w}{\cos\beta}\right)^2\sin^2\gamma}$$

where $h = \overline{QR}\sin\gamma$

$$d1 = \frac{w}{\cos\alpha}\sqrt{(1+\cos\gamma)^2 + \sin^2\gamma} = \frac{w}{\cos\alpha}\sqrt{1+2\cos\gamma+\sin^2\gamma+\cos^2\gamma}$$

$$d1 = \frac{\sqrt{2}w}{\cos\alpha}\sqrt{1+\cos\gamma} = \frac{\sqrt{2}w}{\cos\alpha}\sqrt{1+\cos\left(\sin^{-1}\left(\sqrt{1-\sin^2\alpha\sin^2\beta}\right)\right)}$$

$$d2 = \sqrt{(\overline{PQ} - h\cot\gamma) + h^2}$$

$$d2 = \frac{\sqrt{2}w}{\cos\alpha}\sqrt{1-\cos\gamma} = \frac{\sqrt{2}w}{\cos\alpha}\sqrt{1-\cos\left(\sin^{-1}\left(\sqrt{1-\sin^2\alpha\sin^2\beta}\right)\right)}$$

(39)

and h is the minimum distance between segments $\overline{PQ}$ and $\overline{RS}$.

Now the geometry of the section cut by through the body by the water surface plane is defined; however, it is the geometry of the section cut through the body by a

plane orthogonal to the water surface plane that is of interest. The geometry of this orthogonal section is described in a similar manner. The orthogonal plane which cuts through the body is parallel to a plane which is orthogonal to the water surface plane and intersects the *xy* plane along the same line as the water surface plane. The parallel plane then forms an angle with the *y* axis in the *yz* plane of $(\pi/2-\beta)$ and an angle with the *x* axis in the *xz* plane of $(\pi/2-\alpha)$. The interior angles of a parallelogram cut by a plane through the leg orthogonal to the water surface plane can now be derived similar to the parallelogram cut through the leg by the water surface plane. In actuality, there are an infinite number of planes orthogonal to the water surface plane which transect the leg in the section where slamming forces may be present. However, all of the parallelograms thus formed are identical except for the location along the axis of the leg where they intercept the leg. Similar to Equations (36) and (38), the angles ξ and ζ are found to be:

$$\xi = \sin^{-1}\left(\sqrt{1-\sin^2(\tfrac{\pi}{2}-\alpha)\sin^2(\tfrac{\pi}{2}-\beta)}\right) = \sin^{-1}\left(\sqrt{1-\cos^2\alpha\cos^2\beta}\right) = \tan^{-1}\left(\frac{d4}{d3}\right) \tag{40}$$

$$\zeta = \pi - \xi$$

The lengths *d*3 and *d*4 can now be found in the same manner as Equation (39), yielding:

$$d3 = \frac{\sqrt{2}w}{\sin\alpha}\sqrt{1+\cos\xi} = \frac{\sqrt{2}w}{\sin\alpha}\sqrt{1+\cos\left(\sin^{-1}\left(\sqrt{1-\cos^2\alpha\cos^2\beta}\right)\right)}$$

$$d4 = \frac{\sqrt{2}w}{\sin\alpha}\sqrt{1-\cos\xi} = \frac{\sqrt{2}w}{\sin\alpha}\sqrt{1-\cos\left(\sin^{-1}\left(\sqrt{1-\cos^2\alpha\cos^2\beta}\right)\right)} \tag{41}$$

The length of the segment which joins the point where the water surface plane intersects the axis of the leg and the point where the plane orthogonal to the water surface plane intersects the axis of the leg is denoted by *d*5, which is:

$$d5 = \left(\frac{d1^2}{4} + \frac{d3^2}{4} \right)^{1/2} \tag{42}$$

Now the parallelogram cut by the plane orthogonal to the water surface plane has been fully described. However, this geometric analysis does not account for the angle of rotation about the centerline axis of the leg which would add a third degree of freedom to the system. The neglected rotation would result in a slamming section which is not symmetric about the water surface plane normal and, therefore, would require the use of a volume of fluid or other more advanced modeling technique for the slamming force. It should be noted though that the neglected rotation angle does not affect the shape of the slamming section, only the direction of its axis of symmetry.

3.4.2 Slamming Force Calculation

The slamming force created by a fluid impinging upon a body is estimated to be equal to the time rate of change of the momentum of the body. The following derivation follows the theory presented by von Karman (1929). A new coordinate system is adopted for the purposes of this derivation. This new coordinate system, referred to as the slamming section coordinate system, is intermediary in that it will not be utilized directly in the wave force model. The slamming section coordinate system is defined by the x'' and z'' axes as shown in Figure 6. The z″ axis is normal to the water surface plane, corresponding to the major axis of the parallelogram slamming section, and the x'' axis is parallel to the water surface plane, corresponding to the minor axis of the parallelogram slamming section. The origin of the slamming section coordinate system is located

where the plane of the section intersects the centerline axis of the leg which is also the intersection of the minor and major axes of the parallelogram.

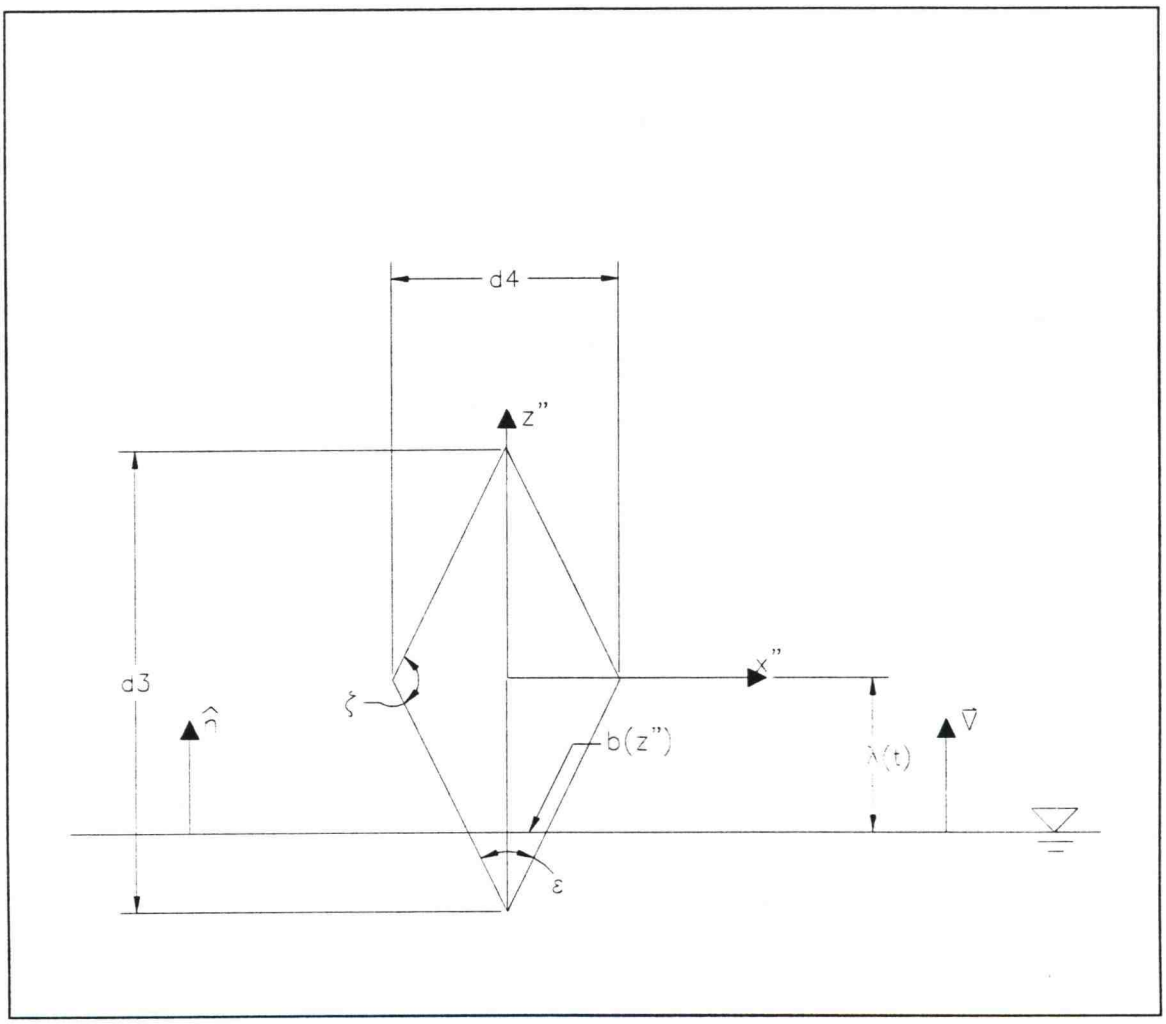

Figure 6: Slamming force calculation definition sketch.

The position of the water surface at time t is denoted $\lambda(t)$ in the slamming section coordinate system. The slamming force , f_{imp}, on a body is estimated as the time rate of change of the total momentum of the added mass of the body as it enters the fluid:

$$\vec{f}_{imp} = \vec{V}\frac{dm_a(t)}{dt} \tag{43}$$

$$\vec{V} = \frac{d\lambda(t)}{dt} = \dot{\eta}\cdot\hat{n} \tag{44}$$

where $\vec{V}$ is the vertical (+z" direction) velocity of the free surface, $\hat{n}$ is water surface normal unit vector, $\vec{f}_{imp}$ is the slamming force, and $m_a(t)$ is the added mass of the system at time t. The added mass is approximated as (von Karman, 1929):

$$m_a(t) = \frac{1}{2}\rho\pi[b(t)]^2 \tag{45}$$

where $b(t)$ is the half width of the waterline of the body at time t and ρ is the fluid density. Differentiating and applying the chain rule yields the magnitude of the slamming force:

$$f_{imp} = V\rho\pi b(t)\frac{db(t)}{dt} = V^2\rho\pi b(\lambda)\frac{db(\lambda)}{d\lambda} \tag{46}$$

where

$$b(\lambda) = \left(\lambda + \frac{d3}{2}\right)\tan\xi = \left(\lambda + \frac{d3}{2}\right)\frac{d4}{d3}$$

$$\frac{b(\lambda)}{d\lambda} = \tan\xi = \frac{d4}{d3} \tag{47}$$

The slamming force for the range of $-d3/2<\lambda<0$ is found to be:

$$\vec{f}_{imp} = \left[(\dot{\eta})^2\rho\pi\left(\lambda + \frac{d3}{2}\right)\left(\frac{d4}{d3}\right)^2\right]\hat{n} \tag{48}$$

A finite number of elements with the cross-sectional geometry described above each having a depth, or length normal to $d3$ and $d4$, of $d\ell$ are located within the region of the leg where the slamming force exists. The force, $d\vec{f}_{imp}$, acting on each of these slamming force coordinate system elements is:

$$d\vec{f}_{imp} = d\ell\left[(\dot{\eta})^2 \rho\pi\left(\lambda + \frac{d3}{2}\right)\left(\frac{d4}{d3}\right)^2\right]\hat{n} \tag{49}$$

The von Karman slamming force equation for the range of $0<\lambda<d3/2$ yields a force in the direction of the relative motion of the body or an "un-slamming" force. This theoretical force does not correspond to experimental observation and is therefore ignored. In other words, if $\frac{db}{dt} > 0$ then the slamming force exists; however, if $\frac{db}{dt} < 0$ then the slamming force does not exist.

The direction of the slamming force must also be defined. The vector $\hat{n}$ is a convenient basis for the slamming force coordinate system. This means that the force will only have one component, in the direction of $\hat{n}$; the force magnitude can then be treated as a scalar and multiplied by $\hat{n}$ to get the force vector in the appropriate coordinate system, thereby preventing the necessity for further coordinate transformations.

The slamming force exists for all elements along the leg which are partially submerged. Thus, any of an infinite number of planes orthogonal to the water surface plane can be defined in the slamming region. The slamming region, shown in Figure 7, is between the intersection of the water surface plane and the centerline axis of the leg (in parallelogram PQRS) and a point on the centerline axis of the leg a distance of $d5$

"above" this point. The slamming force can thus be calculated for any number of discrete elements whose major axis are normal to the water surface plane. Each of these elements has a depth, a third dimension, of length $d\ell$ as shown in Figure 8.

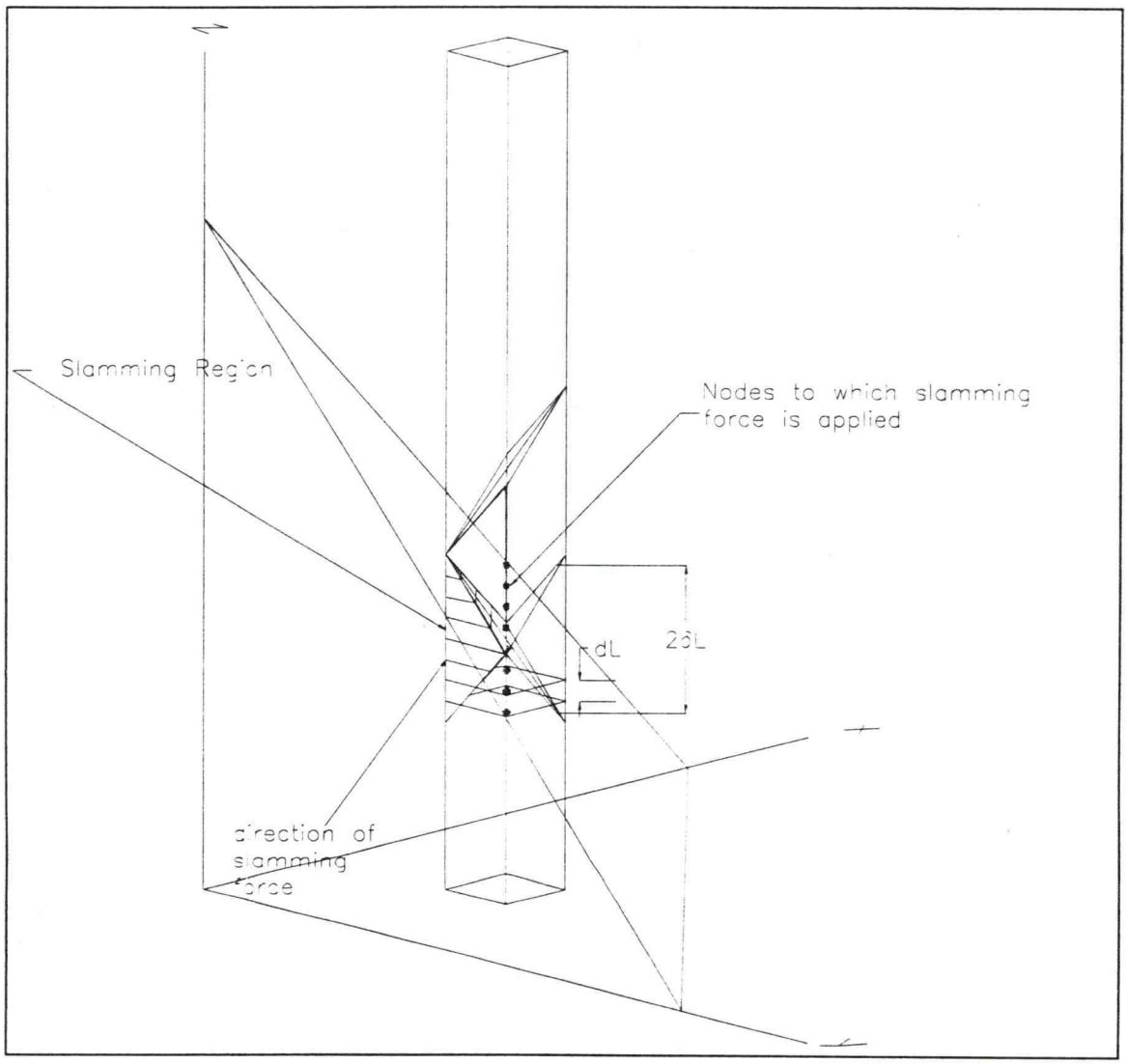

Figure 7: Slamming force region.

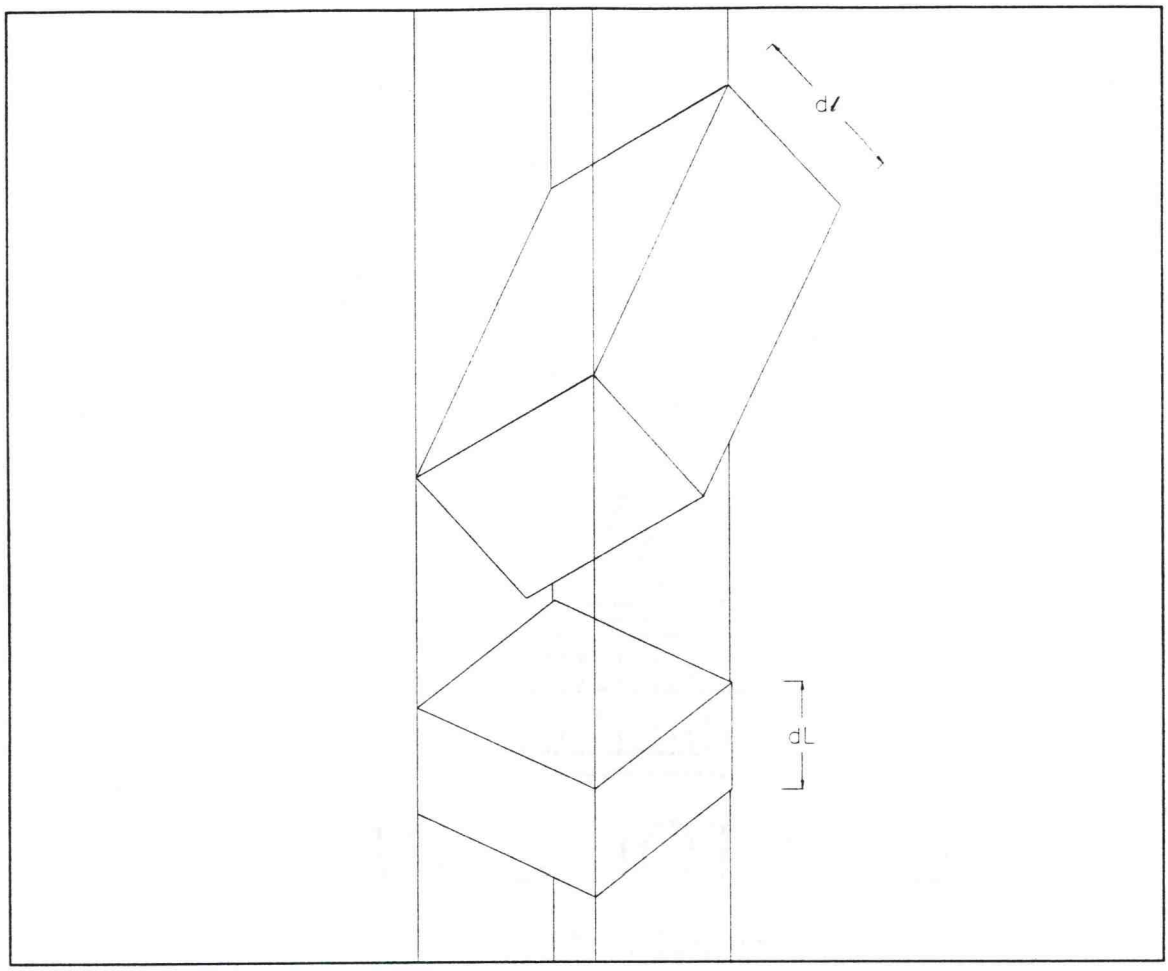

Figure 8: Definition sketch for $d\ell$ and dL.

The total slamming force on the leg is the sum of a finite number of slamming force sections each with length $d\ell$, but this causes the total slamming force to be a function of $d\ell$. Therefore, it is desired to integrate the slamming force with respect to ℓ to find the total slamming force on the leg and to eliminate the dependence on $d\ell$. Once the total slamming force is known it can be distributed among the discrete elements in the body coordinate system, of length dL, corresponding to the slamming region of the

leg. The force $d\vec{f}_{imp}$ is integrated over the length of the slamming section to yield the total slamming force:

$$\vec{F}_{imp} = \int_{SR} d\vec{f}_{imp} = \int_0^{d1/2} \vec{f}_{imp} d\ell \tag{50}$$

where *SR* is the region of the leg where slamming forces exist.

It can be seen from Figure 5 that the slamming force exists in the region of $0 < \ell < d1/2$. The ℓ dependence in $\vec{f}_{imp}$ (Equation (48)) arises in the $\left(\lambda + \frac{d3}{2}\right)$ term where the linear relationship between λ and ℓ is:

$$\lambda = \lambda(\ell)$$

$$\lambda(0) = -\frac{d3}{2} \quad \lambda(d1/2) = 0 \tag{51}$$

$$\lambda(\ell) = \frac{d3}{d1}\ell$$

$\vec{F}_{imp}$ is then found to be:

$$\vec{F}_{imp} = [(\dot{\eta})^2 \rho\pi\left(\frac{d4}{d3}\right)^2]\hat{n} \int_0^{d1/2} \frac{d3}{2}\left(\frac{2\ell}{d1} + 1\right) d\ell \tag{52}$$

Carrying out the integration yields the total slamming force:

$$\vec{F}_{imp} = \frac{3}{8}\frac{d4^2 \cdot d1}{d3}[(\dot{\eta})^2 \rho\pi]\hat{n} \tag{53}$$

The total slamming force can now be distributed over the discrete elements, of length *dL*, in the body coordinate system in the slamming force region of the leg. The central

element to which a slamming force applies is the element whose centerline axis node is at the water surface plane. The exterior elements, "upward" and "downward" from the water surface, to which the slamming force applies are located such that the forces act on the corners of these elements as seen in Figure 7.

Since slender body assumptions are being used, meaning that the forces are assumed to act on the centerline of the body not its surface, the forces are translated diagonally to the centerline nodes of these elements. The water surface plane normals passing through these corners intersect the centerline axis of the leg at a distance of $\pm d5$ from the water surface plane intersection with the centerline axis. However, the centerline axis nodes of the exterior elements to which the slamming force applies are located a distance of δL from the intersection as seen in Figure 7. The angle, χ, between $d1$ and $d5$ is:

$$\chi = \cos^{-1}\left(\frac{d1/2}{d5}\right) \tag{54}$$

The distance δL is found by to be:

$$\delta L = \frac{d1}{2}\cos\chi = \frac{d1^2}{4 \cdot d5} \tag{55}$$

The total slamming force is evenly distributed to the elements in the slamming region such that each element is subjected to the force $\bar{F}_n$:

$$\vec{F}_n = \frac{dL}{2\cdot\delta L}\frac{3}{8}\frac{d4^2\cdot d1}{d3}[(\dot{\eta})^2\rho\pi]\hat{n}$$

$$= dL\frac{6}{8}\frac{d4^2\cdot d5}{d1\cdot d3}[(\dot{\eta})^2\rho\pi]\hat{n} \qquad (56)$$

$$\text{for} \quad n = 1.2,3,...N \quad \text{where} \quad N = \frac{2\cdot\delta L}{dL}$$

In some cases the slamming force calculation yields unreasonably large forces. This occurs when the free surface hits an almost parallel surface yielding a near infinite force since the mass change occurs instantaneously. Therefore, it is desired to limit the maximum value of the slamming force. Sarpkaya and Isaacson (1981) define a slamming force coefficient, C_s, for a horizontal cylinder as:

$$C_s = \frac{2\left|\vec{F}_{imp}\right|}{\rho DL(U_m)^2} \qquad (57)$$

where D is the diameter of the cylinder, L is the length of the cylinder, and U_m is the maximum vertical water particle velocity at the free surface. Similarly for the slamming section outlined above, the diameter of the cylinder is replaced with the maximum width of the slamming section $d2$ and the length of the cylinder is replaced with the length of the slamming section $2\delta L$, yielding a slamming coefficient:

$$C_s = \frac{4\cdot d5\cdot\left|\vec{F}_{imp}\right|}{\rho\cdot d1^2\cdot d2\cdot(\dot{\eta})^2} \qquad (58)$$

Sarpkaya and Isaacson show that, for a circular cylinder with its axis parallel to the still water line, the maximum theoretical value of the slamming coefficient, based on a von Karman type slamming force analysis, is π. They also discuss experimental results

showing values for the slamming coefficient ranging from 1.88 to 5.11. Although the geometry differs, for the purpose of this model the slamming force coefficient is limited to a maximum value of $C_s=\pi$ yielding a maximum force per element of:

$$\vec{F}_n^{\max} = \frac{dL}{2 \cdot \delta L} \frac{d1^2 \cdot d2}{4 \cdot d5} \rho \pi (\dot{\eta})^2 \hat{n} = dL \frac{d2}{2} \rho \pi (\dot{\eta})^2 \hat{n} \tag{59}$$

3.5 Wave Force Model

The previous sections of this chapter have dealt with the theoretical development of the principles governing the forces on an A-Jacks unit. The numerical model developed uses these principles in the calculation of forces. This section discusses how these principles are implemented in the numerical model. The numerical model is coded and runs in the program MATLAB (version 5.2), distributed by MathWorks, Inc. The numerical model is composed of a number of modules: input, initial coordinate system transformations, wave mechanics, force calculations, rotational motion post-processing calculations, ancillary vector operations (i.e., dot and cross products, etc.), text output, fixed graphical output, and animated graphical output. The interaction of these modules is shown in Figure 9. This section describes the initial coordinate system transformations module **`geometry`**, the kinematics module **`stretchlwt`**, and the force calculations module **`morang`**. (In this and the following section program module names and variable names in these modules will be denoted in **`bold courier`** font.) The rotational motion module **`postrotate`** will be discussed in the next section.

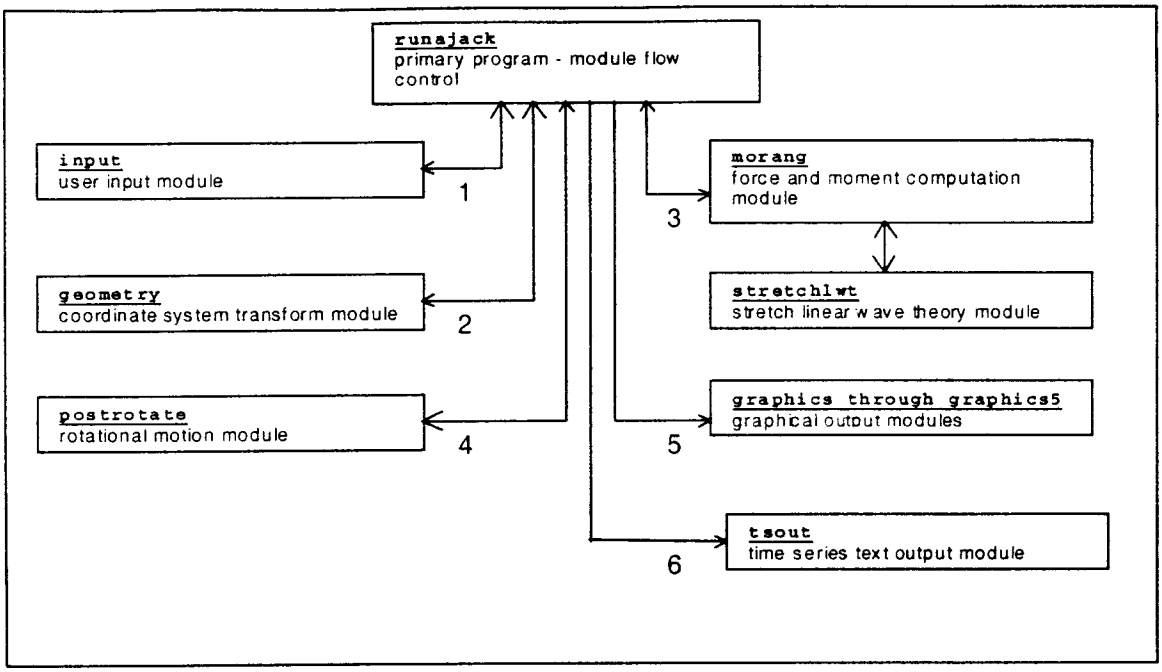

Figure 9: Flow diagram for modules of the numerical wave force model

The module **geometry** computes the transforms described in Section 3.1 and the parametric equations describing the centerline axes of the unit at rest in its initial condition. The module begins by calculating the variables **wavang**, **mu**, **theta**, and **phi**, which correspond to ψ, μ, θ, and ϕ, respectively, in Section 3.1 based on the user inputs of slope, unit rotation on the slope, and body geometry. The vectors **x**, **y**, and **z**, which correspond to $\vec{x}$, $\vec{y}$, and $\vec{z}$ in Equation (5), are calculated and used to form the rotational transformation matrix **L**, corresponding to $\mathbf{R}_1$ in Equation (6). The module **axrot** is used to perform Equation (7) and compute the rotational transformation matrix $\mathbf{R}_2$. The total rotational transformation matrix $\mathbf{R}_1\mathbf{R}_2^T$ used in Equation (14) is computed as the variable **Rg2b** (global to body coordinates transform) and its inverse or transpose, $\mathbf{R}_2\mathbf{R}_1^T$, is **Rb2g** (body to global coordinates transform). The translation matrix $\mathbf{C}_t$

described in Equation (13) is computed as the variable **Ct**. The unit vectors $\vec{a}$, $\vec{b}$, and $\vec{c}$ are defined by the variables **a**, **b**, and **c** and the endpoints of each leg are defined in body coordinates as **a0**, **b0**, **c0**, **a1**, **b1**, and **c1**. The total transformation described by Equation (14) is used to transform these endpoints to their global coordinate equivalents **A0**, **B0**, **C0**, **A1**, **B1**, and **C1** which are then used to define the global coordinate vectors **A**, **B**, and **C** and the corresponding unit vectors **eA**, **eB**, and **eC**. The parametric equations for each leg in global coordinates are described by 2×3 matrices with the beginning points in the first row and the unit vector components in the second. The parametric equations represent the vectors in the form (in global coordinates):

$$(X - X_0)\hat{i} + (Y - Y_0)\hat{j} + (Z - Z_0)\hat{k} = \kappa(A\hat{i} + B\hat{j} + C\hat{k}) \tag{60}$$

where X, Y, Z are the global coordinates of a point on the vector, X_0, Y_0, Z_0 are the global coordinates of the beginning point of the vector, A, B, C are the X, Y, and Z components of the vector, and κ is a parameter describing a points location on the vector.

The **stretchlwt** module computes the local wave length, water level, and the velocity and acceleration vectors using stretch linear wave theory described in Section 3.2. The local wave height, water depth, wave period, water density, gravitational constant, and X, Z, and t coordinates are input to the module. In addition, the local wave length is input. If the local wave length has not previously been computed, a value of zero is passed to the module and the wave length is calculated using the Pade approximations (Tedesco and McDougal, 1999). The water level, horizontal velocity amplitude, and the velocity and acceleration vectors are calculated by the appropriate equations for stretch linear wave theory given in Section 3.2.

The module **morang** computes the forces on the body. Much of the actual code of this module is not discussed here as the comments in the code provide more information on ancillary operations. This module computes the coordinates, in both the global and body systems, of each node where forces are to be calculated with the total number of nodes per leg, **N**, being a user input. Each leg is thus discretized into sections with widths (along the axis of the leg) of **dL**. The coordinates of these nodes are contained in the matrices **Am**, **Bm**, and **Cm** for global coordinates and **am**, **bm**, and **cm** for body coordinates with the first node being a distance of **dL**/2 from the beginning of the leg. The solution is also discretized in the time domain by dividing the wave period, **T**, into equal segments of length **dt**. The remaining computations described in this section occur for each time step.

To determine the slamming force and the portions of the body where it and the Morison's equation forces are applicable, it is necessary to determine what portion of the body is submerged. To do this, the water surface is idealized as an inclined plane defined with respect to the location of the A-Jacks. This is a reasonable assumption if the wave length is much longer than the length of the A-Jacks:

$$L >> D \tag{61}$$

To define this water surface plane, the instantaneous water surface elevation, η, is computed for the global X and Y coordinates of the endpoints of the unit **A1**, **B1**, and **C1**. This gives three points, **j**, **k**, and **l**, on the water surface from which two vectors, **jk** and **jl**, may be defined. Since the global X and Y coordinates of the three endpoints form an equilateral triangle, these two vectors cannot be collinear. The water surface

plane normal, **WSPN**, is defined in global coordinates by the cross product of these two vectors:

$$\mathbf{WSPN} = \mathbf{jk} \times \mathbf{jl} \tag{62}$$

The water surface plane itself is then described by a four element vector, the first three elements of which are the components of the water surface plane normal (*D*, *E*, and *F*) and the last element being:

$$G = Dx_0 + Ey_0 + Fz_0 \tag{63}$$

where *D* is the *X* component of the water surface plane normal (not the length of a leg of the unit), *E* is the *Y* component of the water surface plane normal, *F* is the Z component of the water surface plane normal, x_0 is the *X* coordinate of **A1**, **B1**, or **C1**, y_0 is the *Y* coordinate of **A1**, **B1**, or **C1**, z_0 is the *Z* coordinate of a point on the water surface plane corresponding to the water surface elevation at the *X* and *Y* coordinates of **A1**, **B1**, or **C1**, and *G* is the parameter describing the location of the plane. The parametric equation for the plane is:

$$DX + EY + FZ = G \tag{64}$$

Thus, for each leg the intersection of the centerline axis of the leg and the water surface plane can be located by equating the parametric equations of the plane and the vector (Equations (60) and (64)):

$$\begin{aligned} &D(X_0 + \kappa A) + E(Y_0 + \kappa B) + F(Z_0 + \kappa C) = G \\ &\kappa = \frac{G - (DX_0 + EY_0 + FZ_0)}{DA + EB + FC} \\ &I = (\kappa A + X_0)\hat{i} + (\kappa B + Y_0)\hat{j} + (\kappa C + Z_0)\hat{k} \end{aligned} \tag{65}$$

where I is the location of the intersection of the centerline axis of the leg and the water surface plane (not the mass moment of inertia in this case) and κ is a parameter quantified by solving the expression for κ.

It is now possible to begin computing forces at each node on each of the three legs. The remaining computations are performed for each node on each leg which is below the water surface plane. To assure that forces are not calculated for nodes above the water surface plane (with the exception of slamming forces which will be discussed later), the number of nodes below the water surface plane, **n**, are calculated for each leg as (using leg A as an example):

$$\mathbf{n} = \frac{\mathbf{I} - \mathbf{A0}}{\mathbf{dL}} \tag{66}$$

If **n** is not an integer it is rounded upward to the nearest integer. The Morison's equation forces are then computed for nodes 1 through **n** of each leg.

Morison's equation is used to compute the forces at each submerged node of each leg. The computations are carried out in the body coordinate system. First, the fluid velocity and acceleration, **U** and **A**, at the node are found using the module **stretchlwt**. These vectors are then converted to their body coordinate equivalents, **ub** and **ab**, by multiplying by the rotational transformation matrices **Rg2b**. The normal fluid velocity and accelerations in body coordinates, **un** and **an**, are computed using Equation (21). The magnitude of the normal velocity vector, $\left|\vec{U}_n\right|$, is computed according to Equation (22) using the module **vdot** to perform the vector dot product. $\left|\vec{U}_n\right|$ is used to compute $\mathbf{R_e}$ (**Re**) and **KC** (**KC**) according to Equation (26). The orthogonal components of the normal velocity vector, **un1** and **un2**, are determined using the

modules **vparcomp**, **vprpcomp**, and **vlength**. The angle of attack, Ω in Equation (37), is computed and assigned to the variable name **omega**. The drag coefficient, **Cd**, is found using the values of **Re** and **omega** to linearly interpolate a value from the values shown in Table 1.

The Morison's equation forces described by Equations (19) and (20) can now be computed. The forces are broken into the inertia and drag components and, in addition to Equations (19) and (20), the buoyancy force on each section is calculated. The drag force for each section, **fmd**, is found using the first term on the right hand side of Equation (19) and, if the section is an end element, Equation (20). The inertia force, **fmi**, on each section is computed using the first term on the right hand side of Equation (19). The buoyancy force, **fmf**, on each section is equal to the weight of the displaced fluid of the section:

$$\mathbf{fmf} = \rho g w^2 dL \tag{67}$$

The total Morison's equation forces on each element of each leg, **fma**, **fmb**, and **fmc**, respectively for legs A, B, and C, are taken to be the sum of the drag, inertia, and buoyancy components (using leg A as an example):

$$\mathbf{fma} = \mathbf{fmd} + \mathbf{fmi} + \mathbf{fmf} + \mathbf{fqs} \tag{68}$$

where **fma** is a 3×N matrix of force components at each element in body coordinates and **fqs** is the slamming force (discussed in the next paragraph).

The slamming forces, **fqs**, on each section of the body where they are applicable, are calculated next. First, the intersection angles between the legs and the water surface plane are calculated, and then the lengths $d1$ through $d5$ are calculated using Equations

(40), (41), and (42). The segments to which the slamming force is to be applied are shown in Figure 7. The velocity of the free surface in the body coordinate system is calculated by Equation (44). Equation (56) is used to calculate the slamming force on each segment, and the slamming coefficient, **CS**, is calculated using Equation (58). Where the slamming coefficient exceeds π, the slamming force on each segment is calculated using equation (59).

The total force on each leg, **Fa**, **Fb**, and **Fc** for legs A,B, and C, respectively, is found by summing the components of force for each element in the matrices **fma**, **fmb**, and **fmc**. The total moments about the centroid of the unit, **Ma**, **Mb**, and **Mc** for legs A, B, and C, respectively, created by the forces on each section are computed as (using leg A as an example):

$$\mathbf{Ma} = \sum_{1}^{N} \mathbf{fma}_n \cdot \mathbf{am}_n \tag{69}$$

where $\mathbf{fma}_n$ is the n^{th} force component triad of the matrix **fma** (i.e., the force on the n^{th} section) and $\mathbf{am}_n$ is the n^{th} coordinate triad of the matrix **am** (i.e., the coordinates of the n^{th} node). The total force on the unit, **F**, and the total moment about the centroid of the unit, **M**, (in body coordinates) are taken as the sum of the force and moment components from each leg:

$$\begin{aligned} \mathbf{F} &= \mathbf{Fa} + \mathbf{Fb} + \mathbf{Fc} \\ \mathbf{M} &= \mathbf{Ma} + \mathbf{Mb} + \mathbf{Mc} \end{aligned} \tag{70}$$

The body coordinate system forces and moments are converted to their global coordinate system equivalents by multiplying by the matrices **Rb2g**.

3.6 Rotational Motion About Base Axes

The rotational motion of an A-Jacks unit about the base axes upon which it rests is also numerically modeled. The moment about the centroid of the unit has been described in the previous section. The force and moment at the centroid of the unit are used to determine the moment about the base axes using statics. Knowing the moment about the base axes, the rotation about that axis obeys the general second order ordinary differential equation:

$$I\ddot{\theta} + C(\dot{\theta})\dot{\theta} + K(\theta)\theta = M(t) \tag{71}$$

where θ is the rotation about the base axis, $\dot{\theta} = {d\theta}/{dt}$ is the angular velocity about the axis of rotation, $\ddot{\theta} = {d^2\theta}/{dt^2}$ is the angular acceleration about the axis of rotation, I is the mass moment of inertia of the body about the axis of rotation, $C(\dot{\theta})$ is viscous damping, $K(\theta)$ is the rotational stiffness of the body about the axis of rotation, and $M(t)$ is the moment about the axis of rotation.

The solution of this differential equation will be discussed in this section beginning with a brief discussion on the definition of the base axes and the derivation of the mass moments of inertia about those axes. Next the moments about the base axes are derived and the rotational stiffness discussed. Finally, the differential equation is solved by numerical integration using the 4th order Runge-Kutta technique assuming small rotations.

The first task before solving for the rotational motion of the unit is to describe the base axes about which the unit may rotate. Three base axes are defined by the vectors between the contact points of the legs with the subgrade. The rotation points are the corners of the unit adjacent to the leg endpoints, not the endpoints themselves which are located along the centerlines of the legs and thus slightly above the plane on which the unit sits. The directions of the vectors are defined such that positive moments about the axes tend to produce a rotation for a unit at rest. The three base axes (defined in the body coordinate system), $\overrightarrow{a0b0}$, $\overrightarrow{c0a0}$, and $\overrightarrow{b0c0}$, are shown in Figure 10. The vector equations and coordinates of the rotation points, in the body coordinate system, are:

Leg Endpoint	**Adjacent Rotation Point**	**Axes Vector Directions**
$a0$	$\left(-\frac{D}{2},-\frac{D}{13},-\frac{D}{13}\right)$	$dir\left(\overrightarrow{a0b0}\right)=\frac{1}{\sqrt{2}}\hat{i}-\frac{1}{\sqrt{2}}\hat{j}$
$b0$	$\left(-\frac{D}{13},-\frac{D}{2},-\frac{D}{13}\right)$	$dir\left(\overrightarrow{c0a0}\right)=-\frac{1}{\sqrt{2}}\hat{i}+\frac{1}{\sqrt{2}}\hat{k}$
$c0$	$\left(-\frac{D}{13},-\frac{D}{13},-\frac{D}{2}\right)$	$dir\left(\overrightarrow{b0c0}\right)=\frac{1}{\sqrt{2}}\hat{j}-\frac{1}{\sqrt{2}}\hat{k}$

(72)

where *dir*( ) is the vector direction of the argument (the vector direction has a unit length). It is also necessary to determine the distance from the base axes to the unit centroid. The minimum distances from the base axes to the centroid are found to be from the mid-points of the base axes to the unit centroid, forming vectors orthogonal to the base axes. The coordinates of these mid-points and the vectors between the mid-points and the unit centroid are found to be:

Mid - Point Coordiante **Vector from Mid - Point to Centroid**

$$
\begin{aligned}
mid\left(\overrightarrow{a0b0}\right) &= \left(-\frac{15D}{52}, -\frac{15D}{52}, -\frac{D}{13}\right) & \overrightarrow{a0b0 \cdot \mathbf{C}_t} &= \frac{15D}{52}\hat{i} + \frac{15D}{52}\hat{j} + \frac{D}{13}\hat{k} \\
mid\left(\overrightarrow{c0a0}\right) &= \left(-\frac{15D}{52}, -\frac{D}{13}, -\frac{15D}{52}\right) & \overrightarrow{c0a0 \cdot \mathbf{C}_t} &= \frac{15D}{52}\hat{i} + \frac{D}{13}\hat{j} + \frac{15D}{52}\hat{k} \\
mid\left(\overrightarrow{b0c0}\right) &= \left(-\frac{D}{13}, -\frac{15D}{52}, -\frac{15D}{52}\right) & \overrightarrow{b0c0 \cdot \mathbf{C}_t} &= \frac{D}{13}\hat{i} + \frac{15D}{52}\hat{j} + \frac{15D}{52}\hat{k}
\end{aligned}
\tag{73}
$$

where *mid*( ) is the mid-point of the rotation axis. Finally, the length of the vectors from the mid-points of the axes to the centroid is $\sqrt{\frac{266}{16}}\left(\frac{D}{13}\right)$.

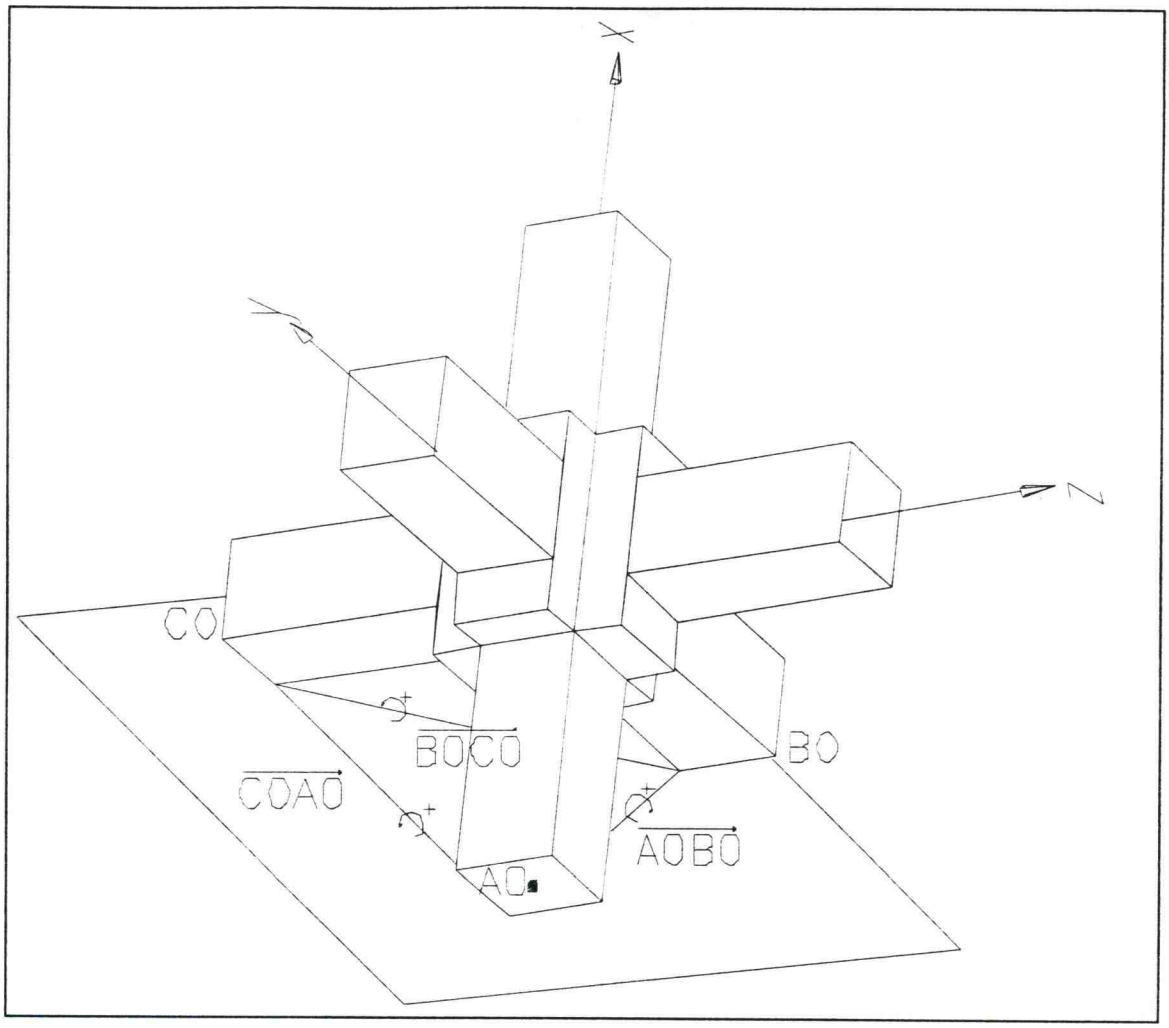

Figure 10: Unit rotation definition sketch.

Next it is necessary to determine the moments of inertia about the base axes. First, the mass moments of inertia were determined for rotation about the major axes of the unit (e.g., the body coordinate system axes). This was accomplished by dividing the unit into four axisymmetric regions comprised of rectangular prisms. Then the mass moments of inertia about the major axes were determined using the mass moment of inertia of each rectangular prism about its centroid and Steiner's parallel axis theorem

(Gieck and Gieck, 1990) to transfer this to the desired axis. The resulting mass moments of inertia about the major axes are:

$$I_{xx} = 1566\rho_u\left(\frac{D}{13}\right)^5$$

$$I_{yy} = 1582\rho_u\left(\frac{D}{13}\right)^5 \tag{74}$$

$$I_{zz} = 1582\rho_u\left(\frac{D}{13}\right)^5$$

where ρ_u is the density of the A-Jacks material (typically concrete). The mass, m_u, weight, W, and buoyant weight, W_b, of the unit were also determined during this analysis to be:

$$m_u = 156\rho_u\left(\frac{D}{13}\right)^3 \cong 0.071\cdot\rho_u D^3$$

$$W = 156\rho_u g\left(\frac{D}{13}\right)^3 \cong 0.071\cdot\rho_u g D^3 \tag{75}$$

$$W_b = 156(\rho_u - \rho)g\left(\frac{D}{13}\right)^3 \cong 0.071\cdot(\rho_u - \rho)gD^3$$

Next, the mass moments of inertia about axes parallel to the base axes passing the centroid of the unit were determined. Again, Steiner's parallel axis theorem was used to transfer these moments of inertia to the base axes. The mass moments of inertia about the base axes were thus found to be:

$$I_{a0b0} = 3030 \cdot \rho_u \left(\frac{D}{13}\right)^5$$

$$I_{c0a0} = 3030 \cdot \rho_u \left(\frac{D}{13}\right)^5 \tag{76}$$

$$I_{b0c0} = 3038 \cdot \rho_u \left(\frac{D}{13}\right)^5$$

Now that the base axes have been defined, the moment about these axes can be determined using statics. The force and moment about a base axis of the unit, $\vec{F}^*$ and $\vec{M}^*$ respectively, are determined from the force, moment, and weight at the centroid of the unit, $\vec{F}$, $\vec{M}$, and $\vec{W}$ respectively, using a force-moment couple. (Note that the force and moment about the centroid already accounts for buoyancy.) The following derivation of this force-moment couple is carried out for the base axis $\overrightarrow{a0b0}$. The sum of forces at the mid-point of axis $\overrightarrow{a0b0}$ gives the relationship:

$$\sum F = 0$$

$$\vec{F} + \vec{W} + \vec{F}^* = 0 \tag{77}$$

$$\vec{F}^* = -\left(\vec{F} + \vec{W}\right)$$

where

$$\vec{W} = \begin{bmatrix} 0 & 0 & -W \end{bmatrix} \cdot \mathbf{Rg2b} \tag{78}$$

where $\vec{W}$ is the unit weight vector in the body coordinate system. The sum of moments about the mid-point of axis $\overrightarrow{a0b0}$ gives:

$$\sum M = 0$$

$$\vec{M} + \left(\vec{F} + \vec{W}\right) \times \overrightarrow{a0b0 \cdot \mathbf{C}_t} + \vec{M}' = 0 \tag{79}$$

$$\vec{M}' = -\vec{M} - \left(\vec{F} + \vec{W}\right) \times \overrightarrow{a0b0 \cdot \mathbf{C}_t}$$

where $\vec{M}'$ is the moment about the mid-point of axis $\overrightarrow{a0b0}$. The component of $\vec{M}'$ parallel to axis $\overrightarrow{a0b0}$ caused by hydrodynamic forcing and the righting moment due to the unit weight is desired; therefore, the moment about the base axis $\overrightarrow{a0b0}$ due to hydrodynamic forcing $\vec{M}^*_{a0b0}$, is:

$$\vec{M}^*_{a0b0} = -\left(\vec{M}' + \left(\left(\vec{F} + \vec{W}\right) \times \overrightarrow{a0b0 \cdot \mathbf{C}_t}\right)\right) \bullet \left(dir\left(\overrightarrow{a0b0}\right)\right) \tag{80}$$

When $\vec{M}^*_{a0b0}$ exceeds zero the unit will tend to rotate about the axis. When $\vec{M}^*_{a0b0}$ is less than zero the unit will either tend to return to its resting position if already in motion, or stay in its resting postion if resting. The moments about the three base axes are then:

$$\begin{aligned}
\vec{M}^*_{a0b0} &= -\left[\vec{M} + \left(\left(\vec{F} + \vec{W}\right) \times \left(\frac{15D}{52}\hat{i} + \frac{15D}{52}\hat{j} + \frac{D}{13}\hat{k}\right)\right)\right] \bullet \left(\frac{1}{\sqrt{2}}\hat{i} - \frac{1}{\sqrt{2}}\hat{j}\right) \\
\vec{M}^*_{c0a0} &= -\left[\vec{M} + \left(\left(\vec{F} + \vec{W}\right) \times \left(\frac{15D}{52}\hat{i} + \frac{D}{13}\hat{j} + \frac{15D}{52}\hat{k}\right)\right)\right] \bullet \left(-\frac{1}{\sqrt{2}}\hat{i} + \frac{1}{\sqrt{2}}\hat{k}\right) \\
\vec{M}^*_{b0c0} &= -\left[\vec{M} + \left(\left(\vec{F} + \vec{W}\right) \times \left(\frac{D}{13}\hat{i} + \frac{15D}{52}\hat{j} + \frac{15D}{52}\hat{k}\right)\right)\right] \bullet \left(\frac{1}{\sqrt{2}}\hat{j} - \frac{1}{\sqrt{2}}\hat{k}\right)
\end{aligned} \tag{81}$$

All three of the base axes moments are defined such that a positive moment will cause the initiation of rotation about that axis for a unit at rest on all three axes.

The rotational stiffness, K, is also needed to solve the differential equation. The rotational stiffness accounts for the resistance to rotation which is proportional to the rotation angle. In this case, the stiffness is caused by the weight of the unit tending to return it to its resting postion. Summing the moments for rotation about axis $\overrightarrow{a0b0}$, for example, gives:

$$I_{a0b0}\ddot{\theta}_{a0b0} = \vec{\ell}\times\vec{W}_n + M = W_n \ell \sin\gamma + M \tag{82}$$

where $\vec{W}_n$ is the component of the weight vector normal to the axis of rotation, $\vec{\ell}$ is the vector from the mid-point of the rotation axis to the unit centroid, and γ is the angle between $\vec{\ell}$ and $\vec{W}_n$.

$$\vec{W}_n = \vec{W} - \left(\vec{W} \bullet dir\left(\overrightarrow{a0b0}\right)\right) dir\left(\overrightarrow{a0b0}\right) \tag{83}$$

The angle γ is the sum of the angle between $\vec{\ell}$ and $\vec{W}_n$ at rest, γ_0, and the rotation about the axis, θ_{a0b0}, which is assumed to be small:

$$\gamma = \gamma_0 - \theta_{a0b0}$$

$$\sin\gamma = \sin(\gamma_0 - \theta_{a0b0}) = \sin\gamma_0 \cos\theta_{a0b0} - \cos\gamma_0 \sin\theta_{a0b0} \tag{84}$$

$$\sin\gamma \equiv \sin\gamma_0 - \theta_{a0b0}\cos\gamma_0 \quad \text{for } \theta_{a0b0} << \frac{\pi}{2}$$

The angle γ_0 is found from the cross product for the righting moment of the unit in its resting position:

$$\gamma_0 = \sin^{-1}\left[\frac{\vec{\ell}\times\vec{W}_n}{W_n \ell dir\left(\overrightarrow{a0b0}\right)}\right] \tag{85}$$

Now the equation of motion for the unit can be written:

$$I_{a0b0}\ddot{\theta}_{a0b0} + W_n \ell \cos\gamma_0 \theta_{a0b0} = M + W_n \ell \sin\gamma_0 = M^*_{a0b0} \tag{86}$$

Therefore, it is shown that the stiffness for the rotational motion is:

$$K = W_n \ell \cos\gamma_0 \tag{87}$$

(The buoyancy of the unit is accounted for in the moment caused by hydrodynamic forcing.) If the assumption is made that the angle of rotation about the axis, θ, is small, then **Rg2b** and K can be considered constant. Otherwise, **Rg2b** and K are functions of the rotation angle θ.

It is now possible to consider the solution of the differential equation. The specific differential equation to be solved is, using axis $\overrightarrow{a0b0}$ as an example:

$$\ddot{\theta}_{a0b0} + \frac{C\left(\dot{\theta}_{a0b0}\right)}{I_{a0b0}}\dot{\theta}_{a0b0} + \frac{K\left(\theta_{a0b0}\right)}{I_{a0b0}}\theta_{a0b0} = \frac{\vec{M}^*_{a0b0}(t)}{I_{a0b0}} \tag{88}$$

The differential equation is integrated using the 4th order Runge-Kutta technique. The solution is carried out using the values of $\vec{M}^*_{a0b0}$ found by assuming negligible rotation about the base axis and neglecting relative motion caused by the rotation. Thus, K is a constant and C=0. In this method, the differential equation is solved after $\vec{M}^*_{a0b0}$ has been determined and, thus, is referred to as post-integrating. The second order differential equation for rotation about axis $\overrightarrow{a0b0}$ can be written as a system of two first order differential equations:

$$y_1 = \theta_{a0b0}$$

$$y_2 = \dot{\theta}_{a0b0}$$

$$\frac{dy_1}{dt} = y_2 \tag{89}$$

$$\frac{dy_2}{dt} = -\frac{K}{I_{a0b0}} y_1 + \frac{\bar{M}^*_{a0b0}}{I_{a0b0}}$$

These first order differential equations can then be solved at the $t_{n+1} = t_n + \Delta t$ time level using the 4th order Runge-Kutta numerical integration technique shown here for a general function $f(t, y)$ (Hoffman, 1992):

$$y_{n+1} = y_n + \frac{1}{6}(\Delta y_1 + 2\Delta y_2 + 2\Delta y_3 + \Delta y_4) + O(\Delta t^4)$$

$$\Delta y_1 = \Delta t \cdot f(t_n, y_n)$$

$$\Delta y_2 = \Delta t \cdot f\left(t_n + \frac{\Delta t}{2}, y_n + \frac{\Delta y_1}{2}\right) \tag{89}$$

$$\Delta y_3 = \Delta t \cdot f\left(t_n + \frac{\Delta t}{2}, y_n + \frac{\Delta y_2}{2}\right)$$

$$\Delta y_4 = \Delta t \cdot f(t_n + \Delta t, y_n + \Delta y_3)$$

This method carries the advantages of a higher order integration method (more accuracy for larger time steps), but does not include relative motion viscous and assume small rotation angles. Since the unit may rotate about only one axis at a time, the appropriate axis of rotation must be chosen. The integration is carried out for the rotation axis which first experiences a moment tending to cause rotation. In most cases moments

tending to cause rotation only occur about one axis. The program module **postrotate** carries out the integration of the differential equation.

4. NUMERICAL MODEL RESULTS

The numerical model was executed for many different conditions to determine under what discretization conditions the model converged. Algorithms were also developed to graphically represent the wave forces and rotational responses. Finally, approximately five thousand cases were analyzed using the numerical model, and the resulting maximum wave forces were investigated to determine simplified expressions for the maximum wave force on a unit.

4.1 Numerical Convergence

To accurately and efficiently run the numerical model, the minimum number of steps in the time and space domains which provides accurate model results must be determined. However, since no analytical solution to the wave force problem or direct physical measurements of wave forces on single armor units are available, determining the minimum number of time and space steps required for the numerical model to converge to a known answer was not possible. Also, since no set of partial differential equations was being solved based on series approximation (such as is done in finite difference methods) determining the step sizes required for convergence could not be performed theoretically either. In fact, the convergence of the numerical model is conceptually better related to a problem of minimum sample spacing required for a certain level of accuracy in a physical experiment (particularly in the time domain). Therefore, model results at different step sizes were compared to results for very small

step sizes to determine under what discretization patterns the model was reasonably convergent to the high resolution set of force predictions.

To determine the minimum number of time and space steps required for reasonably accurate force predictions, the model was run at a series of different space and time steps. The resulting force predictions from these runs was then compared to the force predictions for the highest number of both time and space steps. The difference between the predicted forces for each combination of space and time steps and the predicted forces at the maximum number of space and time steps were normalized by the predicted forces at the maximum number of space and time steps to put the difference in terms of a relative error. Due to the large range of the results, the logarithm (base 10) of the absolute value of the relative error is examined. For example, if for a certain time and space step case a relative error of 10^{-4} was reported, this would indicate a 0.01% difference between this time and space step case and the high resolution case. This procedure was done for a 2 ft. A-Jacks unit in wave conditions which produce an inertia dominated force, a 2 ft. wave with a period of 4 s in 10 ft. water depth with a centroid depth of 4 ft., and for an 8 ft. unit in conditions which produce a drag dominated force, a 4 ft. wave with a period of 12 s in 20 ft. water depth with a centroid depth of 16 ft. For both of these cases, the maximum force magnitude, the integral of the force magnitude over the wave period normalized by the wave period, and the maximum moment magnitude about the unit centroid were analyzed in this manner. Figures 11 through 16 show the results of these tests. In each figure the relative error is indicated by elevation and color versus the number of spatial steps along each leg, *D/dL*, and the number of temporal steps in each wave period, *T/dt*; contours of equal relative error, values

indicated by contour color, are also shown versus the spatial and temporal steps. The relative error values have been linearly interpolated between data points for readability.

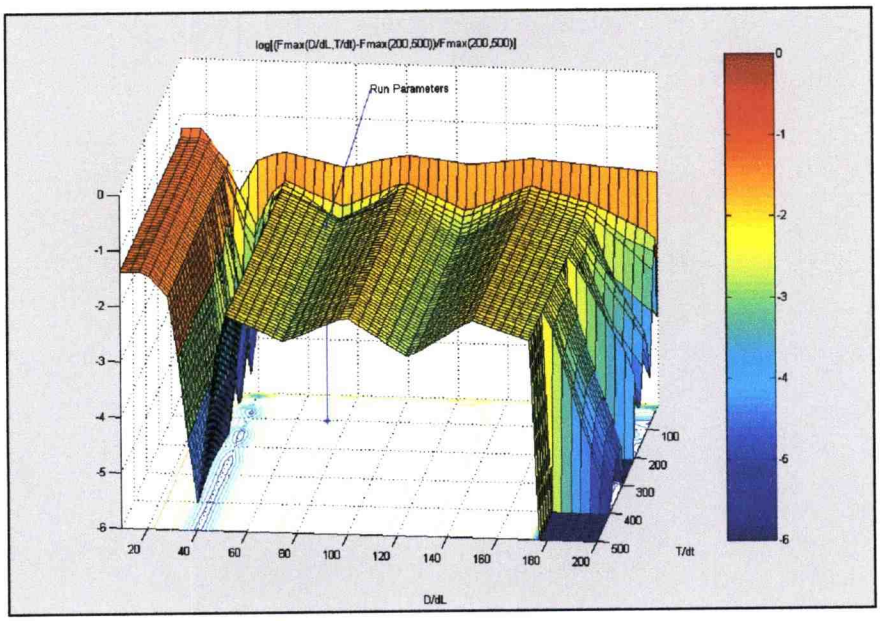

Figure 11: Numerical convergence of the maximum force magnitude for a 2 ft., 4 s wave.

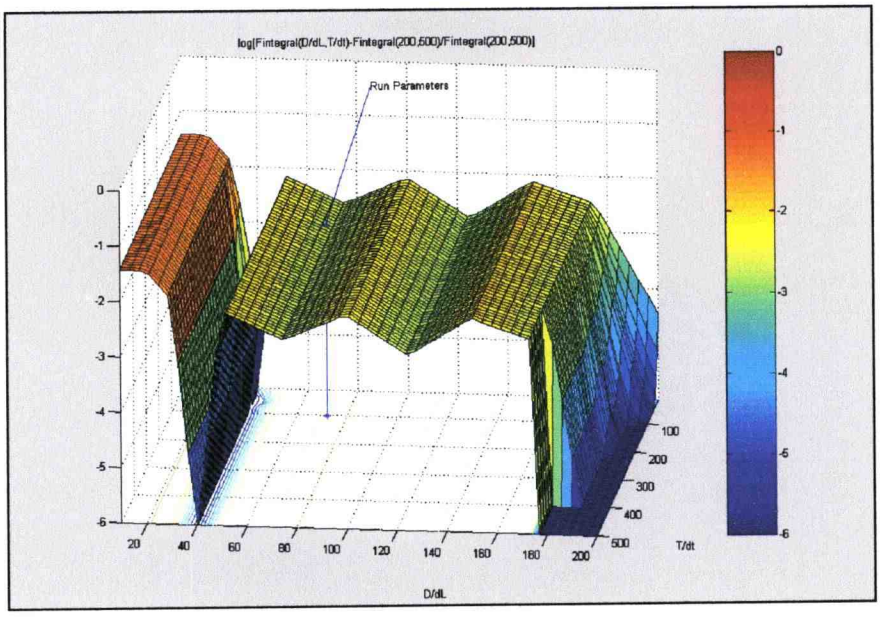

Figure 12: Numerical convergence of the integral of the force over one wave period normalized by the wave period for a 2 ft., 4 s wave.

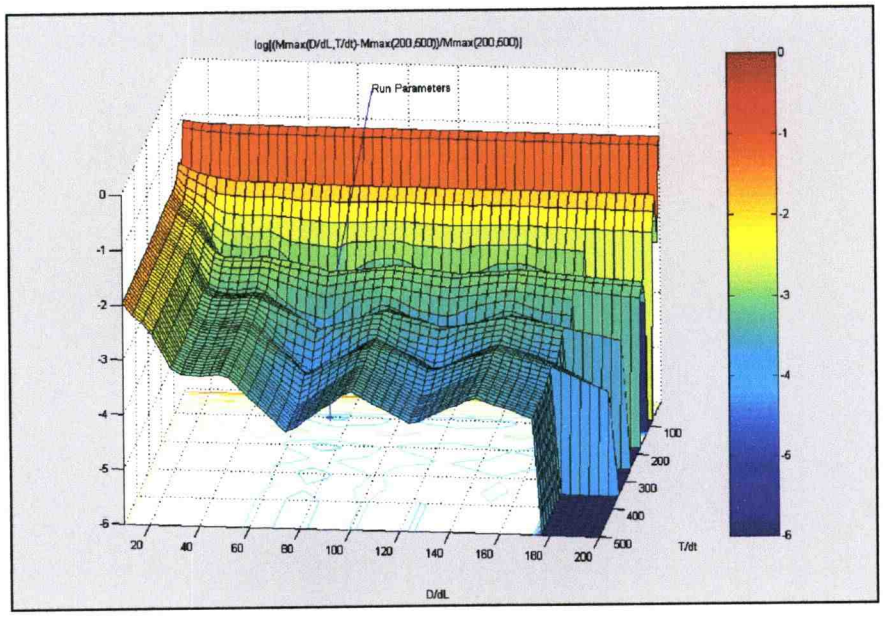

Figure 13: Numerical convergence of the maximum moment magnitude about the unit centroid for a 2 ft., 4 s wave.

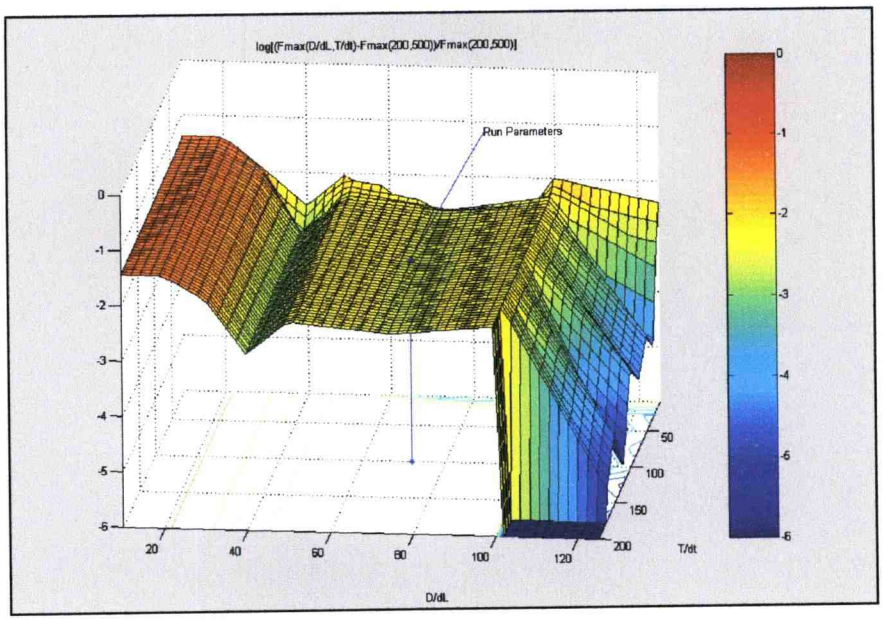

Figure 14: Numerical convergence of the maximum force magnitude for a 4 ft., 12 s wave.

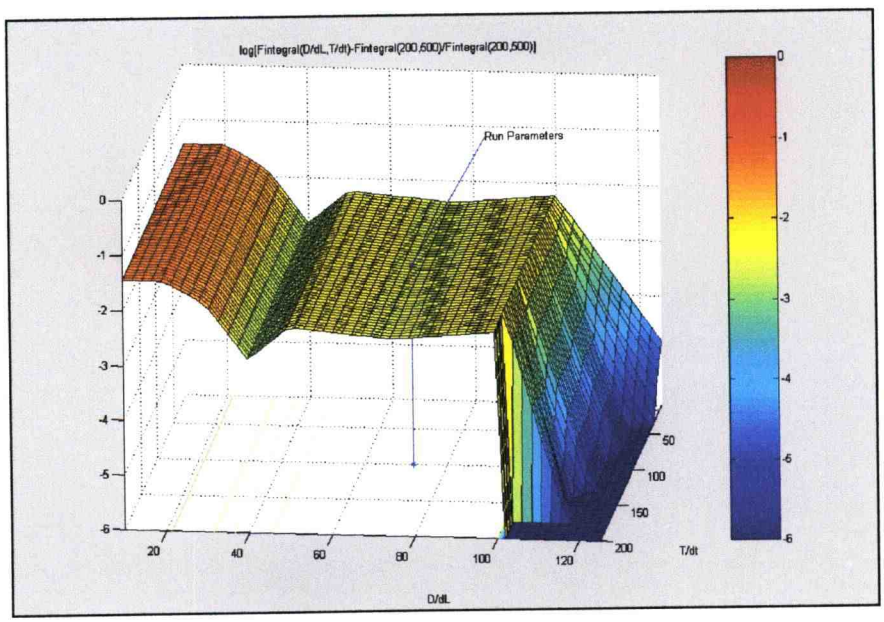

Figure 15: Numerical convergence of the integral of the force over one wave period normalized by the wave period for a 4 ft.,

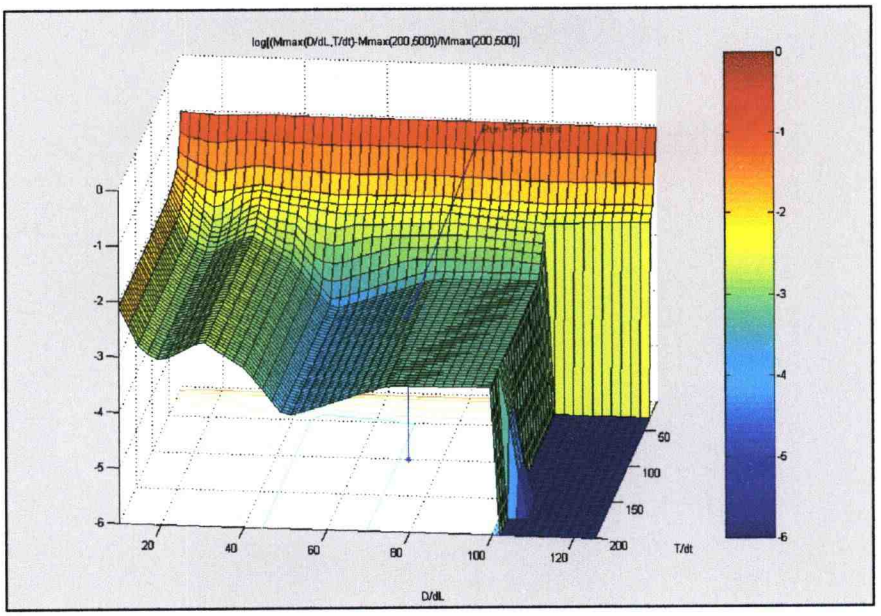

Figure 16: Numerical convergence of the maximum moment magnitude about the unit centroid for a 4 ft., 12 s wave.

As seen in Figures 11 through 16, the model rapidly converges to a relative error of 10^{-2} to 10^{-3}, or 1% to 0.1%, for more than 40 space steps (*D/dL*) and 50 time steps (*T/dt*). After the initial rapid convergence, the relative error varies between 10^{-2} and 10^{-6}; areas of low relative error can be found where the forces at a certain number of spatial and temporal steps is very nearly equal to the value for the maximum number of steps. Based on the convergence patterns, and the necessity of using a relatively low number of steps due to processing time constraints, a standard number of spatial and temporal steps was chosen as 100 temporal steps and 72 spatial steps. The number of spatial steps was chosen in part due to a requirement that the number of spatial steps be a multiple of 36 for compatibility with the structural finite element model. The run parameters chosen are highlighted in Figures 11 through 16. These run parameters were used for all further model runs.

4.2 Wave Forces and Rotational Response

A number of algorithms were developed in the MATLAB language and using the graphical capabilities of the MATLAB software package to represent the wave forces on A-Jacks armor units. In this section, some of the graphical output capabilities are demonstrated by examining one load case corresponding to a 2 ft. unit rotated +34° on a 1:2 slope in 12 ft. of water with its centroid at the still water line acted upon by a 2 ft., 4 s wave. The graphics shown can be produced by the algorithms for any load case and A-Jacks size.

Figure 17 shows the components of the total wave force on a single armor unit for the wave conditions and unit orientation described above. The wave is represented by a cosine function centered at the unit centroid. Therefore, the crest of the wave is at the centroid of the unit at the beginning of the record (t=0 s). The trough reaches the centroid of the unit at one half of the wave period (t=2 s) and the next crest reaches the centroid of the unit at the end of the wave period (t=4 s). The top left subplot shows the drag force on the unit. The global coordinate X, Y, and Z components of the forces are shown in each plot. The maximum drag force component magnitude is approximately 8 lbs. for this case. The period of time when the wave trough is passing the unit and the unit is fully emerged is from approximately 1.5 s to 2.5 s and there are no forces on the unit. The top right subplot shows the inertia force on the unit. The maximum inertia force component magnitude is approximately 10 lbs. The middle left subplot shows the buoyancy force on the unit which has a fully submerged buoyancy force of approximately 28 lbs. The middle right subplot shows the slamming force acting on the

unit as the free surface re-submerges the unit. A peak slamming force of approximately 6 lbs. is predicted at around 3 s. The slamming force shows a very sharp peak as the free surface hits leg B which is closest to parallel with the wave crest in this orientation. The bottom left and right subplots show the water particle velocities and accelerations at the still water level.

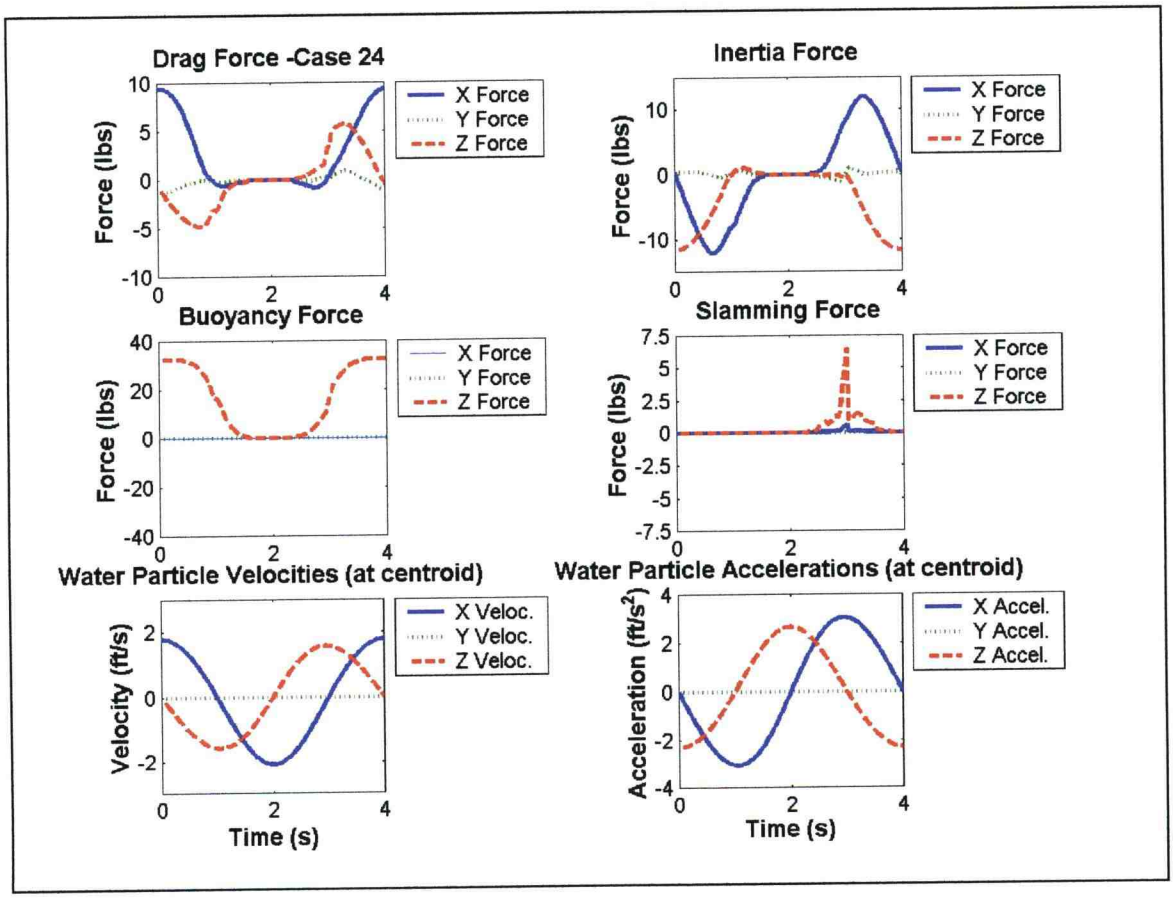

Figure 17: Components of wave force and water particle velocities and accelerations for a 2 ft., 4 s wave.

Figure 18 shows the total combined wave forces and resulting moments about the centroid of the unit for the unit orientation and wave conditions described above. The

upper subplot shows the total wave forces at the centroid of the unit. The total wave forces are a summation of the drag, inertia, buoyancy, and slamming forces shown in Figure 17. The peak total force component magnitude is the vertical force, Z direction, of approximately 30 lbs. at a time of approximately 3.2 s. As seen from Figure 17, this force is a result of uplifting buoyancy and drag forces in conjunction with the upward slamming force. The peak slamming force can be noted as the small peak in the vertical force at approximately 3.0 s. The lower subplot shows the moments about the centroid of the unit caused by the wave forces on the unit. The peak moment is approximately 6 ft.-lbs. in the *Y* direction component which would tend to cause the unit to roll in the direction of wave propagation.

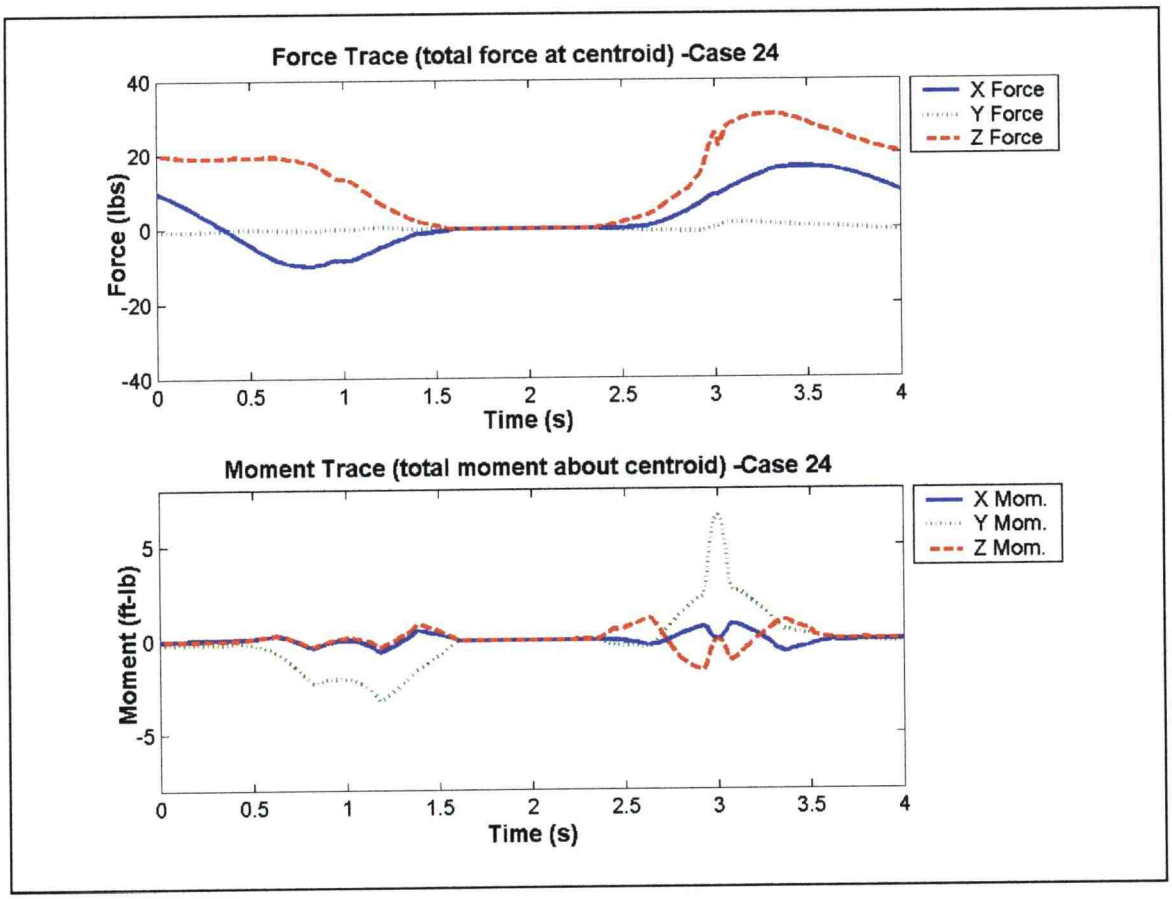

Figure 18: Total wave forces and moments about the unit centroid for a 2 ft., 4 s wave.

Figure 19 shows the results of the rotational motion predictions from the numerical model for this load case. The unit orientation and wave conditions are the same as those described above; however, the plots each cover two wave periods. This is because the rotational motion may not be zero at the beginning of the wave period, which is necessarily its initial condition for the first wave period. Using two or more wave periods is necessary to insure that one complete cycle will be contained in the predicted rotation. The figure is divided into three subplots; the top subplot shows the moment about the base axis $\overrightarrow{a0b0}$ (the moments about the other axes are always negative in this

case and are not shown), the middle subplot shows the rotational angle of the unit about the base axis, and the bottom subplot shows the rotational velocity about the base axis for the unit. As described in Section 3.6, the moments about the base axes are defined such that a positive moment tends to induce rotation from the resting position, while a negative moment tends to inhibit rotation from the resting position or tends to return the unit to its resting position if it is already in motion. Rotation can occur about any of the three axes. However, the axis about which a positive moment is first experienced becomes the dominant axis of rotation and rotation about the other axes is neglected. The middle subplot shows that a maximum rotational angle of 0.062 rad., or 3.6°, is predicted. As discussed above, the rotational motion has the same period as the wave, but the rotational motion can not be fully represented in one wave period. The bottom subplot shows that maximum rotational velocity of approximately 0.15 rad/s, or 8.6°/s, which is also the impact rotational velocity as the end of leg C comes back to its initial position on the slope and rotation is abruptly halted.

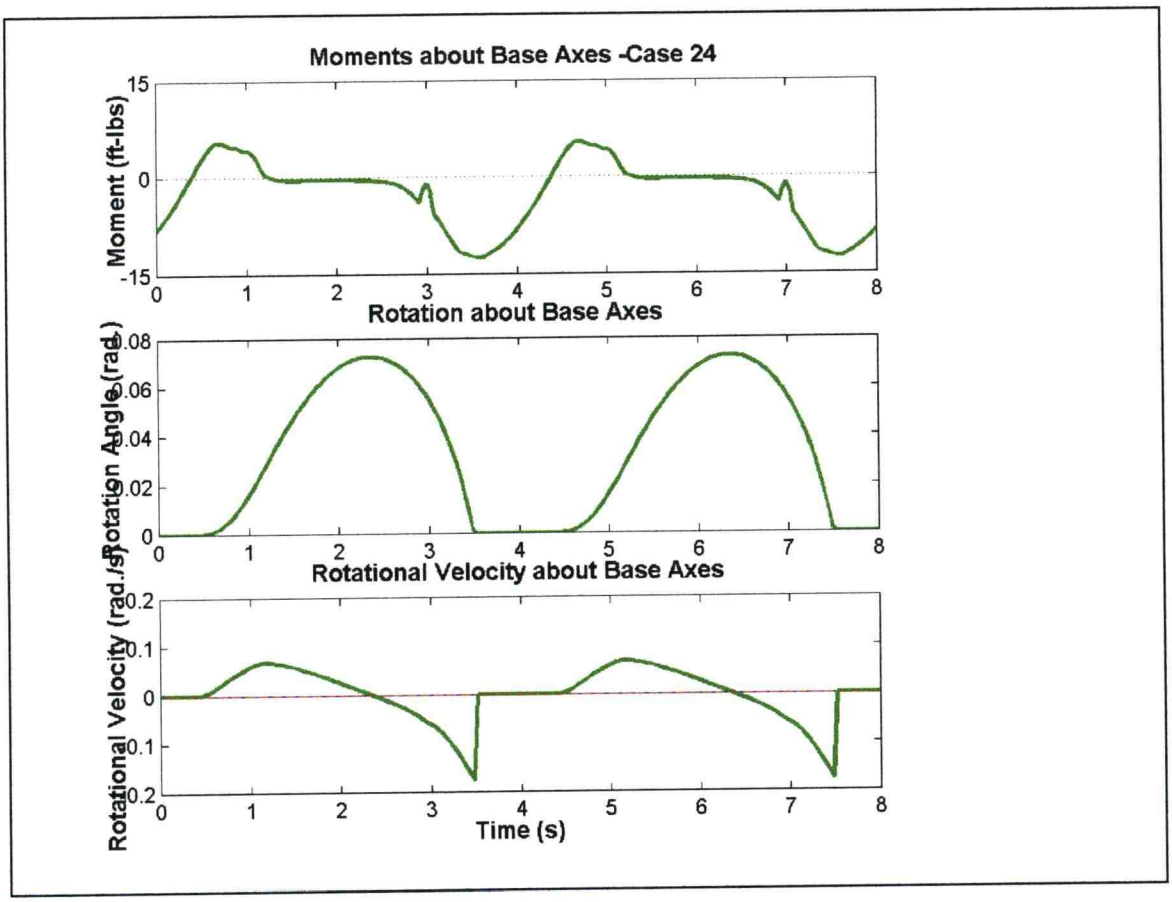

Figure 19: Moments about the base axes, rotational angles, and rotational velocity for a 2 ft., 4 s wave.

An algorithm was also developed to output an animated representation of the forces on each element of a unit. Figure 20 shows several frames from this animated representation. For the purpose of normalizing the force scales on plots with different spatial step sizes, the force on each element has been divided by the area of the element giving units of pressure. However, the forces are represented on the surface for visual interpretation. The calculated forces are actually applied at nodes on the centerline of the leg and are not distributed pressures on the surface of the leg. The color scale on the plots indicates the force on each element, with the central green color representing zero

force, the red colors representing forces acting in the direction of the inward normal of the surface element, and the blue colors representing forces acting in the direction of the outward normal of the surface element. The total force on each element is represented on both the inward and outward normal surfaces so that a given viewing orientation will allow viewing forces in each direction on almost every element. The body coordinate system, x, y, and z, is indicated by vectors on the legs of the unit, while the plot axes are aligned with the global coordinate system, X, Y, and Z. The series of plots shows the distribution of wave forces on the unit, under the orientation and wave conditions mentioned previously, for different times during the wave period. The time is indicated in the plot and a small insert on each plot shows the instantaneous water surface level at the unit centroid. The largest forces on the unit can be seen in the plot for t=3.0 s, which corresponds to high horizontal and vertical forces as discussed previously.

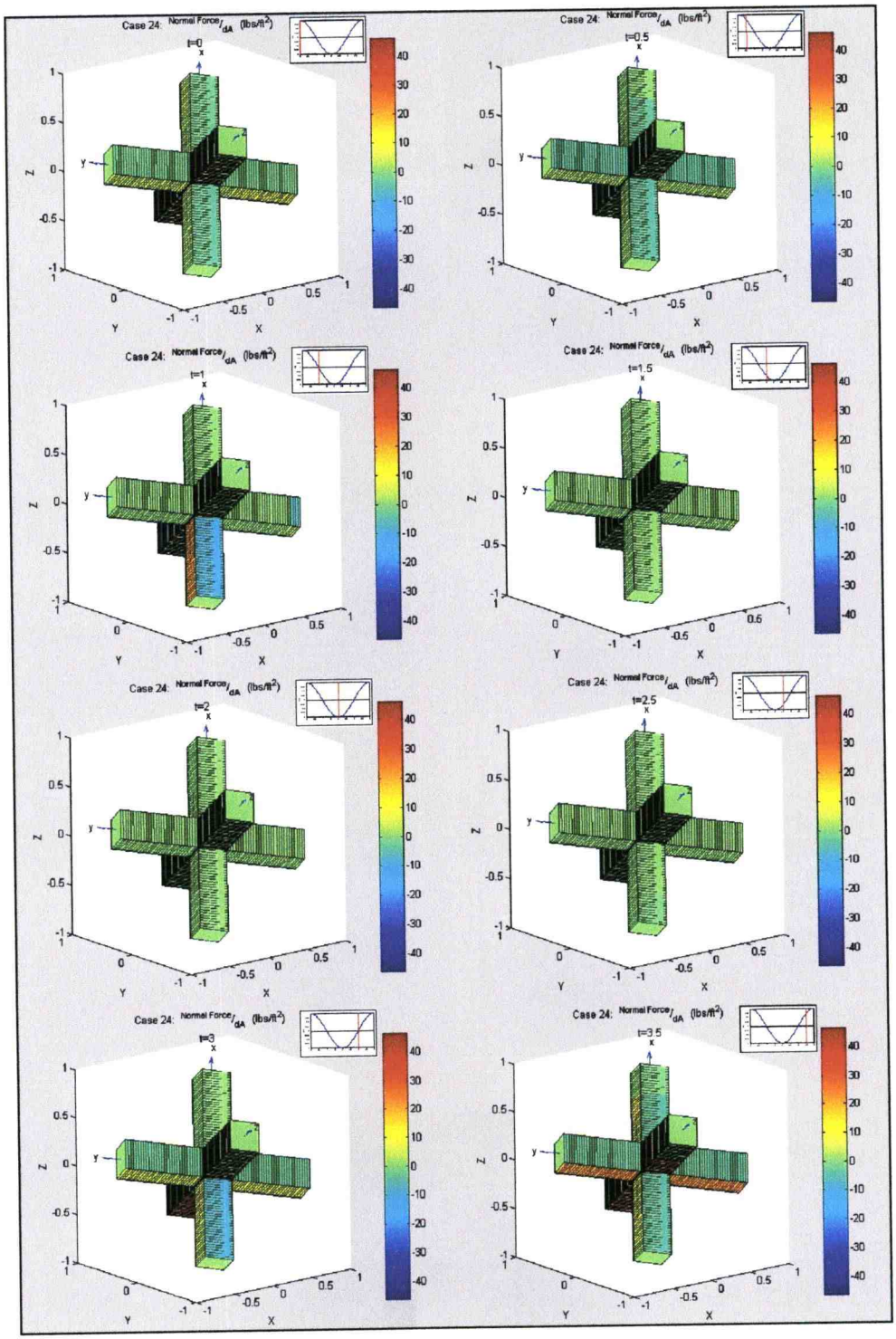

Figure 20: Frames from animated output for a 2 ft, 4 s wave.

4.3 Parametric Analysis of Wave Forces

To determine the effects of the unit orientation parameters of slope, unit rotation, and centroid depth and of the wave parameters of water depth, wave period, and wave height on the wave forces, nearly 5,000 cases were examined using the numerical model. The run case parameters were set by permutations of the factors shown in Table 2. Several of the parameter values are dependent on the values of other parameters. The wave height is dependent upon the maximum wave height, H_{max}, which is defined as the wave height corresponding to a Hudson's equation stability coefficient, K_d, value of 1000. The wave height, H, was also limited by the breaking wave height, H_b, which was defined as the lesser of the following two equations for wave steepness breaking and depth limited breaking, respectively:

$$H_b = \frac{L}{7}\tanh kh \tag{1}$$

$$H_b = 0.78h \tag{2}$$

in which h is the local depth, L is the wave length, and k is the wave number. For each run case the following output variables were written to a text file; the wave length, the Keulegan-Carpenter parameter, the maximum force and phase in each of the global coordinate directions, the maximum total force magnitude and phase, the integral of the force magnitude over the wave period normalized by the wave period, the maximum moment about the centroid of the unit in each of the global coordinate directions and the phases, the maximum total moment about the unit centroid magnitude and phase, the

maximum moment about a base axis and phase, and whether rotational motion or slamming occurred for the case.

Table 2: Parameter values for parametric analysis of wave forces.

Unit Size, D (ft.)	Slope	Unit Rotation	Centroid Depth, d (ft.)	Water Depth, h (ft.)	Wave height, H (ft.)	Wave Period, T (s)
2 4 8 12	1:1.5 1:2 1:3	+34° +84°	*0* *D* 2*D* and at the toe of the slope	1.5*H* 3*H*	$0.1H_{max}$ $0.2H_{max}$ $0.3H_{max}$ $0.5H_{max}$ $0.75H_{max}$ $1.0H_{max}$	4 8 12 16 20

The force and moment results, the unit orientation parameters, and the wave parameters from the run cases were non-dimensionalized using the Buckingham-Pi theorem. For the non-dimensionalization lengths were scaled by the unit size, D, time was scaled by the unit size divided by the maximum horizontal velocity at the unit centroid, D/u_{max}, and mass was scaled by the water density multiplied by the unit size cubed, ρD^3. This scheme yielded the force scaled by the stagnation pressure, the water particle acceleration represented by the Keulegan-Carpenter parameter, gravity represented by the Froude number squared, viscosity represented by the Reynold's number, and the water depth scaled by the unit size. Table 3 presents each of the independent variables for the wave forces problem and how it was scaled.

Table 3: Buckingham-Pi scaling for wave force parameterization

Maximum Wave Force & Moments: $F_{max}, M_{max} = f(u, a, d, m, D, \rho, g, \mu, \theta)$ Scaling Factors: Length $\Rightarrow D$, time $\Rightarrow D/u_{max}$, Mass $\Rightarrow \rho D^3$		
Parameter	Dimensions	Represented by
Maximum force magnitude, F_{max}	$\frac{\text{Mass} \cdot \text{Length}}{\text{Time}^2}$	$F^*_{max} = \frac{F_{max}}{\rho D^2 u^2_{max}}$
Maximum moment about unit centroid magnitude, M_{max}	$\frac{\text{Mass} \cdot \text{Length}^2}{\text{Time}^2}$	$M^*_{max} = \frac{M_{max}}{\rho D^3 u^2_{max}}$
Maximum horizontal water particle acceleration, a_{max} $\left(\text{assuming } a_{max} \approx u_{max}/T\right)$	$\frac{\text{Length}}{\text{Time}^2}$	Keulegan-Carpenter parameter, $\mathbf{KC} = \frac{u_{max} T}{D}$
Centroid depth, d	Length	$d^* = \frac{d}{D}$
Gravity, g	$\frac{\text{Length}}{\text{Time}^2}$	Froude number, $\mathbf{F}^2 = \frac{u^2_{max}}{gD}$
Viscosity, μ	$\frac{\text{Mass}}{\text{Length} \cdot \text{Time}}$	Reynold's number, $\mathbf{R}_e = \frac{\rho D u_{max}}{\mu}$
Slope, m	unitless	m
Unit rotation, θ	radians	θ

The non-dimensionalized forces were compared to the non-dimensionalized parameters in Table 3. The unit centroid depth, structure slope, and unit rotation each showed negligible effect on the maximum force on the unit. However, some correlation was found between the maximum force and the Reynold's number, the Keulegan-Carpenter parameter, and the Froude number. Figures 21 through 23 show the non-

dimensionalized force plotted against these parameters. Since the wave force is non-dimensionalized, in part, by the maximum horizontal velocity squared the relationships with the parameters may appear counter-intuitive at first glance. In Figure 21 four distinct groupings of data are seen; these grouping correspond to the four unit sizes run in the simulations.

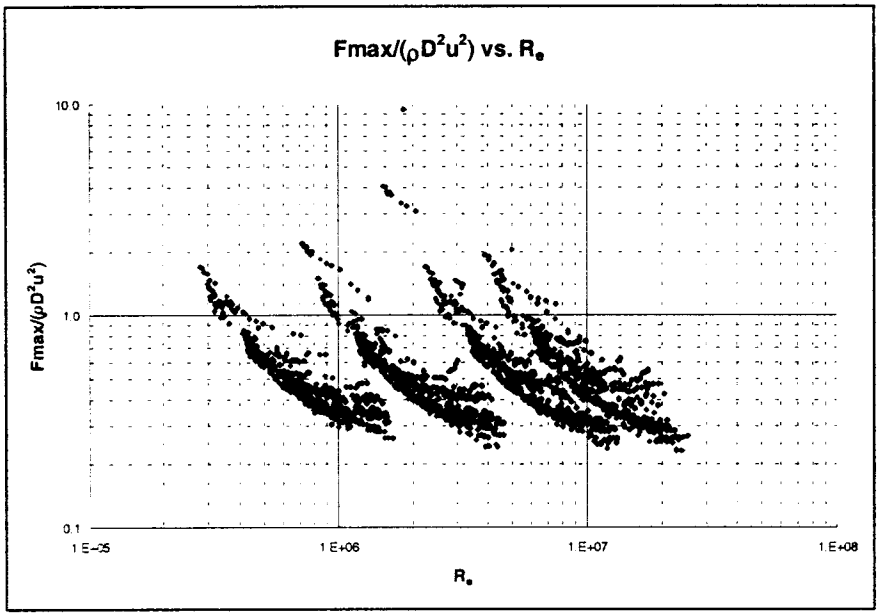

Figure 21: Non-dimensional maximum wave force versus Reynold's number.

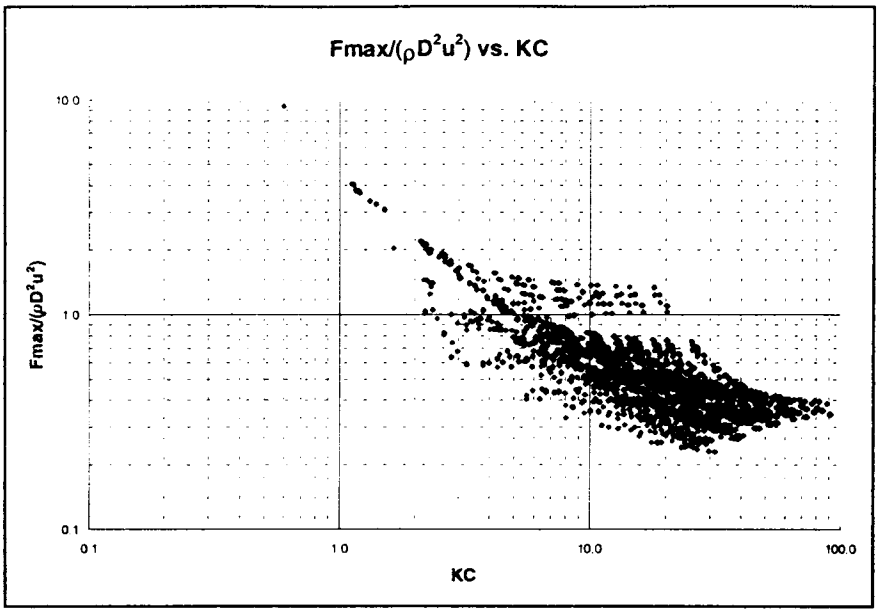

Figure 22: Non-dimensional maximum force versus Keulegan-Carpenter paramter.

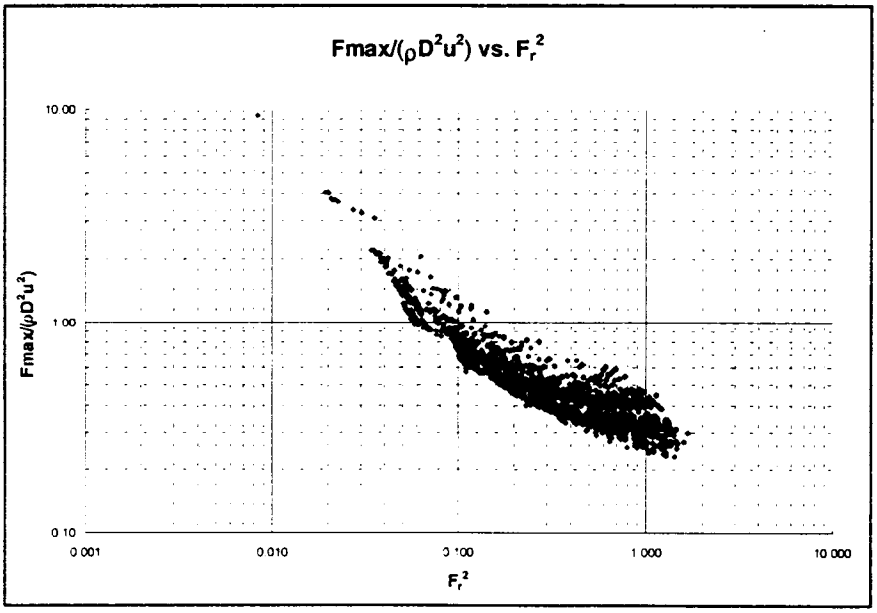

Figure 23: Non-dimensional maximum force versus the Froude number.

The paramterization was also used to find a predictive equation for the maximum wave force on a single A-Jacks armor unit. A simple predictive equation could be used to give first order approximations of the maximum force which might act on a unit. A number of combinations of variables were examined for a simple curve fit. In the end, one simple expression with the maximum wave force non-dimensionalized by the unit weight best fit the data:

$$F_{max} = 2W\mathbf{F}^{2/3} \tag{3}$$

where W is the weight of an A-Jacks unit and $\mathbf{F}$ is the Froude number. The fit of the predictive equation to the calculated maximum wave force is shown in Figure 24. A correlation coefficient of r^2=0.948 was achieved with this predictive equation.

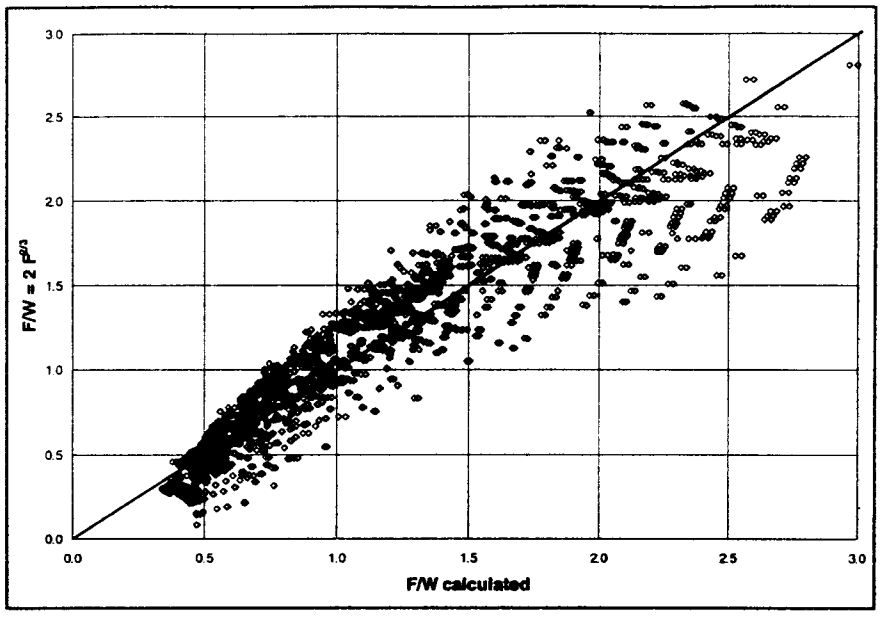

Figure 24: Predictive equation for non-dimensionalized maximum force versus non-dimensionalized maximum force calculated by numerical model.

5. PHYSICAL MODELING RESULTS AND COMPARISON TO NUMERICAL MODELING

To test the numerical wave forces model, three types of small-scale physical model tests were undertaken. In the first of these experiments, the numerical model prediction of incipient rotational motion about a base axis was compared with physical tests under similar wave conditions. The second experiment undertaken was to indirectly measure the forces on a unit under steady flow conditions to determine the drag coefficient. Lastly, the bulk forces on a uniformly placed matrix of A-Jacks units were directly measured in order to calibrate the sheltering effects extrapolation of the numerical model. In this chapter, the set-up and results of each of the three experiments will be discussed and the results of each will be compared with the results predicted by the numerical model.

5.1 Rotational Motion

The numerical wave forces model can predict the rotational motion of individual A-Jacks units on a plane slope. As discussed in Section 3.6 the computed wave forces are used to determine moment about the base axes formed by the corners of the legs upon which the unit rests. The moments about the base axes are defined such that a positive moment tends to induce rotation about the axis while a negative moment impedes motion or tends to restore the unit to its original position if the unit is already rotating. The wave and physical conditions which cause the moment about one of the base axes to just exceed zero correspond to the incipient rotational motion about that axis. The wave and

physical conditions which cause the moment about one of the base axes to be greater than zero are said to exceed incipient rotational motion about that axis and lead to rotational motion.

To confirm the results of the numerical model, physical testing was undertaken to determine the wave conditions that exceed incipient rotational motion conditions. In the tests, observations of the rotational behavior of several sizes of A-Jacks units, placed such that the axis of rotation was easily predicted, were made under different wave conditions. This experiment tests several parts of the numerical model; the inertia and drag forces, the calculation of the moments about the base axes, and to some degree the predicted rotational motions. In addition, this physical test did not require direct or indirect measurement of the forces on the units, only the measurement of wave conditions and observation of the motion of the units.

5.1.1 Testing Procedure

A-Jacks units were placed in the 10 m wave flume in Graf Hall (at Oregon State University) on a level slope (μ=0) and the body x axis was aligned with the direction of wave propagation (θ=0) as described in Section 3.1. A-Jacks units of length 2.5 in., 3 in., 4 in., 6 in., and 8 in. were used. For some of the test runs a shoaling ramp was used to decrease the water depth while still allowing the hinge wavemaker to generate relatively large amplitude waves. In all cases the units were kept several wave lengths from the wavemaker to avoid evanescent modes. Units were also spaced as far from each other as allowable under the space constraints. Figure 25 shows a schematic diagram of the test set-up and Figure 26 shows a photograph of the test set-up.

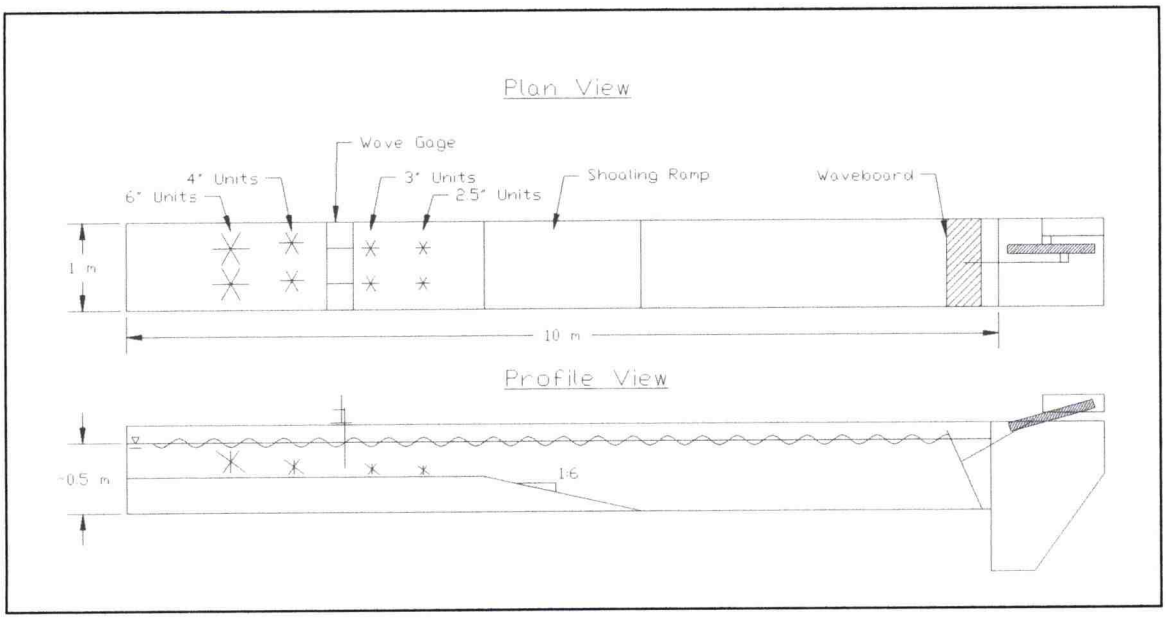

Figure 25: Schematic of the incipient rotational motion experimental set-up.

Figure 26: Incipient rotational motion experiment.

The wave flume was equipped with a hinge wavemaker driven by a variable frequency drive motor. The wave height was controlled by adjusting the maximum throw

(or excursion) of the waveboard and the wave period was controlled by adjusting the frequency of the variable frequency drive (which also affected the wave height). A number of different wave periods and wave heights were tested at several water depths.

A resistance wave gauge, located near the A-Jacks units, was used to measure the wave height. The wave gauges are comprised of two stainless steel wires, separated by approximately 1.5 in. The wave gauge was calibrated by raising and lowering the gauge and correlating the gauge output with the gauge position relative to the still water level. The gauge was found to have a highly linear response pattern.

The water surface elevations were recorded on an analog strip chart recorder and the wave height was interpreted from the strip chart record. For some run cases, wave breaking occurred in the vicinity of the wave gauge. This may have resulted in the recording of larger wave heights than the wave heights at the individual units. For runs 1 through 91, the wave gauge was approximately 2 ft. shoreward of the 2.5 in. A-Jacks units. For runs 92 through 118 the wave gauge was positioned between the 3 in. and 4 in. units to give a more accurate measurement of the wave height at the units. The wave period was measured with a stop watch by recording the time required for 10 full cycles of the waveboard.

The water depth at the A-Jacks units was measured with a ruled steel stick. Direct observation was used to determine whether the A-Jacks units exhibited rotational motion. In addition, for the majority of the runs a video camera was used to record the response of the units.

5.1.2 Results of Physical Model and Numerical Simulation

Although approximately one hundred wave conditions were tested, very few cases resulted in the motion of A-Jacks units. This is largely due to the rather small wave conditions that can be generated in the tank. Rotational motions were observed for both the 2.5 in. and 4 in. units. No other units exhibited rotational motion. The water depths corresponding to the cases with rotational motions varied from approximately 7 in. to approximately 8 in.

The numerical wave force model was used to simulate conditions similar to those in the physical model. The breaking wave conditions formed the upper bound on the wave conditions. The breaking wave height was defined in Section 4.3. An interval halving method was used to determine the wave conditions corresponding to incipient rotational motion about the appropriate base axis. A relative convergence criteria of 1% was used for the incipient motion point. Wave heights above the incipient motion points are expected to cause rotational motion. The numerical model was run at a number of wave periods and two water depths, 1.5 ft and 0.75 ft., to simulate the physical set-up with and without the shoaling ramp. The numerical model was run using parameters (unit size, wave height, etc.) similar to those in the physical testing; therefore, Reynolds number scaling was not required. However, in general the Reynolds numbers for the numerical simulation fell below those for which the drag coefficients were explicitly defined and, thus, the drag coefficients corresponding to the lowest explicitly defined Reynolds numbers were used.

Table 4 summarizes the wave conditions which caused rotational motion in the test cases. Figures 27 and 28 show the results of the test plotted in non-dimensional wave

space (*kh, kH*) along with the predicted incipient motion boundary from the numerical model for a water depth of 0.75 ft. (roughly corresponding to the water depths were rotational motions occurred). Figure 29 shows the rotation of two 2.5 in. units during Run 93.

Table 4: Rotational Motion Experiment Results

Run	h (in.))	T (sec)	H (in.)	2.5" unit Incipient Motion (1=yes 0=no)	4" unit Incipient Motion (1=yes 0=no)	kh	KH
72	6.95	1.312	5.57754	0	1	0.690416	0.277038
84	7.180556	1.228	6.274733	0	1	0.759911	0.332024
94	8	1.218	3.037247	1	0	0.821766	0.30981
104	8.0625	1.203	3.215909	1	0	0.833764	0.333082
107	8.125	1.154	2.858586	1	0	0.878998	0.311073
109	8.125	1.057	3.841225	1	0	0.983113	0.466217
88	7.211207	1.22	6.274733	1	1	0.767717	0.334009
91	7.185345	1.197	7.669118	1	1	0.78355	0.418152
93	8.0625	1.238	3.215909	1	1	0.807342	0.321279

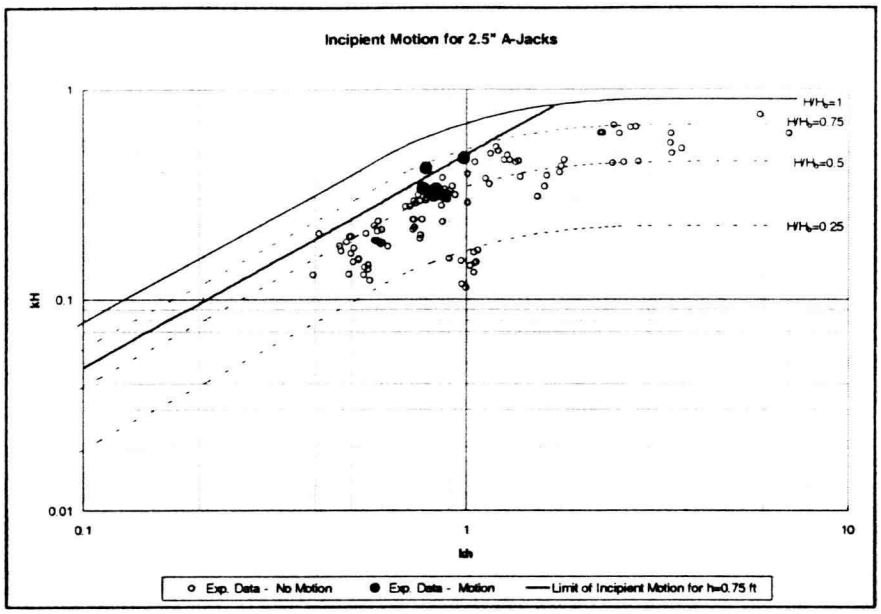

Figure 27: Rotational motion experimental and numerical simulation data for 2.5 in. A-Jacks units.

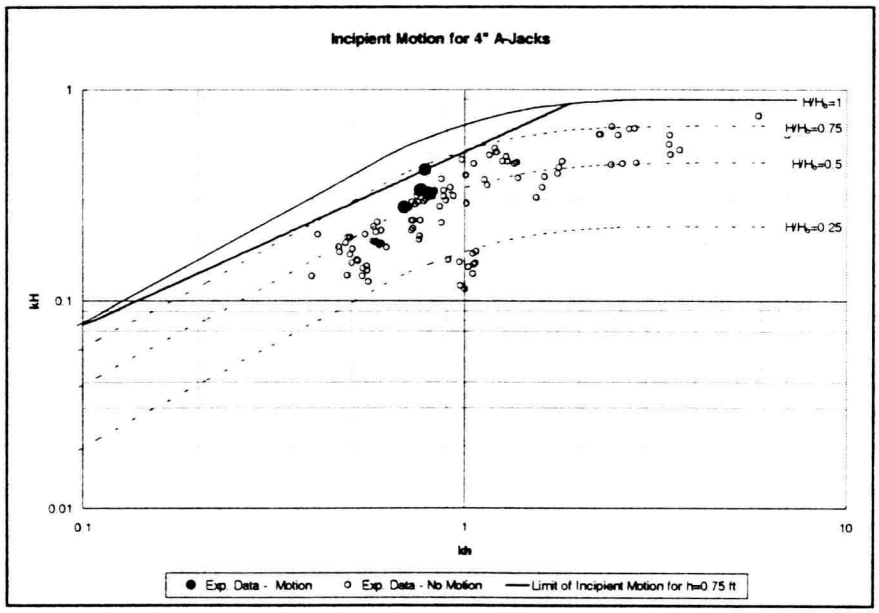

Figure 28: Rotational motion experimental and numerical simulation data for 4 in A-Jacks units.

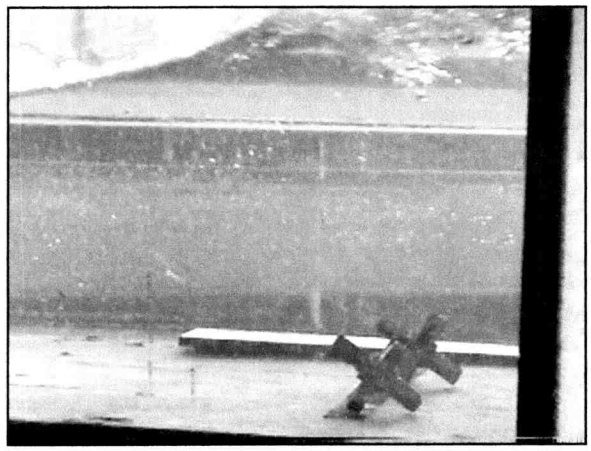

Figure 29: Rotation of 2.5 in. units in Run 93.

5.1.3 Comparison of Numerical Simulation and Physical Model

As seen in Figures 27 and 28, the data from the physical model shows a good agreement with the predictions of the numerical model. Motion was only observed for waves of longer periods close to breaking in both the experiments and numerical model. The lack of rotational motion at the lower wave conditions can also be viewed as a confirmation of the numerical model. It should also be noted again that wave height dissipation due to wave breaking may have caused some of the wave height measurements to be larger than the conditions at the A-Jacks units, especially for depth limited breaking waves. Overall, the rotational motion physical model verified the results of the numerical wave force model reasonably well.

5.2 Steady Flow Drag Coefficient

An experiment was conducted to determine the approximate range of steady flow drag coefficients for the overall A-Jacks armor unit. To simplify the experiment, the overall drag force on the unit was examined rather than the drag force for each element along the legs which is calculated in the numerical model. Thus, this experiment gives some insight into magnitude of drag coefficients for the units and the effect of orientation on the drag force.

5.2.1 Testing Procedure

In this experiment A-Jacks units were suspended as a pendulum in a steady flow and the drag force on the units was determined using statics. The resulting deflection of the unit was used to determine the horizontal drag force on the unit which was, in turn, used to calculate the drag coefficient.

A 10 ft. long, 1 ft. wide hydraulic flume in Graf hall was used for the experiment. The flowrate in the flume was set to its maximum value, 0.33 ft^3/s (cfs), and the tailgate at the end of the flume was used to adjust the depth of flow in the tank. The depth of flow in the tank was measured using a steel ruler. The depth of flow was adjusted to four values between 2.75 in. and 5.875 in. resulting in flow velocities ranging from 0.674 ft/s to 1.440 ft/s.

Harnesses were fashioned for the A-Jacks units onto which a rigid rod was attached. The other end of the rod was attached to a horizontal bar across the top of the

flume in a manner which allowed the unit to rotate freely. Units of three sizes, 2.5 in., 4 in., and 6 in., were suspended in the hydraulic flume. Three different random orientations were used for each unit size and flow depth. The depth of flow limited the use of the larger units for the shallower water depths. In all, twenty four tests were conducted. The distances from the freely rotating connection at the top of the tank to the centroid of the unit, L, and to the water surface, dZ, were measured. The horizontal displacement of the unit, dX, was measured using a carpenters square and the water surface for a horizontal datum. In some cases, especially for high flow velocities and the smallest unit size, some fluctuations in the horizontal displacement were observed and the average displacement was estimated. Figure 30 shows a unit suspended in the hydraulic flume.

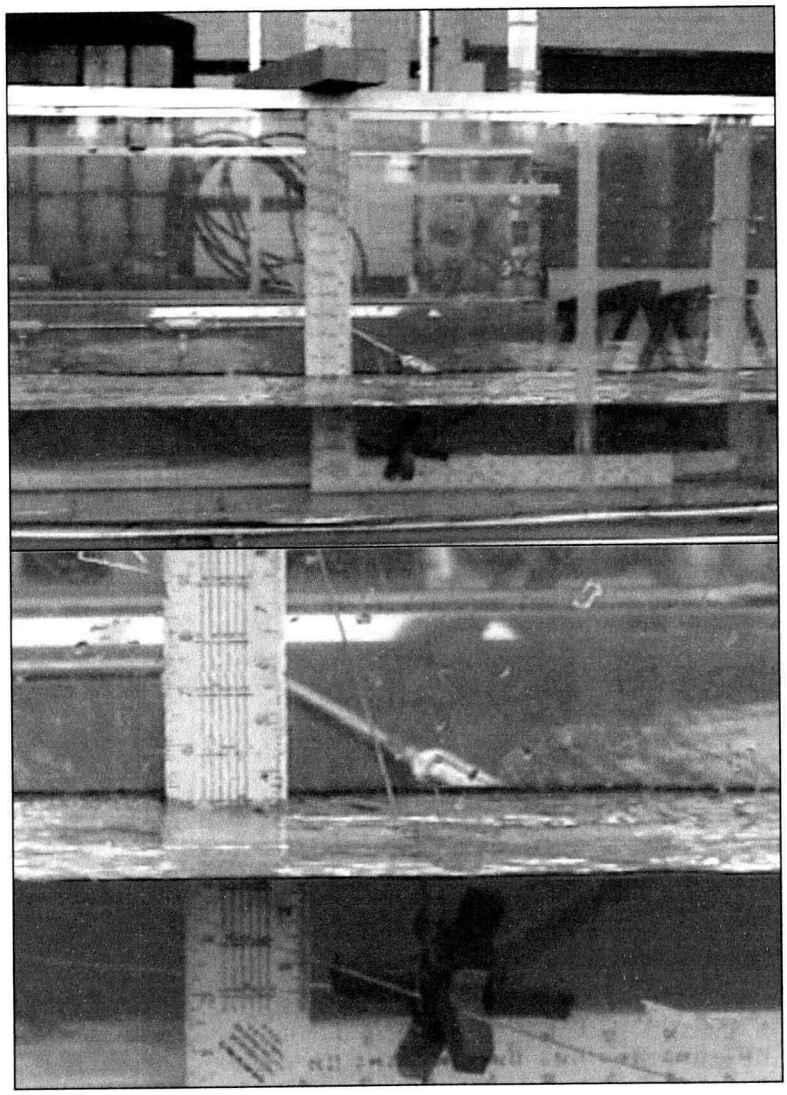

Figure 30: 2.5 in. A-Jacks unit suspended in steady flow.

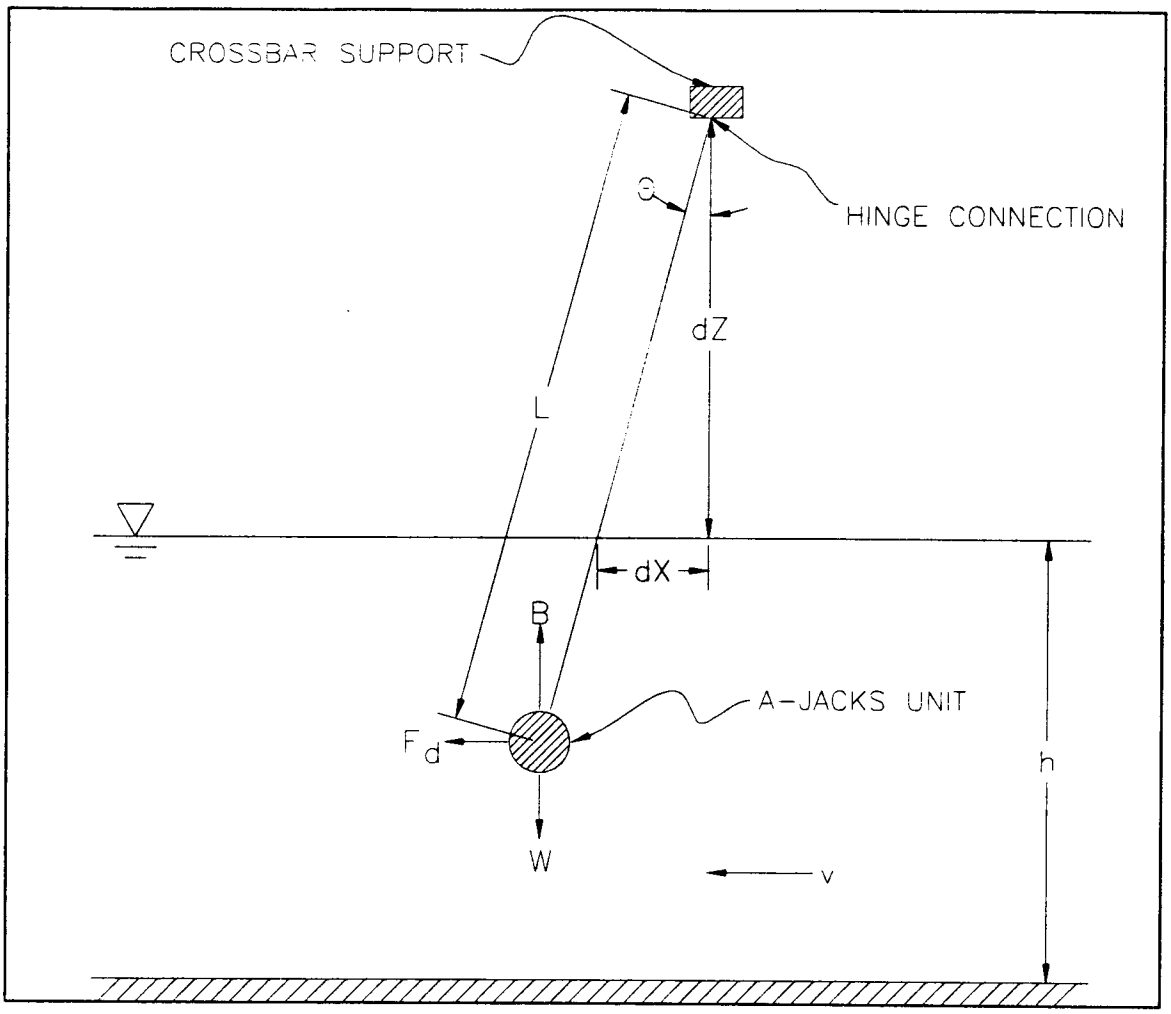

Figure 31: Free body diagram for steady flow drag coefficient.

Static relationships were used to determine the horizontal force on the unit. Figure 31 shows a free body diagram for the experimental setup. Setting the sum of moments about the hinge connection equal to zero for static equilibrium and assuming that the weight of the rod is negligible gives the expression for the horizontal drag force, F_d, on the unit:

$$F_d = (W - B)\tan\theta \qquad (1)$$

where W is the saturated weight of the unit, B is the buoyancy force on the unit, and $\tan\theta = \frac{dX}{dZ}$. The saturated weight of the units was measured using an analytical balance and the buoyancy force was calculated using the equation for the volume of an A-Jacks unit. The drag force is related to the flow velocity, v, unit projected area, A, and steady flow drag coefficient, C_d, by the equation:

$$F_d = \frac{1}{2}\rho C_d A v^2 \tag{2}$$

where ρ is the fluid density. Solving for the steady flow drag coefficient yields:

$$C_d = \frac{2F_d}{\rho A v^2} \tag{3}$$

During the testing it was observed that the unit orientation had little effect on the horizontal displacement of the unit and, furthermore, the projected area is relatively constant for different orientations. Therefore, the projected area of the unit was approximated using the frontal area with one leg parallel to the flow. Because there are three such orientations, one of which does not have a contribution due to the central hub fillets and the others have contributions from four fillets, the approximate frontal area was calculated including two fillets. The approximate frontal area was thus calculated as:

$$A = (2r - r^2 + 2s^2 r^2)D^2 \cong 0.3D^2 \tag{4}$$

where r is the waist ratio (defined in Section 3.1) and s is the fillet ratio (defined in Section 3.1).

5.2.2 Results

Steady flow drag coefficients ranging from 0.848 to 1.718 were calculated from the experimental data. The steady flow drag coefficients were compared with the Reynold's number which was calculated as:

$$\mathbf{R}_e = \frac{vD}{\upsilon} \tag{5}$$

where D is the unit size and v is the kinematic viscosity of the fluid. Reynold's numbers ranging from 1.00×10^{4} to 2.41×10^{4} were calculated. Figure 32 shows a comparison of the steady flow drag coefficients with the Reynold's number. There is a large amount of scatter in the data, but a linear equation was fit to the data. The experiment shows that, although defined differently, the steady flow drag coefficients are in the general range of values used for the numerical wave force model.

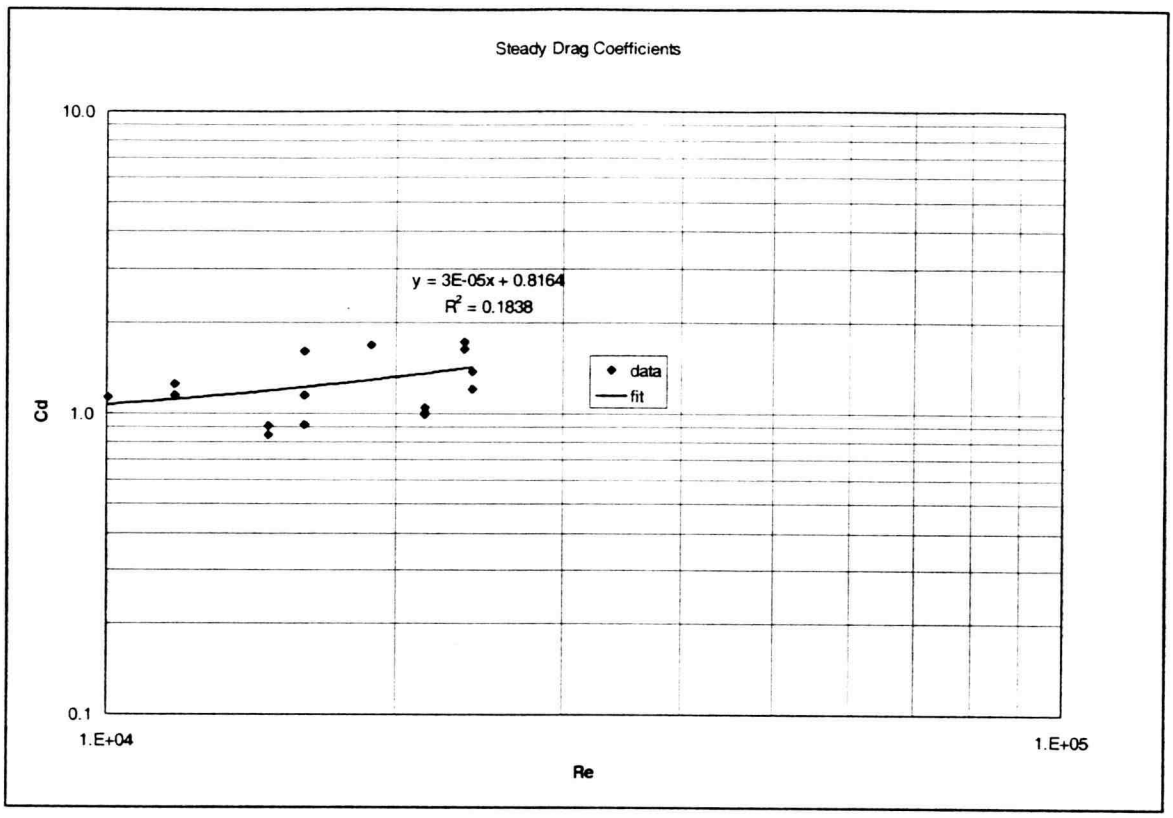

Figure 32: Steady flow drag coefficients vs. Reynold's number

As mentioned previously, the orientation of the unit had little, if any, effect on the drag force on the unit. Because there is little effect due to orientation on the projected area of the unit, this was an expected result. The numerical wave force model which calculates the actual projected area also showed no effect due to orientation on the maximum force magnitude in oscillatory flow.

5.3 Bulk Forces on Matrices of Units

The numerical model for single A-Jacks units was extended to estimate the forces on a matrix of units based on the results of physical model experiments. A load frame was constructed and model experiments were conducted to measure the forces on a matrix of units under various wave conditions. The extension of the model is based on semi-empirical sheltering coefficients applied to the predicted forces. The sheltering coefficients account for the reduction in projected frontal area and the effect other units in a matrix have on the water kinematics. The sheltering coefficients were used to fit the output from the numerical model to the measured forces.

5.3.1 Testing Procedure

A load frame was constructed to measure the wave forces on a matrix of units. A schematic profile view and free body diagram of the load frame are shown in Figure 33. Figure 34 shows a view of the load frame loaded with 2.5 in. A-Jacks units. The load frame was constructed to be a statically determinant structure and measure the bulk force in the horizontal and vertical directions. Strain rings, aluminum rings with strain gages, were used to measure tensile forces. A set of elastic cords was used to keep the horizontal force strain ring in tension and to increase the horizontal stiffness of the load frame. The forces in the cross-tank direction were assumed to be negligible. The slope surface of the load frame, corresponding to the under layer in a breakwater, was constructed from expanded steel grating and had a very high porosity.

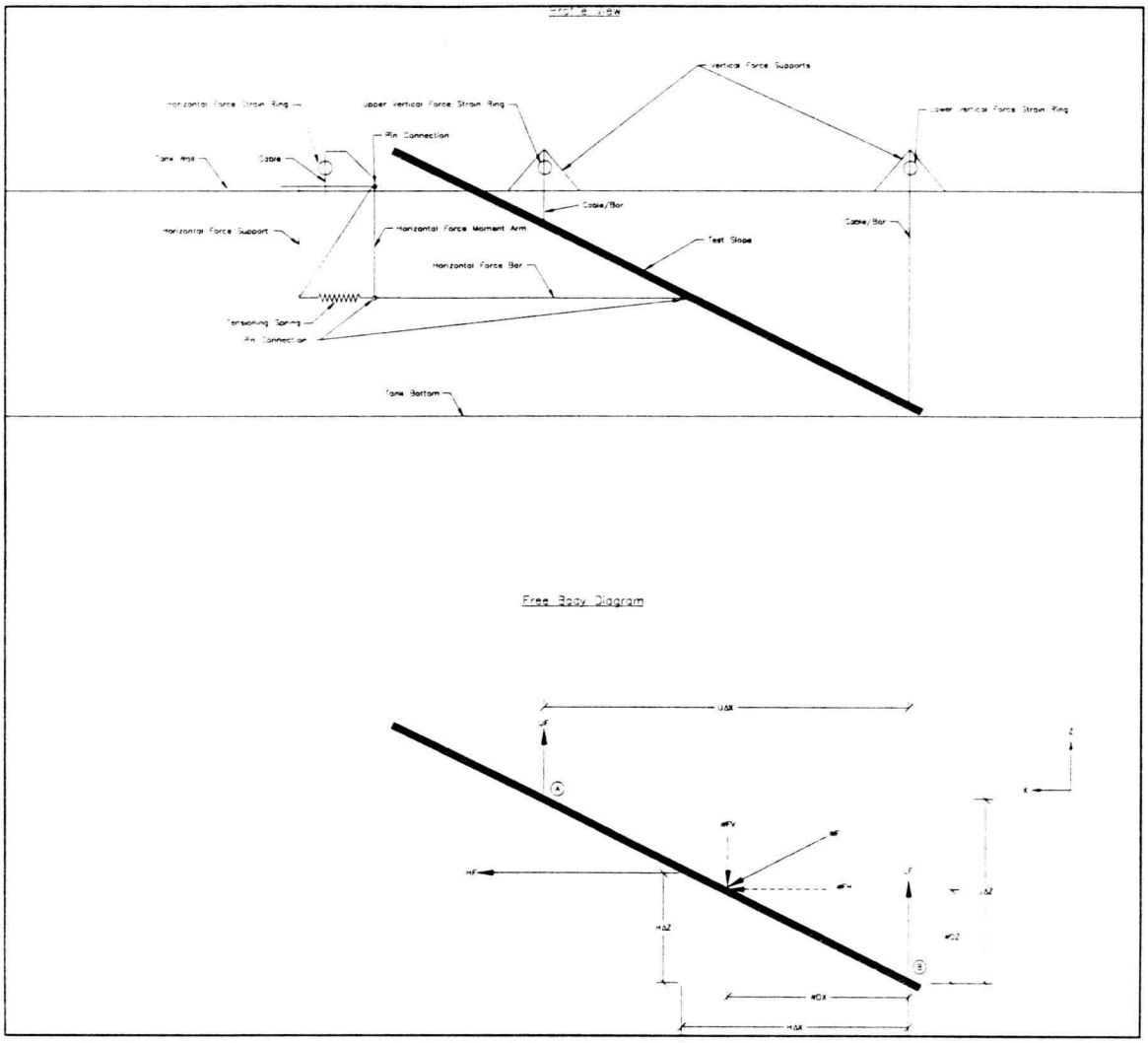

Figure 33: Schematic profile view and free body diagram of the bulk forces load frame.

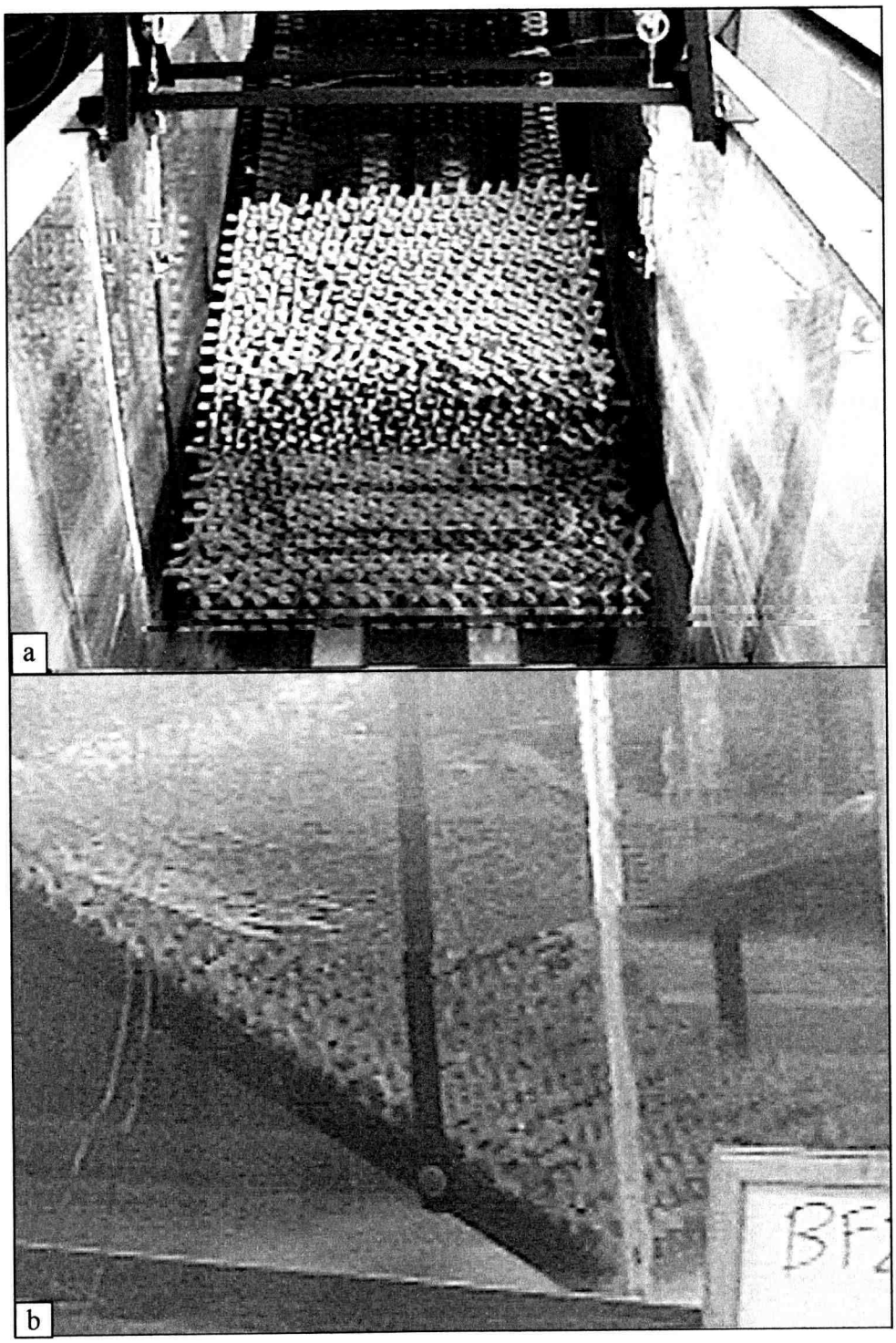

Figure 34: (a) View down the wave tank at the load frame with 2.5 in. units. (b) Oblique view of load frame with 2.5 in. units during a run (wave trough is near the middle of the structure slope).

The measured forces on the load frame were analyzed using static relationships to determine the total horizontal and vertical wave forces as follows:

$$WFV = UF + LF \tag{6}$$

$$WFH = HF \tag{7}$$

where WFV is the total vertical wave force on the structure, WFH is the total horizontal wave force on the structure, and UF, LF, and HF are the measured forces as shown in the free body diagram (Figure 33). The magnitude of the total wave force, WF, and the angle between the total wave force and vertical, ϕ, were also determined as follows:

$$WF = \left[WFV^2 + WFH^2\right]^{1/2} \tag{8}$$

$$\begin{aligned} \phi &= \sin^{-1}\left(\frac{-WFH}{WF}\right) \quad \text{for } WFV > 0 \\ \phi &= \pi + \sin^{-1}\left(\frac{-WFH}{WF}\right) \quad \text{for } WFV < 0 \end{aligned} \tag{9}$$

The vertical location, $W\Delta Z$, and horizontal location, $W\Delta X$, of the centroid of the wave forces were also determined from the measured data according to the following relationships:

$$W\Delta Z = \frac{-HF(H\Delta Z) + UF(U\Delta Z)m}{(UF + LF)m - HF} \tag{10}$$

$$W\Delta X = (W\Delta Z)m \tag{11}$$

where m is the run/rise of the structure slope and $U\Delta Z$ and $H\Delta Z$ are the vertical distances from the point B to the upper connector and the horizontal bar connector, respectively, as shown on Figure 33

Data collection for the experiment was performed using a data acquisition card on an IBM compatible computer and the LABVIEW software package. In addition to the force measurements, the water surface profile was measured at a location approximately 15 ft. from the toe of the structure using the wave gauge described in Section 5.1.1. Data acquisition was performed at a frequency of 30 Hz and all data was analog filtered at a cutoff frequency of 15 Hz. Water depth, $U\Delta Z$, and $H\Delta Z$ were measured with a steel ruler, as was the distance from the toe of the structure to the wave gauge denoted as *Xoffset*. The strain rings were calibrated by applying known forces and recording the voltage output. All of the strain rings were found to have linear response patterns.

During experimental runs some horizontal motion, less than 1/16 in., was observed in the load frame. This motion results in inertial forces caused by the acceleration of the load frame and is believed to cause some error in the force measurements. To attempt to correct for the introduction of the inertial force due to frame motion, the load frame has been idealized as a spring-mass-damper system as shown in Figure 35. The measured horizontal force, denoted here as $F(t)$, can be used to determine the applied horizontal force on the structure, denoted here as $f(t)$, using a linear transfer function. It should be noted that the applied horizontal force contains forces

arising from the radiation of waves caused the structure motion away from the structure which are not accounted for.

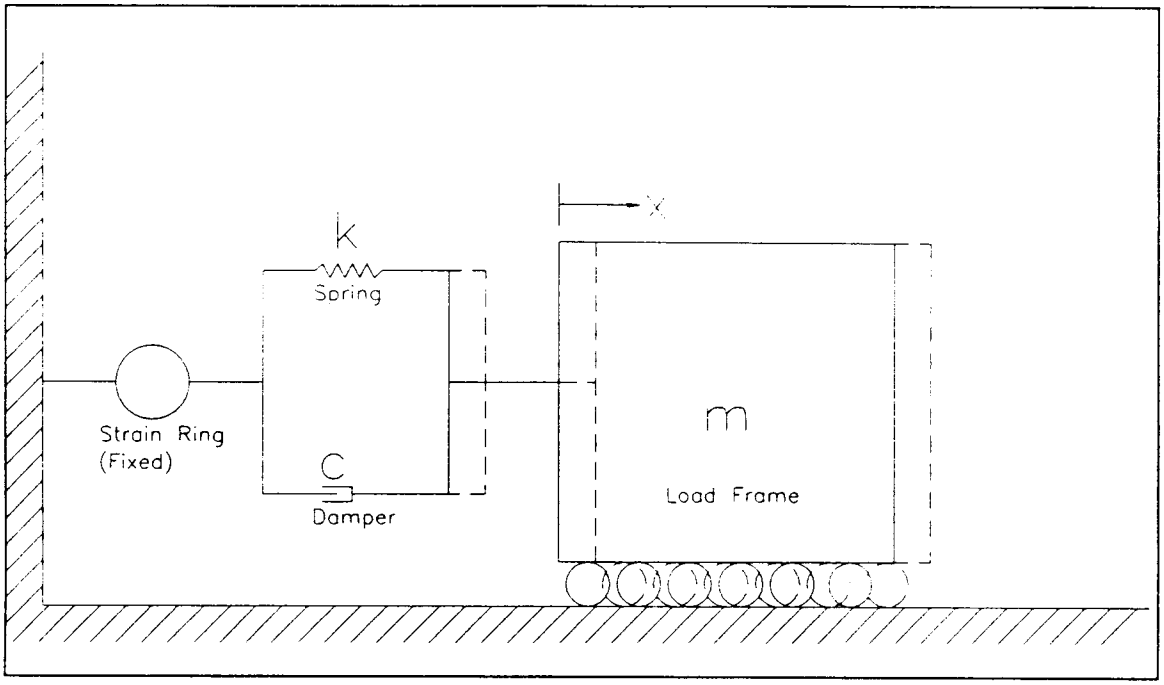

Figure 35: Schematic diagram of bulk force load frame response.

First the transfer function must be derived. The equation of motion is written for the load frame with the applied horizontal load as follows:

$$m\ddot{x} + c\dot{x} + kx = f(t) \tag{12}$$

where x is the horizontal displacement of the system, over-dots denote the time derivatives of the horizontal displacement, m is the mass of the system (constant), c is the damping coefficient of the system (constant), and k is the horizontal stiffness of the system (constant). The measured force, $F(t)$, can be written as:

$$F(t) = kx + c\dot{x} \tag{13}$$

The measured and applied horizontal loads can be represented using a discrete, complex valued Fourier series:

$$f(t) = \sum_{n=-\infty}^{\infty} f_n e^{-i\omega_n t}$$
$$F(t) = \sum_{n=-\infty}^{\infty} F_n e^{-i\omega_n t} \tag{14}$$

where f_n are the complex Fourier coefficients for the applied force, F_n are the complex Fourier coefficients for the measured force, and ω_n are the discrete frequency components of the Fourier series. Similarly, a discrete, complex-valued Fourier series can be written for the horizontal displacement of the load frame and its derivatives:

$$x(t) = \sum_{n=-\infty}^{\infty} x_n e^{-i\omega_n t}$$
$$\dot{x}(t) = -i\omega_n \sum_{n=-\infty}^{\infty} x_n e^{-i\omega_n t} \tag{15}$$
$$\ddot{x}(t) = -\omega_n^2 \sum_{n=-\infty}^{\infty} x_n e^{-i\omega_n t}$$

Equations 12 and 13 can now be rewritten in terms of the discrete Fourier series representations to give:

$$\sum_{n=-\infty}^{\infty} \left(-\omega_n^2 m - i\omega_n c + k\right) x_n e^{-i\omega_n t} = \sum_{n=-\infty}^{\infty} f_n e^{-i\omega_n t} \tag{16}$$

$$\sum_{n=-\infty}^{\infty} F_n e^{-i\omega_n t} = \sum_{n=-\infty}^{\infty} \left(k - i\omega_n c\right) x_n e^{-i\omega_n t} \tag{17}$$

Combining Equations 16 and 17 then gives the final transfer function:

$$\sum_{n=-\infty}^{\infty} f_n e^{-i\omega_n t} = \sum_{n=-\infty}^{\infty} \left(\frac{-\omega_n^2 m - i\omega_n c + k}{k - i\omega_n c} \right) F_n e^{-i\omega_n t} \tag{18}$$

The weight of the load frame and the A-Jacks units was estimated to be 100 lbs., giving a mass of approximately 3.11 slugs. The horizontal stiffness of the structure was determined by measuring the horizontal displacement with the application of known loads. A horizontal stiffness of approximately 2400 lbs/ft was measured. To determine the system damping, the load frame was displaced a known distance, released, and allowed to oscillate freely. It was observed that at the completion of one complete oscillation the horizontal displacement was approximately half of the initial displacement. Analyzing the homogeneous equation of motion with the already determined mass and horizontal stiffness yielded a damping coefficient of approximately 20 lbs-s/ft. These values were used to compute the time series for the applied horizontal force. This series is also denoted as the inertia corrected horizontal wave force.

An algorithm written in the MATLAB language was used to process the raw data file from the data acquisition software. The algorithm read and analyzed the raw data. A series of ten waves was chosen from the early part of the time series, after the wave forces on the structure were fully developed, but before a re-reflected wave reached the structure. The water surface time series was phase shifted to the toe of the structure using the linear wave theory celerity and *Xoffset*. The MATLAB Radix-2 fast Fourier transform (FFT) algorithm was used to compute the discrete, complex-valued Fourier series for the water surface profile and measured force data series. The resulting power spectra showed very narrow banded results with the same peak frequency for each wave and measured force series, with secondary peaks occurring at higher order harmonics for the measured forces. The ten wave record for the water surface profile and the measured forces was printed and the crest amplitude and trough amplitude for each was visually

interpreted. The total amplitude was taken as the average of the crest and trough amplitudes.

5.3.2 *Results of Physical Model and Numerical Simulation*

Physical model experiments were performed for more than four hundred different sets of conditions. These included two different A-Jacks sizes (2.5 in. and 6 in.), different water depths, wave periods, wave heights, uniform placement and three different random placement densities, and three different structure slopes (1:1, 1:2, and 1:3). The relative packing coefficient, K_p, has been calculated for each random placement scheme where:

$$K_p = \frac{(\text{number of units})}{\text{area}} \frac{D^2}{4} \tag{19}$$

The relative packing coefficient is the ratio of the measured unit placement density to the unit placement density for a uniform placement pattern (K_p=1). A series of experiments was also performed in which the number of rows of A-Jacks units was varied from zero (just the load frame) to a fully armored slope in an attempt to quantify the wave force on the load frame.

The data from the bulk force experiments was non-dimensionalized and analyzed. The measured horizontal wave force amplitudes, $aWFH$, (which do not have buoyancy forces) were non-dimensionalized by the weight of a single A-Jacks unit, W, and were compared with the wave steepness (kH), Froude number, Reynold's number, and Keulegan-Carpenter parameter as defined in Table 3. The measured vertical wave force

amplitudes, $aWFV$, were also compared with the measured horizontal wave force amplitude and the wave steepness. The results of the bulk forces experiments are illustrated in Figures 36 through 65. In each figure curves have been fit to the data and the correlation coefficient, R^2, is shown for each curve. The figures are grouped according to the slope. The runs used to fit the sheltering coefficients are also denoted. Figures 54 through 59 show a comparison of the results for the uniform, fully armored slopes for 2.5 in. units. The last group of figures show the results for a partially armored 1:2 slope with the number of rows of units from the toe denoted. Finally, Figure 66 presents a comparison between force measurements, for all wave heights and periods, and the number of rows on the partially armored slope.

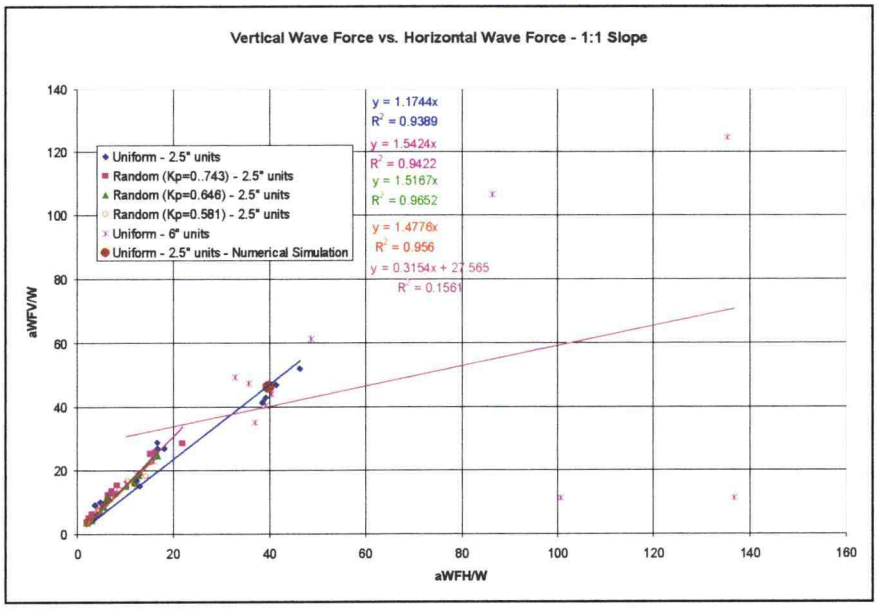

Figure 36: Vertical wave force vs. horizontal wave force for 1:1 slope.

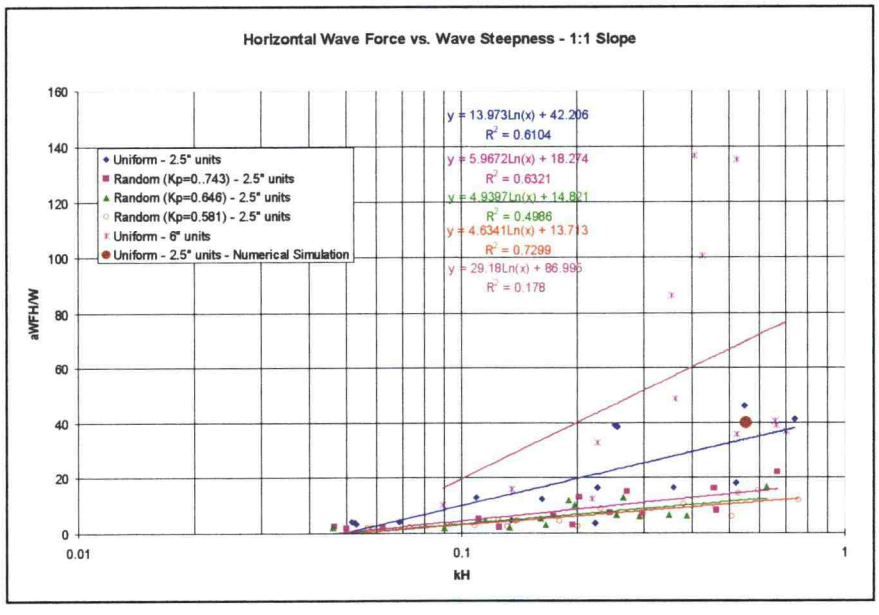

Figure 37: Horizontal wave force vs. wave steepness for 1:1 slope.

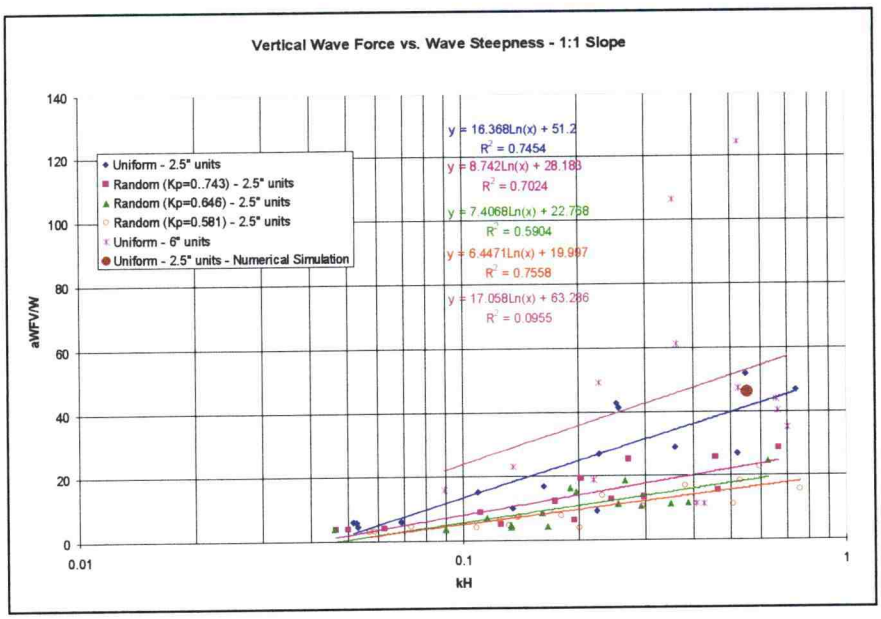

Figure 38: Vertical wave force vs. wave steepness for 1:1 slope.

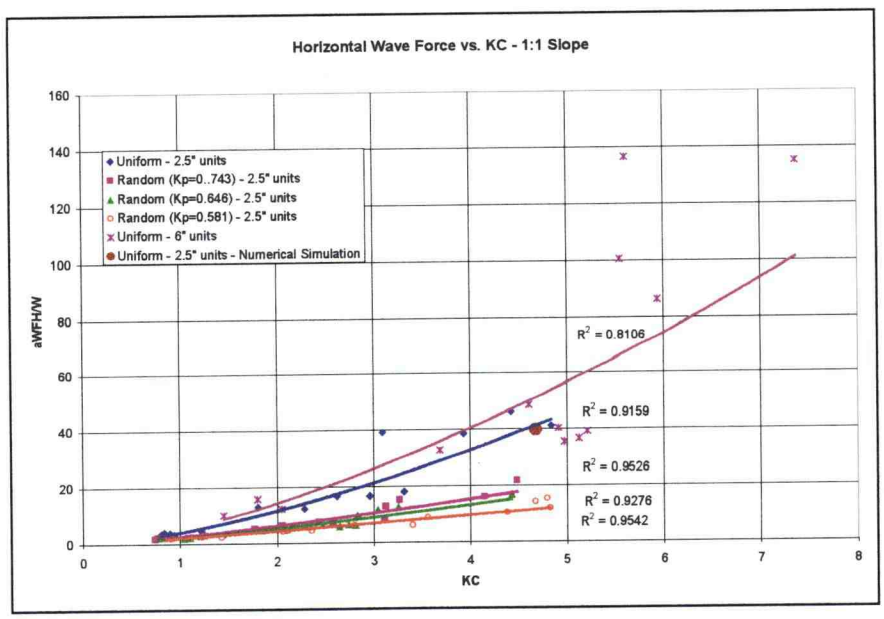

Figure 39: Horizontal wave force vs. Keulegan-Carpenter parameter for 1:1 slope..

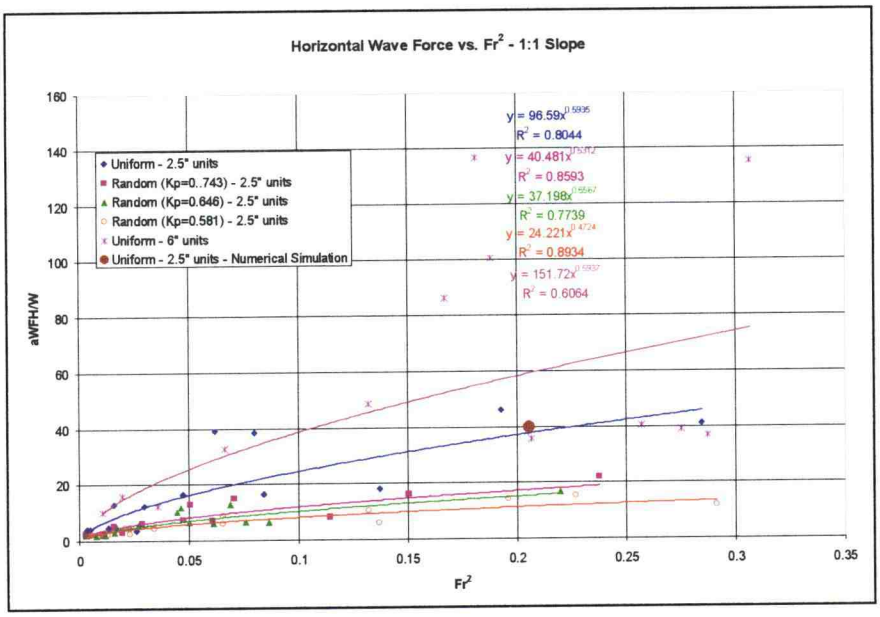

Figure 40: Horizontal wave force vs. Froude number parameter for 1:1 slope.

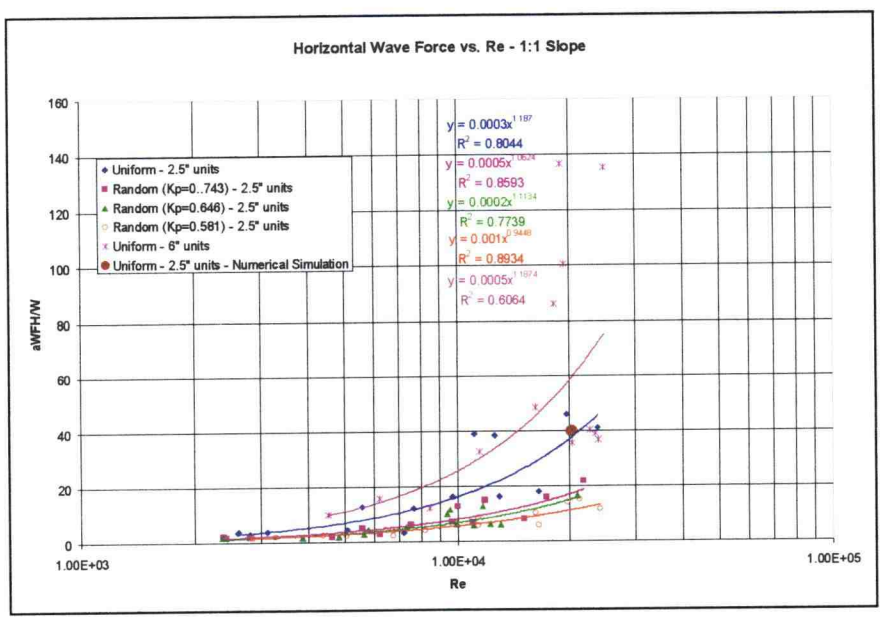

Figure 41: Horizontal wave force vs. Reynold's number for 1:1 slope.

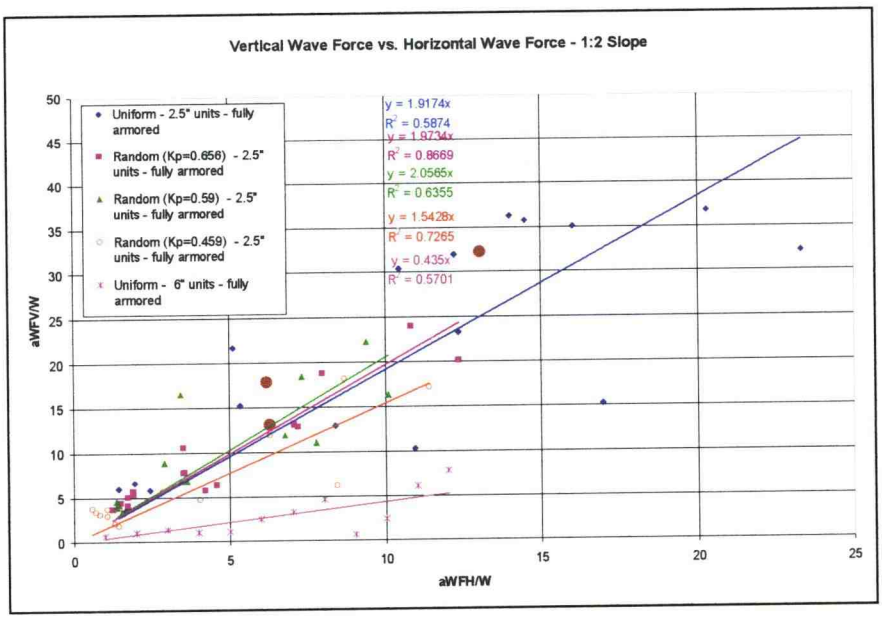

Figure 42: Vertical wave force vs. horizontal wave force for 1:2 slope.

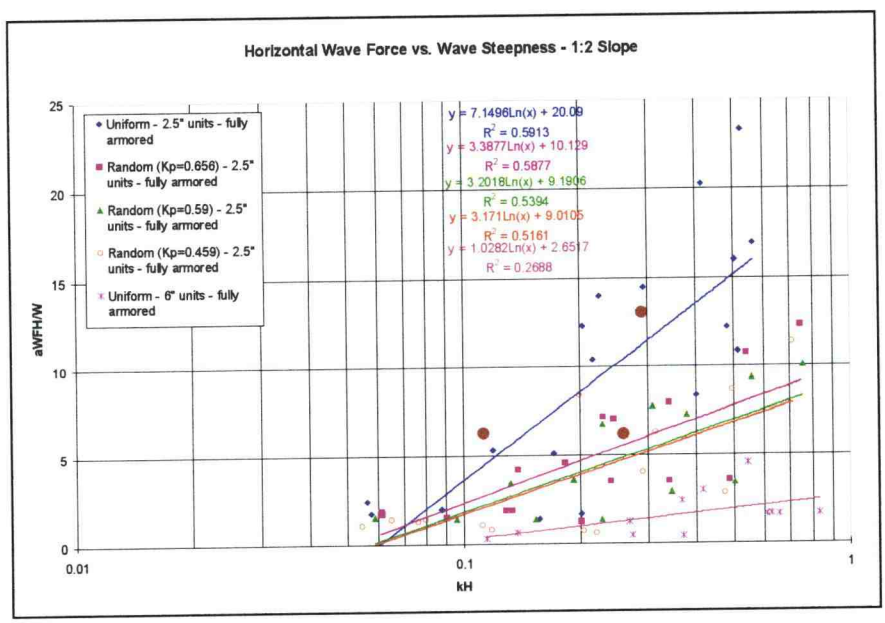

Figure 43: Horizontal wave force vs. wave steepness for 1:2 slope.

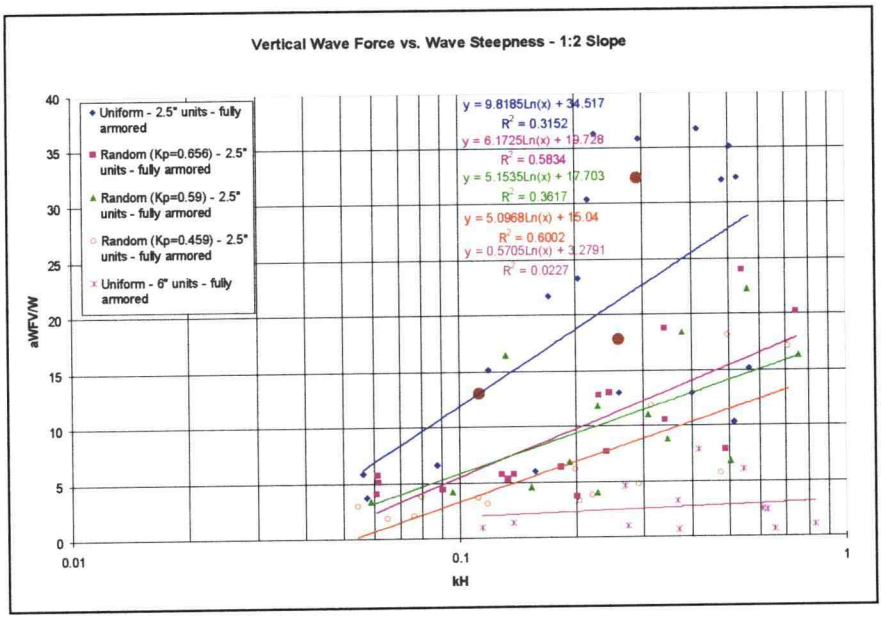

Figure 44: Vertical wave force vs. wave steepness for 1:2 slope.

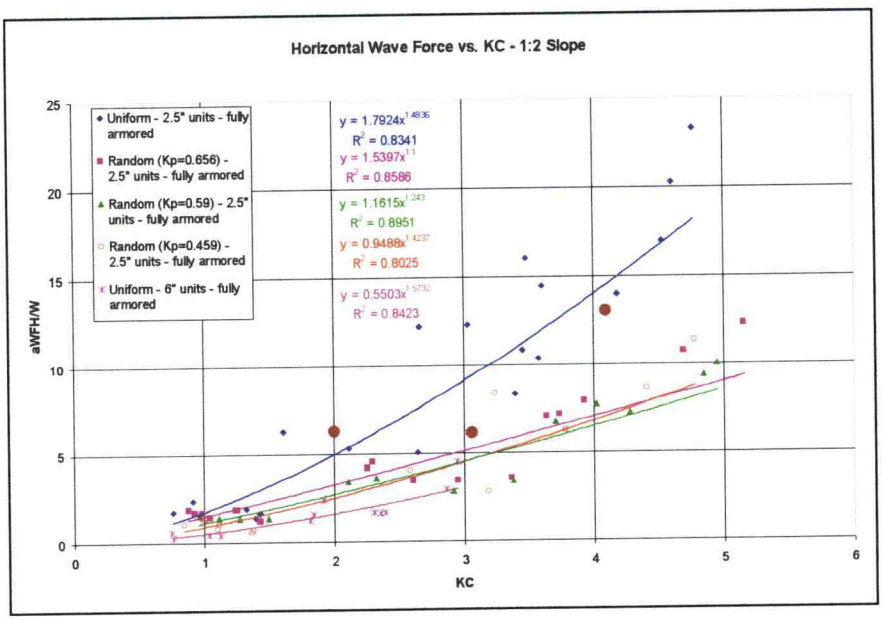

Figure 45: Horizontal wave force vs. Keulegan-Carpenter parameter for 1:2 slope.

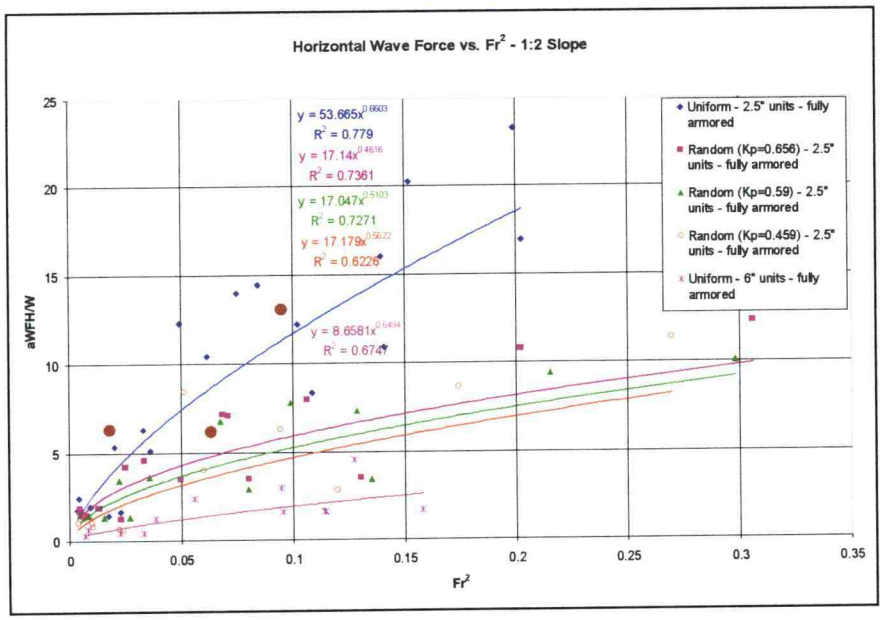

Figure 46: Horizontal wave force vs. Froude number parameter for 1:2 slope.

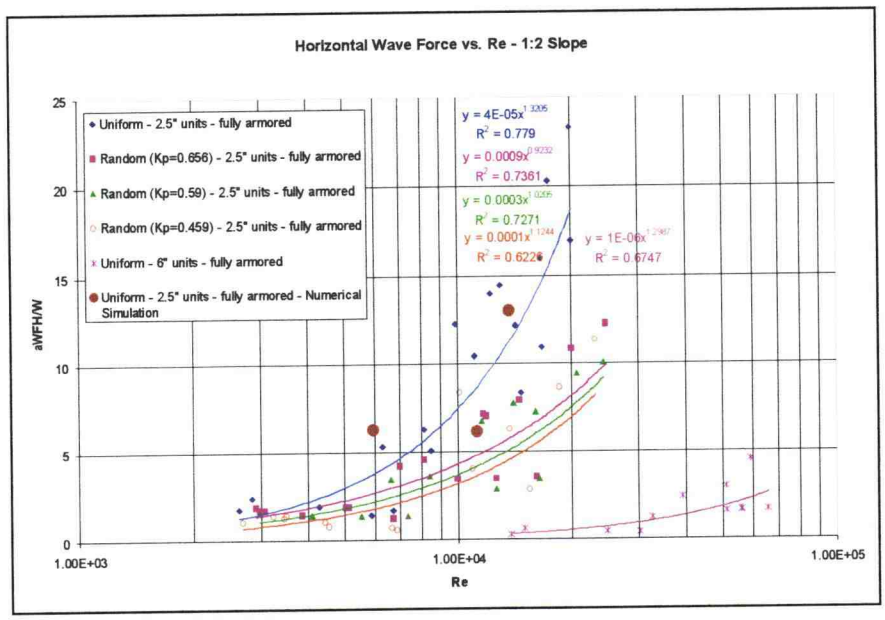

Figure 47: Horizontal wave force vs. Reynold's number for 1:2 slope.

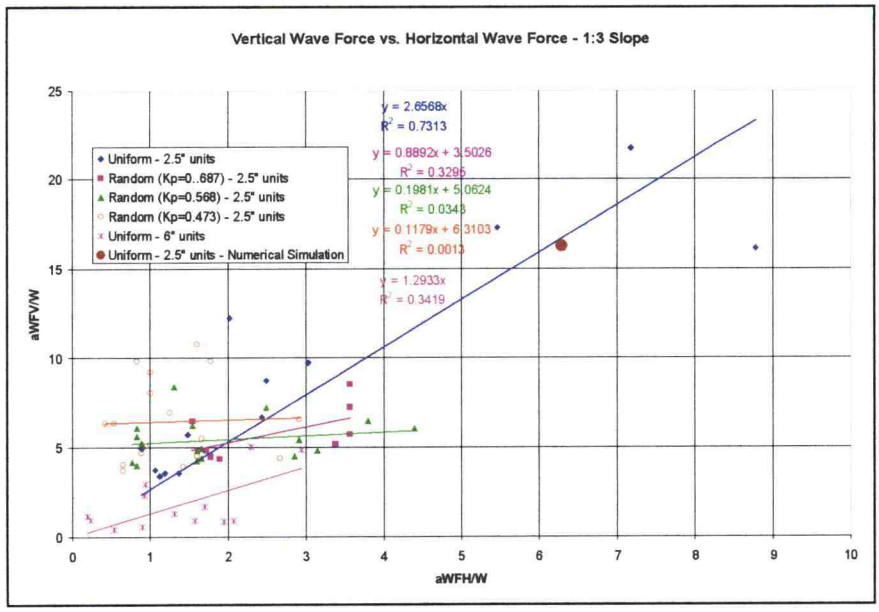

Figure 48: Vertical wave force vs. horizontal wave force for 1:3 slope.

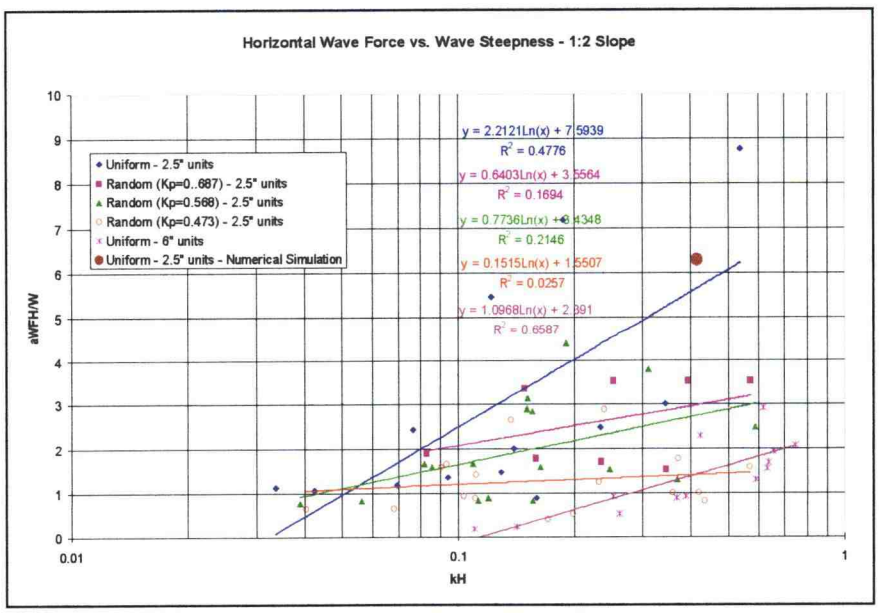

Figure 49: Horizontal wave force vs. wave steepness for 1:3 slope.

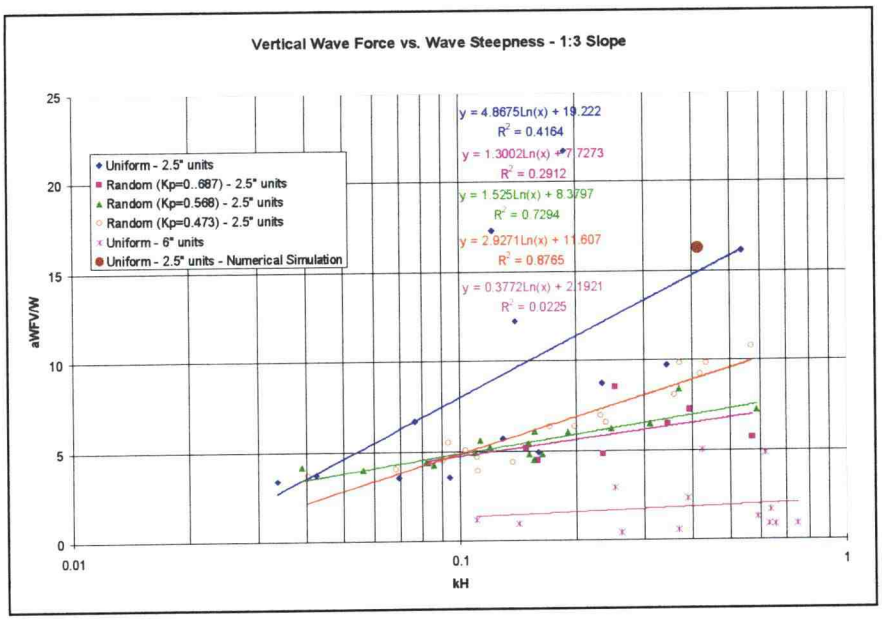

Figure 50: Vertical wave force vs. wave steepness for 1:3 slope.

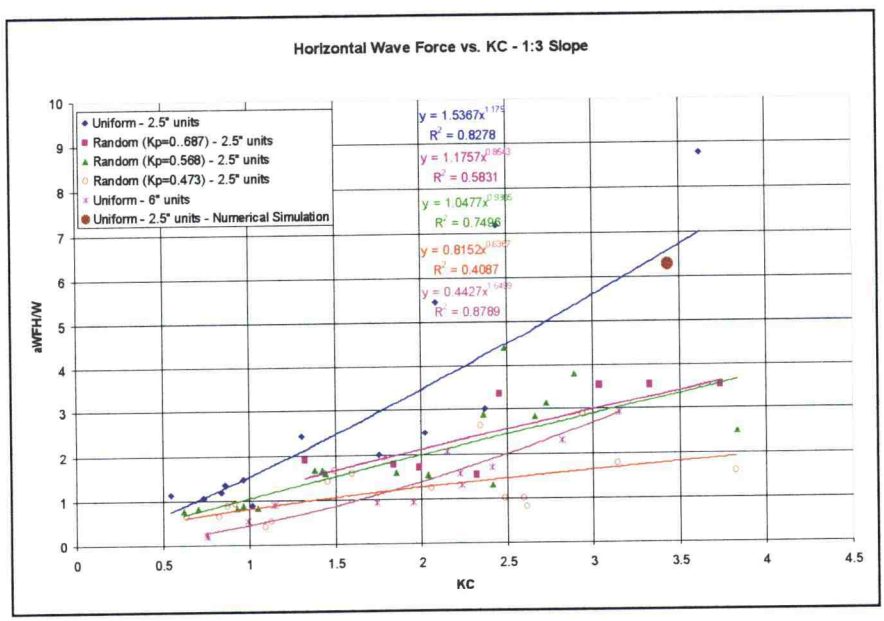

Figure 51: Horizontal wave force vs. Keulegan-Carpenter parameter for 1:3 slope.

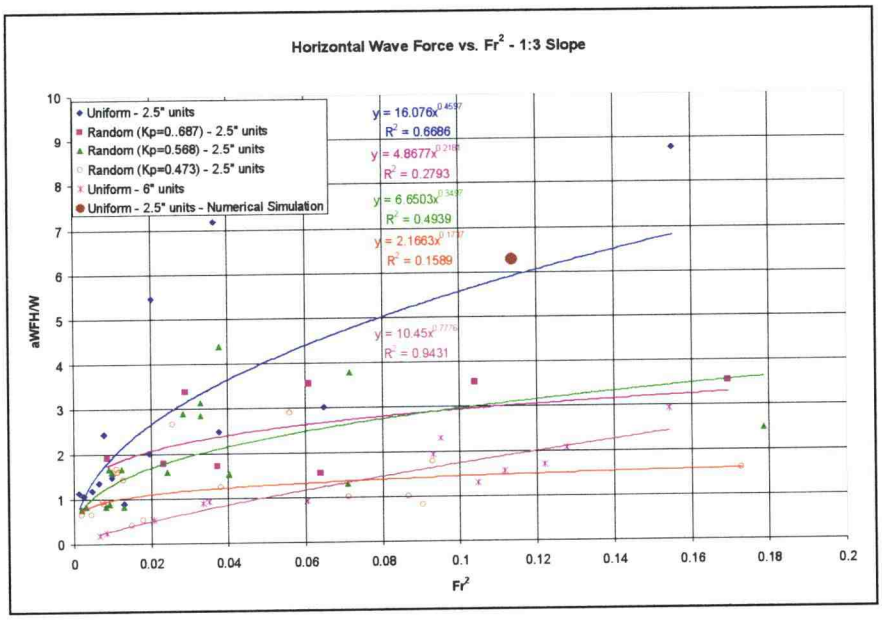

Figure 52: Horizontal wave force vs. Froude number parameter for 1:3 slope.

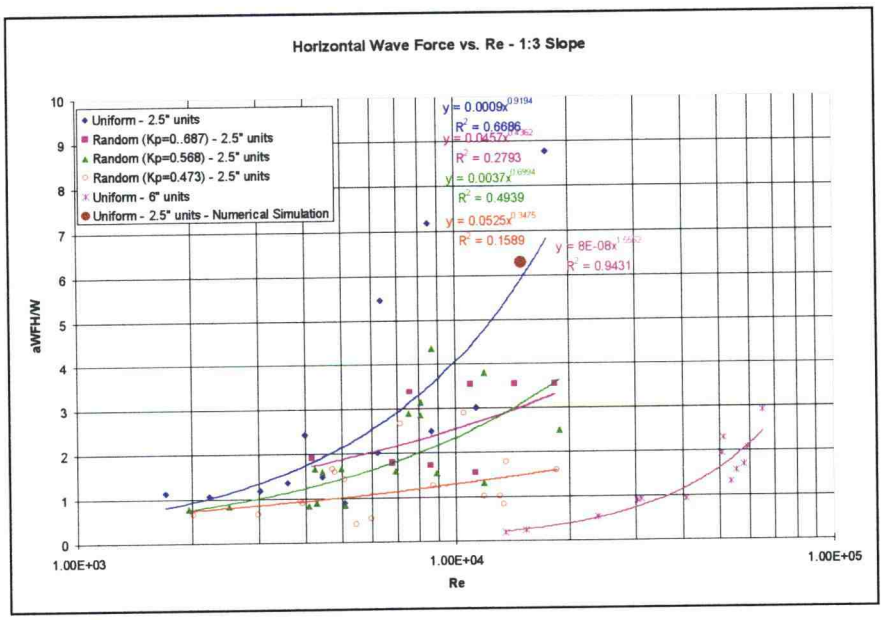

Figure 53: Horizontal wave force vs. Reynold's number for 1:3 slope.

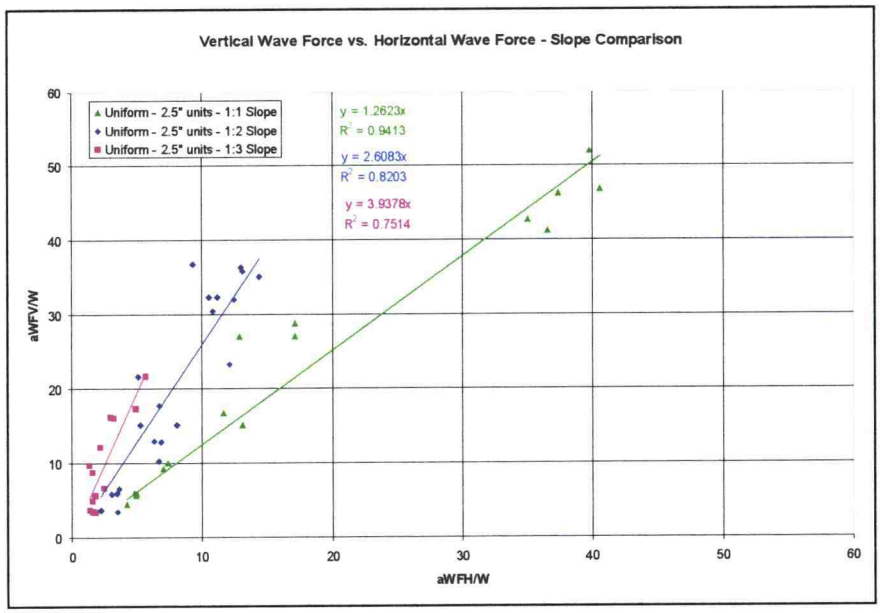

Figure 54: Slope comparison of vertical wave force vs. horizontal wave force.

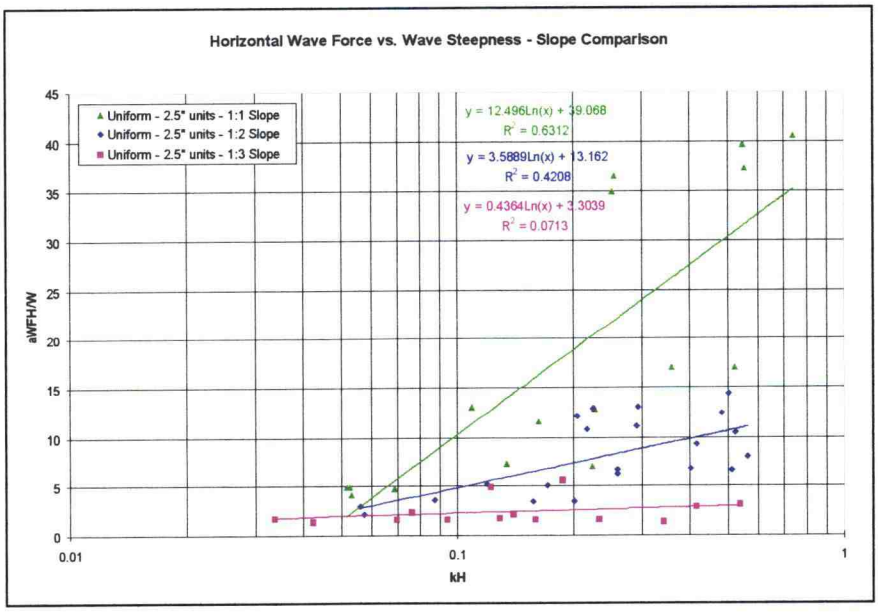

Figure 55: Slope comparison of horizontal wave force vs. wave steepness.

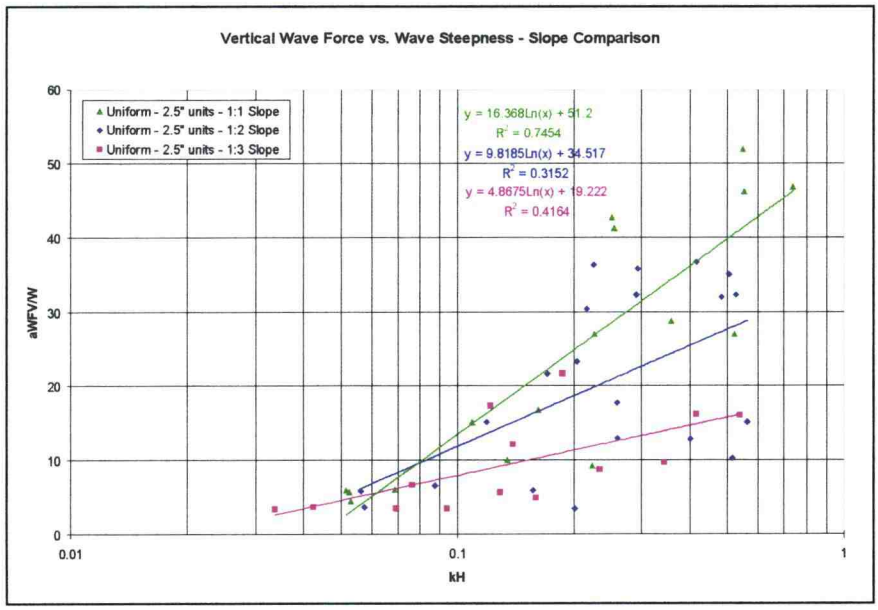

Figure 56: Slope comparison of vertical wave force vs. wave steepness.

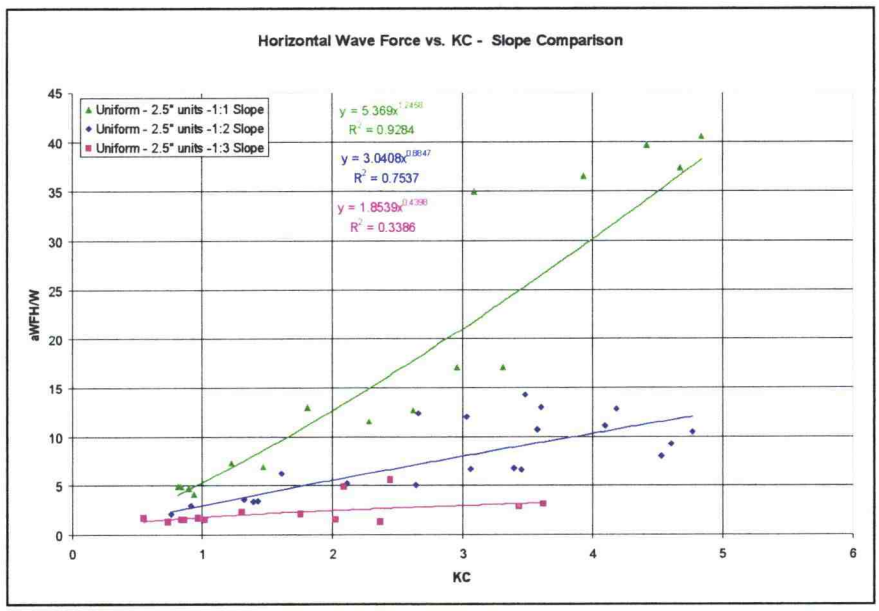

Figure 57: Slope comparison of horizontal wave force vs. Keulegan-Carpenter parameter.

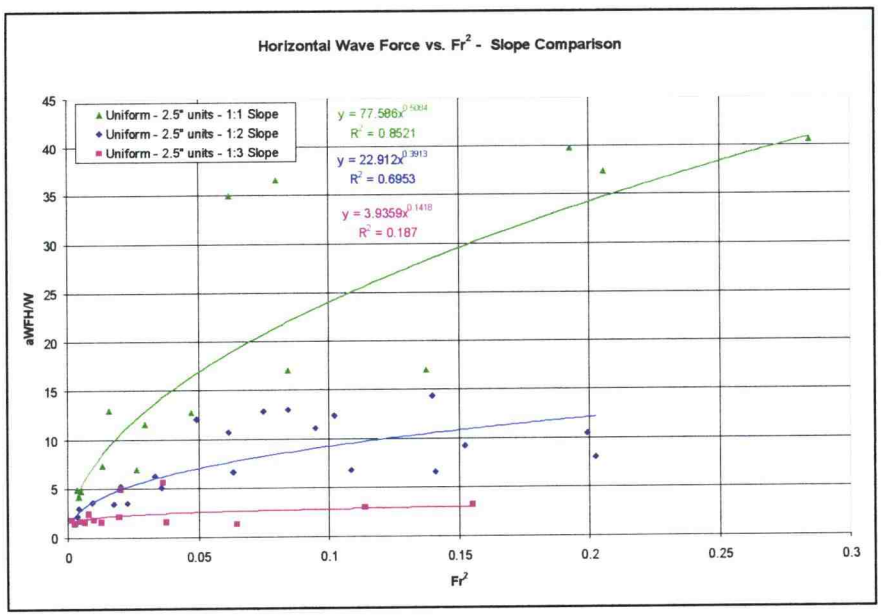

Figure 58: Slope comparison of horizontal wave force vs. Froude number parameter.

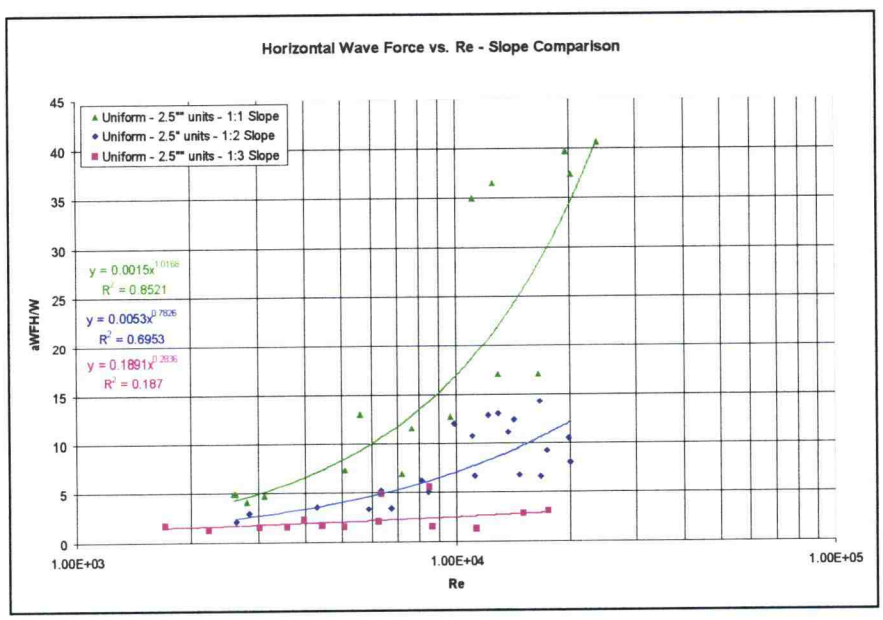

Figure 59: Slope comparison of horizontal wave force vs. Reynold's number.

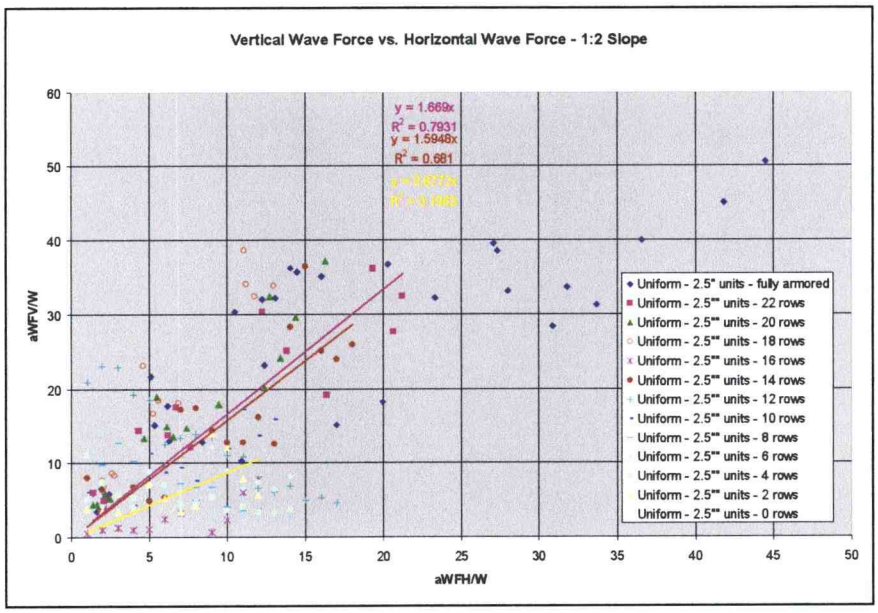

Figure 60: Vertical wave force vs. horizontal wave force for partially armored 1:2 slope.

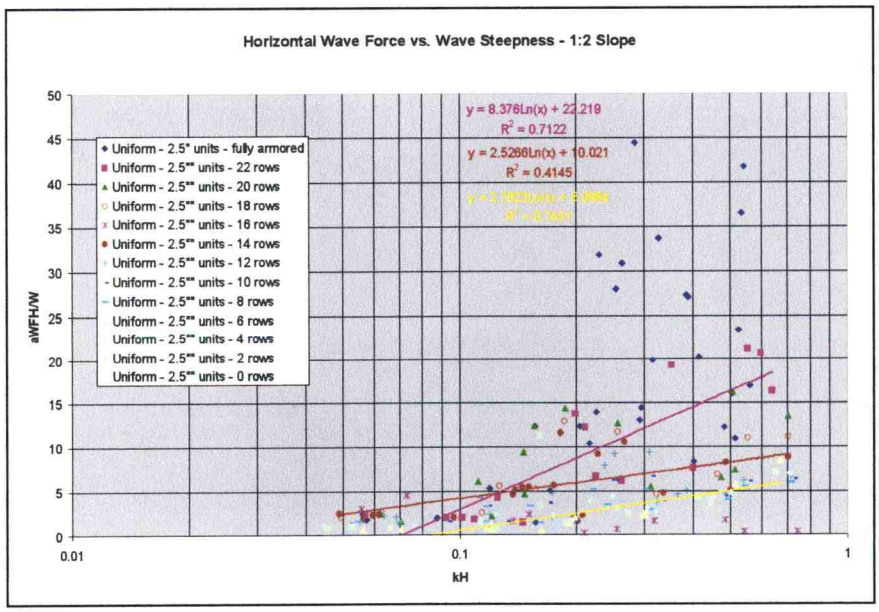

Figure 61: Horizontal wave force vs. wave steepness for partially armored 1:2 slope.

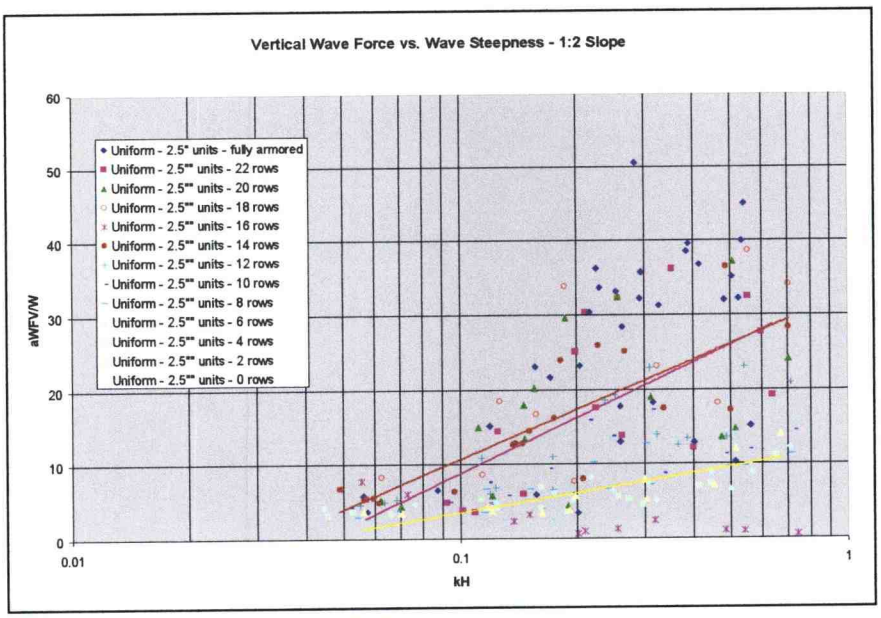

Figure 62: Vertical wave force vs. wave steepness for partially armored 1:2 slope.

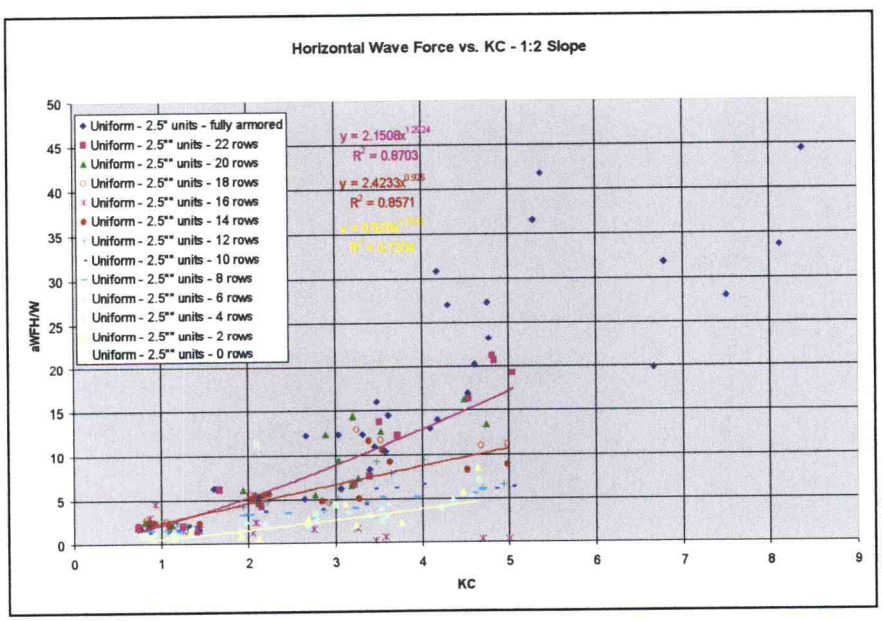

Figure 63: Horizontal wave force vs. Keulegan-Carpenter parameter for partially armored 1:2 slope.

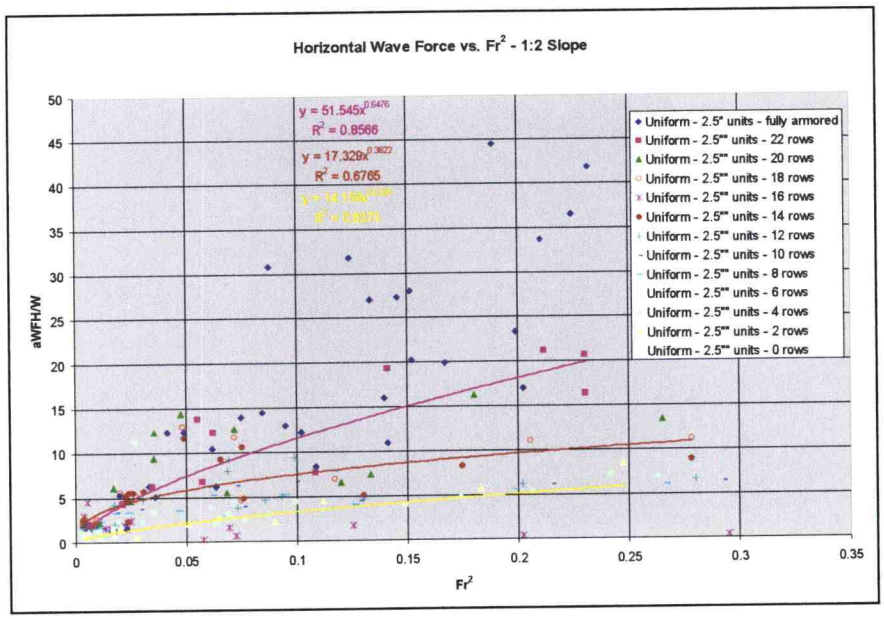

Figure 64: Horizontal wave force vs. Froude number parameter for partially armored 1:2 slope.

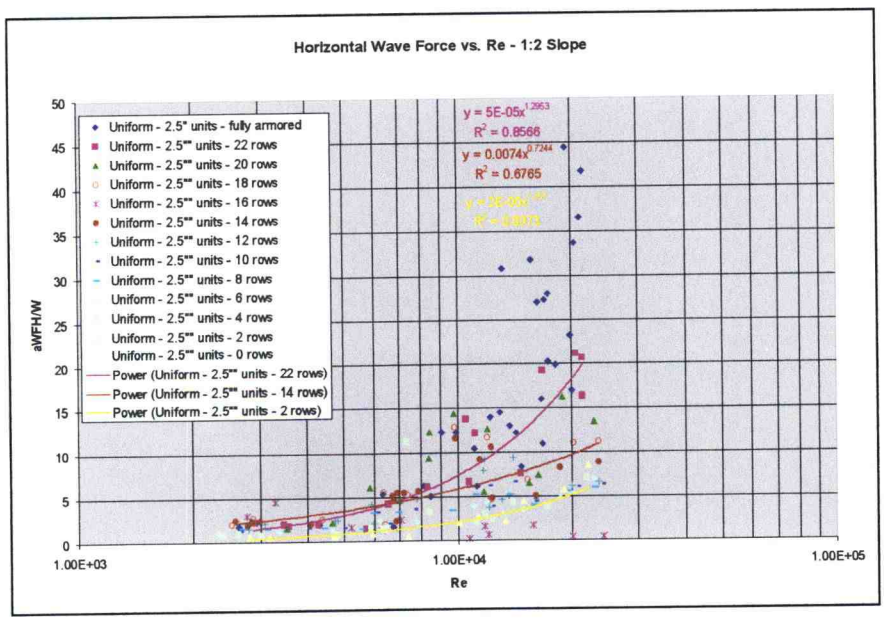

Figure 65: Horizontal wave force vs. Reynold's number for partially armored 1:2 slope.

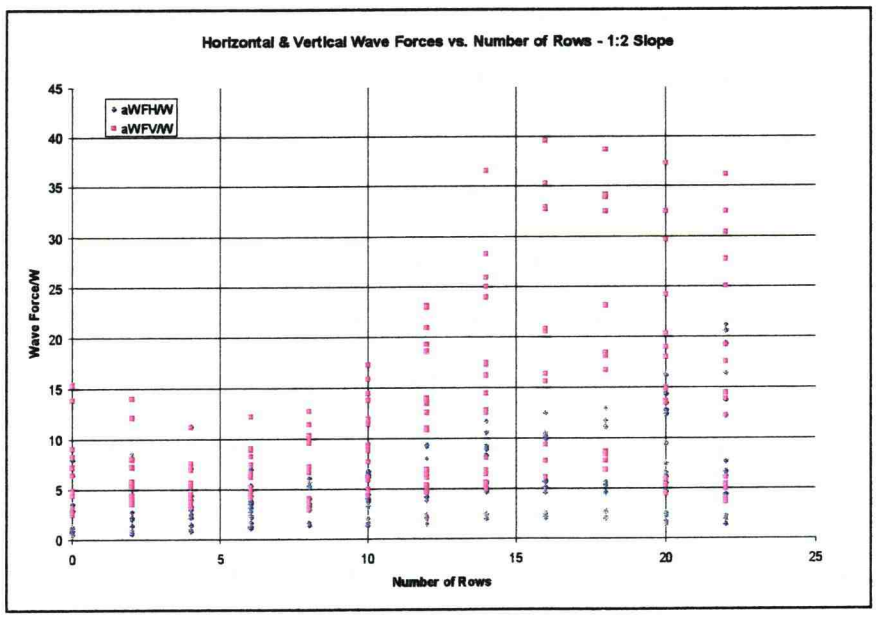

Figure 66: Measured forces vs. number of rows for partially armored 1:2 slope.

Several general observations can be made on the bulk forces data. It can be seen that the wave force is a function of the unit packing density; as the packing density decreases so do the wave forces. Results for randomly placed units also exhibited slightly lower correlations with the fit curves. The horizontal and vertical wave forces are also found to be fairly well correlated, especially for steeper structure slopes. The wave forces exhibited some correlation with the wave steepness, again with better correlation for steeper slopes. Generally, good correlation was found with the Froude number, the Reynold's number, and the Keulegan-Carpenter parameter. The 6 in. units generally exhibited similar correlation as the 2.5 in. units; however, for the 1:1 slope the 6 in. unit test exhibited lower correlation. When comparing the 6 in. unit test data with the data for the 2.5 in. unit test data it should be kept in mind that the forces have been non-dimensionalized by the unit weight where the unit weight for the 6 in. units is almost

14 times greater than that of the 2.5 in. units. It can also be seen that for the partially armored slope the wave force increases as the number of rows of units increases.

Several relationships can also been seen when comparing the data from the different structure slopes. Larger forces in both the horizontal and vertical directions were found for the steep slopes. It is also shown in Figure 54 that the vertical wave forces are larger in comparison to the horizontal wave forces for milder slopes. This is due to the fact that there is a greater buoyancy effect for the milder slopes since more units are fully emerged and submerged for the same wave height. Generally higher correlation coefficients for the fitted curves were found with the steeper slope. One possible cause of variability in the milder slopes is that more of the wave, relative to its wave length, is over the structure at any time which leads to opposing forces on different parts of the structure. Run-up and run-down on the structure slope may also have a larger effect for milder slopes.

Numerical simulation was run for only five of the test cases due to the computer processing time required for each numerical simulation and the time required to fit the sheltering coefficients. As with the incipient rotational motion experiments, the numerical model was run at the physical model scale. For the numerical simulations, the wave force model was run for each row of A-Jacks units on the structure slope. The unit centroid depth and the horizontal offset of each row from the toe of the structure were taken into account. The horizontal and vertical force time series for the rows of units were summed and multiplied by the number of units across the structure to give the total force time series for the structure. The total force time series was output from MATLAB in a text format and imported into a spreadsheet program to fit the sheltering coefficients.

Sheltering coefficients were applied to the horizontal and vertical components of the drag and slamming forces. These coefficients were used to scale the values of the drag and slamming forces for each row of units. In addition, the horizontal and vertical inertia force on the structure was scaled to account for the change in added mass for an inclined structure. Blevins (1979) presents empirically determined added mass coefficients for ellipsoids with varying ratios of major to minor axis length for fluid acceleration parallel to the major axis. As the major to minor axis length ratio increased the added mass coefficient decreased. Similarly, as the structure slope changes, the added mass for the entire slope is affected. The scaling of the inertia is different in nature than the sheltering coefficients. The sheltering and horizontal inertia force coefficients were modified until a visual best-fit was found between the numerical bulk forces estimate and the measured forces.

5.3.3 Comparison of Numerical Simulation and Physical Model

The measured wave height, period, water depth, and the structure slope and unit size for each case analyzed are presented in Table 5. The fit between the measured bulk force data and the numerical simulation of the bulk forces is shown in Figures 67 through 71. The sheltering coefficients used to fit the bulk forces data and the scaling factors for the inertia forces are shown in each figure. For four of the five cases, sheltering coefficients of 0.25 were used for both horizontal and vertical components of drag and slamming. For run BF359 a horizontal drag sheltering coefficient of 1.00 was used, but a value of 0.25 for the other sheltering coefficients still provide the best fit. Run BF359

was for a 1:1 slope, which may have affected the horizontal drag sheltering coefficient. The horizontal inertia force was scaled by 0.10 for all of the case except for run BF38 where a scaling factor of 0.25 was used. The vertical inertia forces were scaled by a factor between 0.7 and 1.0 for all case except BF266 where a value of 0.5 was used. Run BF266 was for a 1:3 slope and the vertical wave forces were buoyancy dominated. A summary of the sheltering coefficients and inertia scaling factors used to fit the numerical model data is presented in Table 6.

Table 5: Physical parameters for run cases used to fit sheltering coefficients.

Run Case	H (in.)	T (s)	h (in.)	Slope	D (in.)
BF27	2.7714	1.07	12	1:2	2.5
BF35	2.1714	0.98	11.94	1:2	2.5
BF38	1.2571	0.71	12	1:2	2.5
BF266	2.5333	0.82	12	1:3	2.5
BF359	3.5429	0.83	12	1:1	2.5

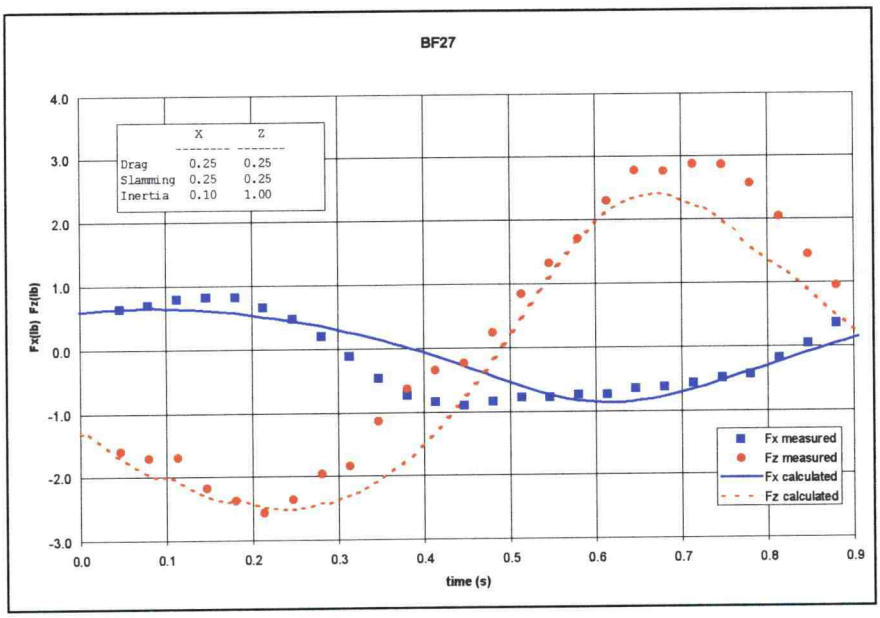

Figure 67: Bulk forces curve fit using sheltering coefficients for run BF27.

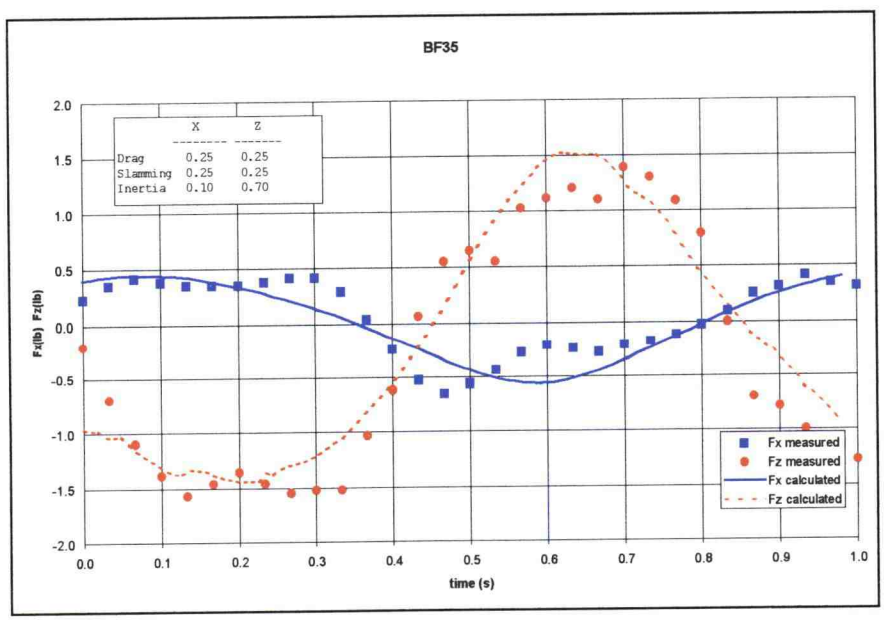

Figure 68: Bulk forces curve fit using sheltering coefficients for run BF35.

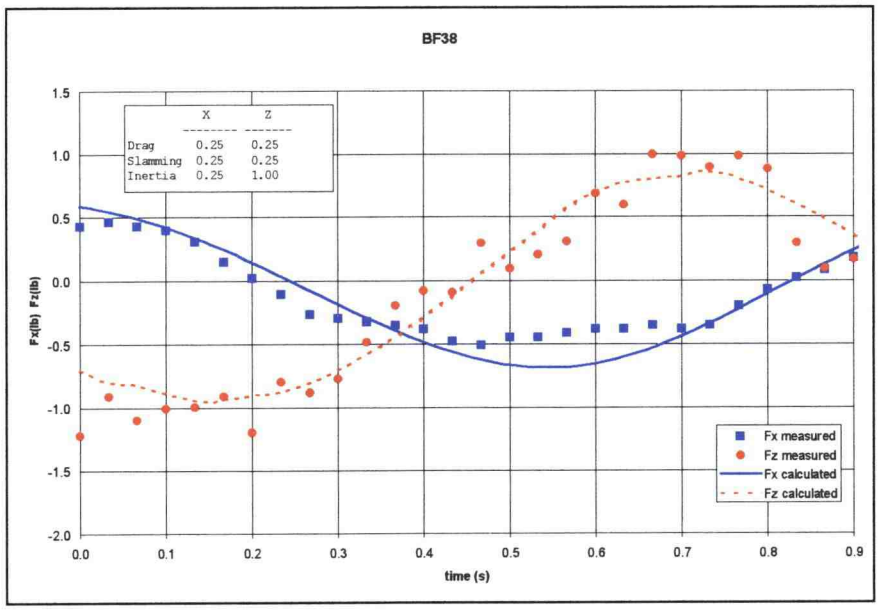

Figure 69: Bulk forces curve fit using sheltering coefficients for run BF38.

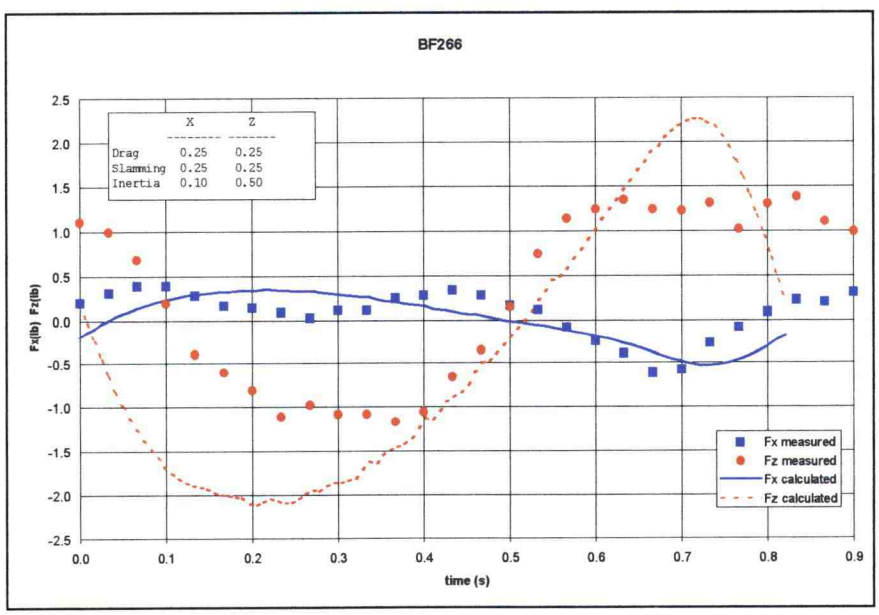

Figure 70: Bulk forces curve fit using sheltering coefficients for run BF266.

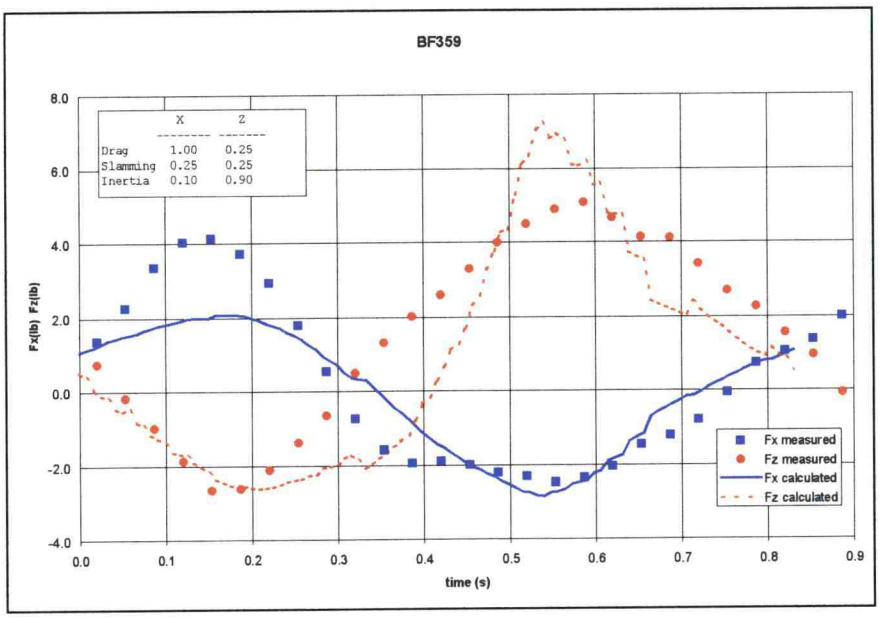

Figure 71: Bulk forces curve fit using sheltering coefficients for run BF359.

Table 6: Sheltering coefficients and inertia scaling factors.

Run	*X* direction drag sheltering coefficient	*Z* direction drag sheltering coefficient	*X* direction slamming sheltering coefficient	*Z* direction slamming sheltering coefficient	*X* direction inertia scaling factor	*Z* direction inertia scaling factor
BF27	0.25	0.25	0.25	0.25	0.10	1.00
BF35	0.25	0.25	0.25	0.25	0.10	0.70
BF38	0.25	0.25	0.25	0.25	0.25	1.00
BF266	0.25	0.25	0.25	0.25	0.10	0.50
BF359	1.00	0.25	0.25	0.25	0.10	0.90

The empirically fit curves based on the numerical model results provide good fits to the measured data. The general trend of the data was followed by each curve fit and the sheltering coefficients used to fit the data were consistent. The bulk force data provide further evidence of the validity of the wave force model and allows the extension of the model to estimate forces on entire structures. The bulk force data showed some secondary peaks which are believed to be inertial forces due to the movement of the load frame. The inertial correction method described in this section smoothed the data for most cases; however, for some cases the inertial correction caused unreasonable results and, therefore, was not used to analyze the data presented here. Overall the bulk force experiment was successful.

6. CONCLUSIONS

A numerical model has been developed to predict wave forces on A-Jacks armor units. The model allows for the specification of any unit orientation in a system based on the structure slope and unit rotation on the slope. The model also accepts waves which are not normally incident to the structure toe. The drag, inertia, buoyancy, and slamming forces on the units are calculated and the rotations of the units induced by these forces are estimated by integrating the equation of motion. The numerical calculation of these forces was found to converge to a single value as the spatial and temporal step sizes decreased. The model can be run, using the MATLAB software package, on a number of operating systems and is acceptably fast on a desktop computer. Graphical output routines which make the model results easy to interpret have also been developed.

The numerical model is capable of calculating the bulk forces on a matrix of uniformly placed A-Jacks units. Sheltering coefficients and inertia scaling factors can be input to the model. The model determines the location of each row of units on the structure slope and computes the forces (per unit across the slope) on each. The computed drag and slamming forces are multiplied by the sheltering coefficients and the inertia force is scaled by the inertia scaling factors. The model sums the forces and outputs the total force on each row of units and the total force on the slope.

Nearly 5,000 runs of the numerical wave force model were performed. The maximum forces from these runs were analyzed and compared with the Reynold's number, Keulegan-Carpenter parameter, and the Froude number. This analysis showed that there is strong correlation between these parameters and the predicted maximum wave force. A simplified expression, with a good correlation to the numerical model

predictions, was developed for the calculation of the maximum wave force on an isolated unit.

Three physical experiments were conducted to validate the results of the numerical model. In the first, the model predictions for the onset of rotational motion were verified by observation of units subjected to different wave conditions in a wave flume. The numerical model results were largely in agreement with the observations in the experiments. In the second experiment, the drag coefficient for steady flow was experimentally determined. This experiment showed that the unit orientation has little effect on the drag force. This is similar to predictions made by the wave force model. It was also found that the steady flow drag coefficient is similar to the drag coefficient used in the numerical model. In the third experiment, the bulk forces on matrices of units were measured using a load frame in a wave flume. The effects of slope, packing density, and unit size on the measured forces were examined for a variety of wave conditions. The measured forces were used to develop sheltering coefficients for the numerical bulk forces model. The sheltering coefficients were fit to the results of five experimental runs and were consistent. The wave force predictions of the numerical model were thus partially confirmed by direct measurement.

There is further work which could be done to validate and potentially improve the wave force model. First, determining sheltering coefficients for more bulk force runs would increase confidence in the coefficients and an analysis of their variation with physical parameters could be performed. Second, an improved method of modeling water particle kinematics at and near the armor units could be developed, perhaps similar to Kobayashi et al. (1990) or McDougal and Sulisz (1990). Third, a more accurate

determination of the drag and inertia coefficients for oscillatory flow used in the model could be conducted, particularly for prototype scale Reynold's numbers. Lastly, measurements of actual wave forces on isolated and nested units would be useful. This is especially true for the slamming forces on units which, although the magnitudes seem reasonable, have not yet been directly or indirectly measured for isolated units.

Although the results from the numerical model are interesting in their own right, the application of the model to the larger problem of armor unit and coastal structure stability is a key reason for its development. The development of this model provides a basis for progress towards an analytical stability model for breakwaters with A-Jacks armor units. Potential applications of the model follow Bruun's (1990) categories for breakwater stability (overall stability, unit-in-place stability, and unit structural stability).

As mentioned in Chapter 1, a finite element model (FEM) of the unit structural stability is a primary impetus for the development of the wave force model. The predicted forces from the numerical model and the empirically estimated bulk forces on matrices of units will be used as the input for a FEM to determine the stresses induced in units by these forces. This work is being performed by Joseph Tedesco and Trent Latta at Auburn University. The wave force induced rigid body motions and the resulting reaction forces with the sub-base and other units will also be analyzed and input to the FEM. For A-Jacks in uniform placement, these motions and reaction forces are deterministic, unlike for randomly placed units. Failures in armor units are frequently attributed to unit movements; therefore, it is likely that the rigid body motions and reaction forces, along with the self-weight of the units, will be much more important to the unit structural stability than the wave forces themselves.

The wave force model may also be used to examine the unit-in-place stability. Mickel (1999) conducted tests to determine the ability of matrices of A-Jacks units to resist the displacement of units in a non-submerged environment with static loads. It may be possible to use the estimates of bulk forces to estimate the response of a matrix of units based on a similar approach with oscillatory loads.

The ultimate application for the wave force model is to determine overall structural stability for breakwaters. The bulk forces on a matrix of units could be applied in a slope stability model that accounts for interlocking between units using discrete element modeling. Such a model, combined with improved wave force model hydrodynamics, could be developed for the regularly placed A-Jacks armor units. If possible this type of model could lead to the first completely analytical model for overall breakwater stability. This would be a major advance in coastal engineering and could lead to improved and less costly breakwater designs.

REFERENCES

Arai, M., L. Y. Cheng, and Y. Inoue (1995) "Hydrodynamic impact loads on horizontal members of offshore structures." ***Proc., 14th Int. Conf. on Offshore Mechanics and Arctic Engineering (Copenhagen, Denmark)***, ASME, New York, N.Y., 199-206

Blevins, Robert D. (1979) ***Formulas for Natural Frequency and Mode Shape***, Van Nostrand Reinhold Co., New York, N.Y.

Bruun, Per (1990) "Design criteria and procedures for mounds for breakwaters and coastal protection." ***Journal of Coastal Research - Special Issue #7***, Coastal Education and Research Foundation, Fort Lauderdale, Florida, 1-4

Burcharth, Hans F. (1985) "Structural unit stability." ***Design and Construction of Mounds for Breakwaters and Coastal Protection***, Ed. Per Bruun, Elsevier, Amsterdam, Netherlands, 270-287

Chisholm, J.S.R. (1978) ***Vectors in Three-Dimensional Space***, Cambridge University Press, Cambridge, United Kingdom

Epstein, H. and F. C. Tyrell (1949) "Design of rubble-mound breakwaters." ***Proc., 17th Int. Navigation Congress (Lisbon, Portugal)***, Section 2, Communication 4, 81-98

Gasson, Peter C. (1993) ***Geometry of Spatial Forms***, John Wiley & Sons, New York, N.Y.

Geick, Kurt and R. Geick (1990) ***Engineering Formulas, 6th English ed.***, McGraw-Hill, New York, N.Y.

Hofman, Joe D. (1992) ***Numerical Methods for Engineers and Scientists***, McGraw-Hill, New York, N.Y.

Howell, G. L. (1988) "Measurements of forces on Dolos armor units at prototype scale." ***Proc., 21st Int. Conf. On Coastal Engineering***, ASCE, New York, N.Y.,

Hudson, R. Y. (1958) "Design of quarry-stone cover layers for rubble-mound breakwaters." ***Research Report No. 2-2***, U.S. Army Corps of Engineers Waterways Experiment Station, Vicksburg, Mississippi

Irrabaren, R. (1938) "Una formula para el calculo de los diques de escollera." (A formula for the calculation of rock filled dikes), Revista de Obras Publicas, Madrid, Spain. Translated by D. Heinrich, Fluid Mechanics Laboratory, University of California, Berkeley, California, ***Technical Report HE-116-295***, 1948

Juhl, Jorgen and O. J. Jensen (1990) "Forces on Breakwater Armor Units." ***Proc., 22nd Coastal Engineering Conf.***, ASCE, New York, N.Y.,1538-1551

Kobayashi, Nobuhisha and A. K. Otta (1987) "Hydraulic stability analysis of armor units." ***Journal of Waterway, Port, Coastal, and Ocean Engineering***, ASCE, 113(2), 171-186

Kobayashi, Nobuhisha and A. Wurjanto (1990) "Numerical model for waves on rough permeable slopes." ***Journal of Coastal Research - Special Issue #7***, Coastal Education and Research Foundation, Fort Lauderdale, Florida, 149-166

Kobayashi, Nobuhisha, A.Wurjanto, and D. T. Cox (1990) "Irregular waves on rough permeable slopes." ***Journal of Coastal Research - Special Issue #7***, Coastal Education and Research Foundation, Fort Lauderdale, Florida, 167-184

McDougal, William. G. and W. Sulisz (1990) "Wave interaction with rubble bases." ***Journal of Coastal Research - Special Issue #7***, Coastal Education and Research Foundation, Fort Lauderdale, Florida, 139-148

McDougal, William G., J. A. Melby, and J. W. Tedesco (1987) "Wave forces on concrete armor units." ***Proc., Computer Aided Simulation of Fluid-Structure Interaction Problems (Atlantic City, New Jersey)***, ASCE, New York, N.Y., 1-21

Mickel, Joshua J. (1999) ***A-Jacks Matrix Stability: Deflection Due to Static Normal Loads***, Engineering Report in Partial Fulfillment of Master of Science Degree, Department of Civil, Environmental, and Construction Engineering, Oregon State University, Corvallis, Oregon

Mortenson, Micheal E. (1985) ***Geometric Modeling***, John Wiley & Sons, New York, N.Y.

Mott, Robert L. (1994) ***Applied Fluid Mechanics***, Maxwell Macmillan, Toronto, Canada

Rufin, Teofilo M., Jr., N. Mizutani, and K. Iwata (1996) "Estimation method of stable weight of spherical armor unit of a submerged wide-crown breakwater." ***Coastal Engineering***, 28(1-4), Elsevier, 183-228

Sarpkaya, Turgut and M. Isaacson (1981) ***Mechanics of Wave Forces on Offshore Structures***, Van Nostrand Reinhold Co., New York, N.Y.

Silva, R. and I. J. Losada (1997) "Numerical model to predict wave forces on permeable breakwaters." ***Proc., Int. Conf. on Computer Modeling of Seas and Coastal Regions***, Ashurst, United Kingdom, 265-274

Sulisz, Wojciech (1994) "Stability analysis for multilayered rubble bases." ***Journal of Waterway, Port, Coastal, and Ocean Engineering***. ASCE, 102(3), 269-282

Tedesco, Joseph W., W. G. McDougal, and C. A. Ross (1999) ***Structural Dynamics: Theory and Applications***, Addison-Wesley, Menlo Park, California

Tedesco, Joseph W., W. G. McDougal, J. A. Melby, and P. B. McGill (1987) "Dynamic response of Dolos armor units." ***Computers & Structures***, 26(1-2), 67-77

Von Karman, Theodore (1929) "The impact on seaplane floats during landing." ***National Committee for Aeronautics Technical Note No. 321***, Washington, D.C.

Whalin, Robert W. (1994) "An overview of rubble-mound breakwater development in the United States." ***Case Histories of the Design, Construction, and Maintenance of Rubble Mound Structures Seminar (Eureka, Calif.)***, ASCE, New York, N.Y., 1-15